EXPERIMENTAL STUDY AND NUMERICAL OPTIMIZATION OF A THERMAL SWING ADSORBER FOR BIOGAS UPGRADING

JACKLINE MWENDE MUTUNGA

DOCTOR OF PHILOSOPHY IN MECHANICAL ENGINEERING

JOMO KENYATTA UNIVERSITY OF AGRICULTURE AND TECHNOLOGY

2026

Experimental Study and Numerical Optimization of a Thermal Swing Adsorber for Biogas Upgrading

Jackline Mwende Mutunga

A Thesis Submitted in Partial Fulfillment of the Requirements for the Degree of Doctor of Philosophy in Mechanical Engineering of the Jomo Kenyatta University of Agriculture and Technology

2026

DECLARATION

This thesis is my original work and has not been presented for a degree in any other University

Signature ..... ……Date.....

Jackline Mwende Mutunga

This thesis has been submitted for examination with our approval as the University Supervisors

Signature ..... ……Date.....

Prof. (Eng.) Hiram M. Ndiritu, PhD

JKUAT, Kenya

Signature ..... ……Date.....

Dr. Meshack Hawi, PhD

JKUAT, Kenya

Signature ..... ……Date.....

Dr. Ing Peter Oketch, PhD

JKUAT, Kenya

DEDICATION

To the Mutungas, Kimathis, and Kang’entus.

ACKNOWLEDGEMENT

I am grateful to Almighty God for His mercies and for providing strength and resources to carry out this study. This research thesis would not have been completed without the guidance and invaluable input of my supervisors, Prof. Eng. Hiram Ndiritu, Dr. Meshack Hawi, and Dr. Ing. Peter Oketch. I sincerely appreciate the time and effort they dedicated to reviewing my work and making significant contributions, as well as the invaluable guidance and mentorship they provided. The technical team at JKUAT's mechanical engineering workshops greatly assisted in the successful completion of this work. I particularly appreciate Mr. Joseph Muigai from the Thermodynamics lab.

I acknowledge the financial support of the German Academic Exchange Service (DAAD) and Japan International Cooperation Agency (JICA) for funding this research. Their assistance was crucial in allowing me to complete this work with minimal financial constraints. Additionally, I am grateful to the Erasmus+ exchange program for facilitating my research stay at Politecnico di Torino in Italy.

Finally, I would like to express my appreciation to my family and friends who provided me with both direct and indirect support throughout the research process; their insights and advice were truly invaluable.

TABLE OF CONTENTS

LIST OF TABLES

LIST OF FIGURES

LIST OF APPENDICES

ACRONYMS AND ABBREVIATIONS

AC	Activated Carbon
ANN	Artificial Neural Networks
ANOVA	Analysis of Variance
BBD	Box-Behnken Design
BET	Brunauer Emmett Teller
BJH	Barrett-Joyner-Halenda
DOE	Design of Experiment
Db	Dry Basis
dF	Degree of Freedom
IP	Isotherm Parameter
LDF	Linear Driving Force
MTC	Mass Transfer Coefficient
pH	Potential of Hydrogen
PID	Proportional Integral Derivative
Pr	Prandtl Number
P/F	Purge-to-Feed Flow Rate Ratio
PSA	Pressure Swing Adsorption
RMSE	Root Mean Square Error
RSS	Residual Sum of Squares
RSM	Response Surface Methodology
SEM	Scanning Electron Microscopy
SD	Standard Deviation
SDGs	Sustainable Development Goals
slpm	Standard Liters Per Minute
TSA	Thermal Swing Adsorption
TGA	Thermogravimetric Analysis
v/v	Volume per Volume
VPSA	Vacuum Pressure Swing Adsorption
VSA	Vacuum Swing Adsorption

LIST OF NOMECLATURE

A	Cross-Sectional Area: m^2
a_p	Particle Surface Area/Volume of Bed:m^{-1}
$\mathbf{B_{xi}}$	Systematic Uncertainty
C_{pg}	Fluid Phase Heat Capacity: $kJ/kg.K$
C_{ps}	Specific Heat Capacity of Adsorbent: $kJ/kg.K$
C_{pw}	Specific Heat Capacity of Wall: $kJ/kg.K$
d_{AC}	Average Particle Diameter: m
D_b	Internal Diameter of Bed: m
$\mathbf{d_p}$	Particle Diameter: m
F_{bm}	Optimal Biomethane Flow rate: m^3/s
H_b	Height of Bed: m
h_w	Gas-wall Heat Transfer Coefficient: $W/m^2.K$
k_{LDF,CH_4}	Methane Mass Transfer Coefficient: 1/s
k_{LDF,CO_2}	Carbon Dioxide Mass Transfer Coefficient: 1/s
k_w	Bed Wall Thermal Conductivity: W/mK
k_s	Solid Phase Thermal Conductivity: W/mK
$\mathbf{k_g}$	Gas Phase Thermal Conductivity: W/mK
$\mathbf{M_w}$	Molecular Weight of the Gaseous Mixture
o	Regression Model Output Response
$\mathbf{P_{xi}}$	Random Uncertainty
$\mathbf{P_i}$	Equilibrium Pressure of Component i: bar
$\mathbf{q_i^*}$	Loading of Component i: $kmol/kg$
q	Molar Flow rate: mol/s
R	Gas Constant: $m^3.Pa/mol.K$
r_p	Particle Radius: m
v_g	Fluid Phase Velocity: m/s
w_t	Wall Thickness of Bed: m
y_i	Mole Fraction of Component i in Gas Phase
$\boldsymbol{\beta_o}$	Regression Coefficient for Intercept

β_i	Linear Regression Coefficient
β_{ii}	Quadratic Regression Coefficient
β_{ij}	Interaction Terms
ε_b	Interparticle Voidage
ε_p	Particle Porosity
ϕ	Internal Frictional Angle
ϕ_r	Residual
ϕ_{CH_4}	Biomethane Concentration in Volume Fraction
μ	Dynamic Viscosity: Pa. s
ψ	Particle Sphericity
ΔP	Pressure change: Pa
Δt	Time Step: s
ρ_{AC}	Activated Carbon Pellet Density: kg/m^3
ρ_w	Bed Wall Density: kg/m^3
ρ_g	Fluid Phase Density: kg/m^3
σ	Total Uncertainty

ABSTRACT

Biogas is a renewable energy source that can be adopted as a reliable and sustainable alternative when upgraded. The composition of carbon dioxide in biogas of up to 45% reduces its energy density. Thermal swing adsorption has proven to be a promising technology in the biogas upgrading process, due to its ease of integration with renewable electricity sources and its suitability for water-deficient areas. The experimental study of the biogas upgrading process has been complicated by the dynamic nature of the process and the high sensitivity to operating conditions, such as pressure, temperature, and gas flow rate. To understand the complex interaction between the process parameters, numerical simulation was utilised. There are, however, limited numerical studies evaluating multi-objective optimization of these process parameters. This study assessed the performance of thermal swing adsorption technology, utilising resistive heating, in upgrading biogas produced from the anaerobic digestion of organic waste. Commercial coconut shell-based activated carbon was used as an adsorbent in the experimental cyclic process to capture carbon dioxide. Aspen Adsorption software was used to develop a thermal swing adsorption numerical model. The simulation model was validated using experimental data obtained from a laboratory-scale setup. A good agreement was observed between the simulation and experimental carbon dioxide breakthrough times, with a mean absolute percentage error of 2%. Dynamic adsorption tests were conducted to evaluate the system performance in carbon dioxide capture. The maximum resistive heating regeneration temperature of 60℃ resulted in a peak carbon dioxide concentration of 39% in the waste gas, an energy requirement of 0.1538 kWh per cycle, and an energy efficiency of 87%. This was a good trade-off between adsorbent recovery for subsequent biogas upgrading cycles and system energy efficiency. In the second phase of the study, the adsorbent particle radius, regeneration temperature, and purge-to-feed flow rate ratio were investigated to determine the system's sensitivity. The adsorption and desorption processes were based on methane and carbon dioxide adsorption isotherms, which were fitted to the Langmuir-Freundlich model. The model described the adsorption behaviour on a heterogeneous adsorbent surface, where adsorption sites had different affinities and capacities. Adsorbent particle radius, steam regeneration temperature, and purge-to-feed flow rate ratio range of 1 to 9 mm, 77 to 227℃, and 0.1 to 0.7, respectively, were adopted. Multi-objective numerical optimization of the selected variables was carried out using the Box-Behnken design response surface methodology. The target output responses maximized were the methane purity and recovery. From the analysis of variance, the purge-to-feed flow rate ratio made the highest contribution to both methane purity and recovery, of 92.37% and 99.90%, respectively. While the particle radius had a negligible influence on the methane recovery model, its contribution to the methane purity was significant. The optimal values for maximum methane purity and recovery obtained were 82.12% and 37.21%, respectively, achieved at a particle radius of 9 mm, steam regenerating temperature of 227℃, and a purge-to-feed flow rate ratio of 0.4152. This study offers valuable insights into the design of a thermal swing adsorption biogas upgrading model, as well as the impact of various variables and configurations on the process. The developed model provides practical guidelines for selecting optimal biogas upgrading process parameters to maximize both methane purity and recovery.

CHAPTER ONE

INTRODUCTION

1.1 Background

Projections of global energy demand indicate a growing trend, with primary demand increasing by 2% in 2024, reaching a new high of 592 EJ. A 1% increase in global carbon dioxide(CO_2) emissions to 40.8 $GtCO_2e$, primarily from industrial processes was recorded in 2024 compared to 2023 (Energy Institute, 2025). Fossil fuels occupy a significant share of the energy mix in Africa with oil at 26.27% and natural gas at 7.38% (African Energy Commission, 2024). Renewable energy generation is a reliable alternative due to its environmental sustainability and the continuous ability to replenish itself. In 2023, while fossil fuels accounted for 81.5% of the global primary energy use, renewable energy adoption increased by 0.4% compared to the previous year, accounting for 14.6% of total energy consumption (Energy Institute, 2024). The adoption of renewable energies as the primary energy source aims to mitigate the adverse effects of emissions released into the environment.

Renewable energies originate directly from the sun (such as photoelectric, photochemical, and thermal energy), indirectly from the sun (for example, hydropower, wind, and biomass), or are derived from other natural mechanisms (such as tidal energy and geothermal heat). The growing utilisation of wind and solar energy offers a more environmentally friendly alternative to conventional energy sources. However, these systems are characterised by highly fluctuating and poorly predictable production profiles (Kalpana *et al*., 2023; Wu *et al*., 2023). Hydro, geothermal, and tidal energy sources are location-specific, which hinders their exploitation in some regions (Owusu & Asumadu-Sarkodie, 2016). Biomass energy, on the other hand, is capable of producing a constant base load, in addition to balancing out the supply-demand variations (Schneider *et al*., 2020). Its utilisation is also significantly independent of geographical location and seasons (Pöschl *et al*., 2010). A previous study identified agricultural waste to have a higher environmental efficiency compared to fossil fuel-based energy generation technologies (Anand *et al*., 2021).

Biomass is broadly classified into two categories: organic waste and natural vegetation, as shown in Figure 1.1 (Akula, 2013). Organic waste primarily originates from the byproducts of human and animal activities. They include livestock manure, slaughterhouse waste, kitchen waste, sewage sludge, and industrial organic waste. Most biogas plants use organic wastes due to their fast degradability, in addition to being a waste management solution (Arifan *et al*., 2021; Siddiki *et al*., 2021).

Natural vegetation encompasses naturally occurring plant biomass, including aquatic plants, forestry residues, grasses, and herbaceous plants. The high lignocellulosic content in them necessitates their pretreatment to make them more accessible to microorganisms during anaerobic digestion (Czubaszek *et al*., 2023). The use of agricultural plant residues as a co-substrate to organic waste in anaerobic digestion has resulted in increased biogas production (Frankowski & Czekała, 2023).

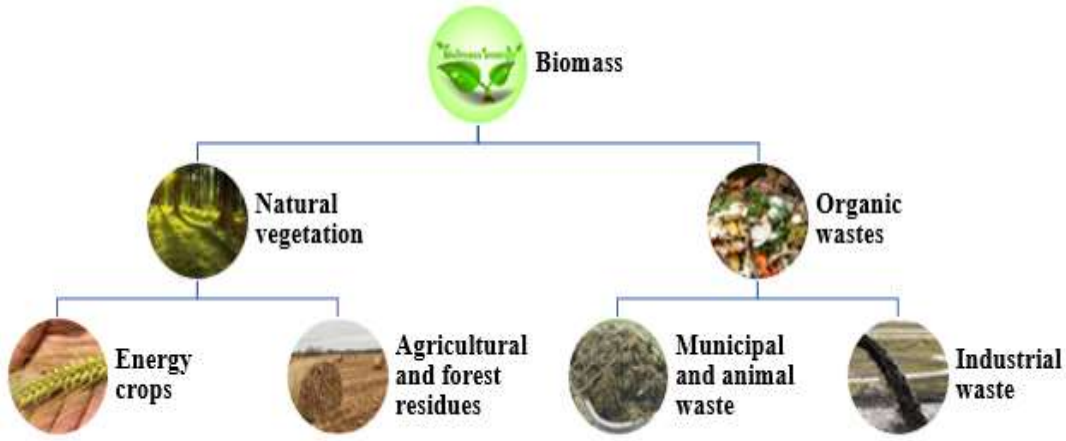

Figure 1.1: Classification of Biomass

Source: (Akula, 2013)

Energy from biomass can be obtained through gasification, pyrolysis, combustion, or anaerobic digestion. Biomass combustion is the process of burning organic materials to generate heat. The chemical energy stored in biomass is released as heat through an exothermic reaction with oxygen (Briones-Hidrovo *et al.*, 2021). The gasification process involves converting carbonaceous material at high temperatures (>700°C)

using a controlled amount of oxygen to produce syngas (Tezer *et al.*, 2022). The pyrolysis process is similar to gasification but operates with almost no oxygen, at temperatures ranging from 250℃ to 600℃ (Aboelela *et al.*, 2023). Anaerobic digestion is a biological process in which microorganisms break down organic matter in the absence of oxygen to produce biogas.

Biomass combustion processes have a low thermal efficiency of 20% to 30%, and a higher number of pollutants such as particulate matter, nitrogen oxides, sulphur oxides, and carbon monoxide, attributed to incomplete combustion (Zhai *et al*., 2021). Differences related to the heating values of biogas (20 - 26 MJ/m^3) and syngas (10 - 18 MJ/m^3) suggest that the use of biogas is preferred over syngas to achieve high energy production (Solarte-Toro *et al*., 2018). Furthermore, syngas production has a complex and energy-intensive production process (Centi & Perathoner, 2020).

1.2 Biogas Production and Utilization

Biogas, generated from anaerobic digestion of biodegradable organic waste by bacteria, offers more excellent prospects as an alternative energy source (Karuppiah & Azariah, 2019). Given the high population density in urban areas, most biogas plants utilize organic waste, while natural vegetation is more common in rural areas. The main constituents of biogas are methane (CH_4) (50 to 75% (v/v)) and carbon dioxide (20 to 45% (v/v)), with water vapour at given temperatures. Other important minor constituents include oxygen, nitrogen, hydrogen sulphide, siloxanes, and ammonia (DOSH, 2016; Sun *et al*., 2015). Furthermore, the digestate, a by-product of anaerobic digestion, is used as a fertilizer to enhance crop productivity.

The complete anaerobic digestion process consists of four main stages: hydrolysis, acidogenesis, acetogenesis, and methanogenesis, as illustrated in Figure 1.2. During hydrolysis, complex molecules are broken down into soluble monomers such as glucose and fructose. Enzymes secreted by bacteria, including cellulase, protease, and lipase, act as catalysts in this process. Acidogenesis refers to the stage during which acid-forming bacteria convert the solubilised monomers produced during hydrolysis into simple organic compounds, primarily short-chain volatile fatty acids, ketones, and

alcohols. The specific concentrations of products formed at this stage vary depending on the type of bacteria, temperature, and pH values.

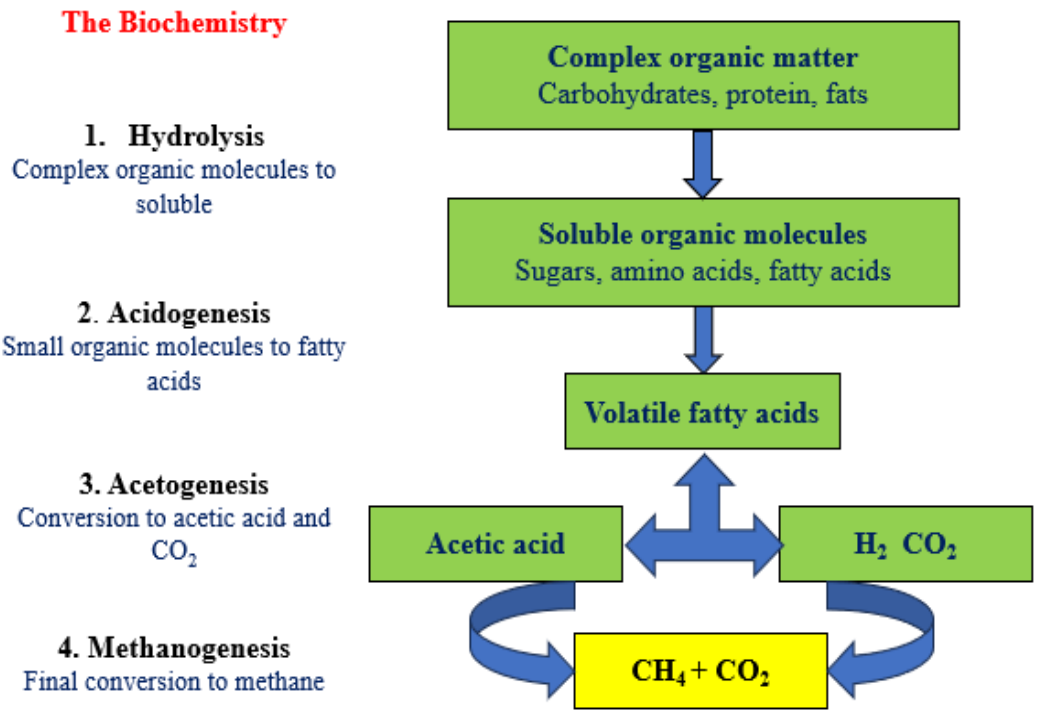

Figure 1.2: Anaerobic Digestion Biochemical Conversion Pathways

Source: (Fatma A. Alfarjani, 2012)

The acetogenesis process involves converting the fatty acids into hydrogen and acetic acid by acetogenic bacteria through oxidation. The acetogenic bacteria require a low hydrogen partial pressure to conserve energy for growth. Methanogenic bacteria involved in methanogenesis facilitates the production of methane in two ways. This can occur through the cleavage of acetic acid molecules to generate carbon dioxide and methane, or by the reduction of carbon dioxide using hydrogen as an electron donor, resulting in the production of methane and carbon dioxide (Ostrem *et al*., 2004).

Biogas is a viable energy carrier and an enabler of sustainable development, with applications in various sectors. The two main utilisation pathways for biogas are electricity and heat generation. The power generated by using biogas in internal combustion engines or gas turbines is fed into the grid. When used for heat generation,

biogas is combusted directly in a boiler, and the heat is mainly used to heat the digesters, buildings, or dry agricultural products. Combined heat and power generation, however, represents a better approach, achieving energy efficiency of up to 90% (Hakawati *et al*., 2017). When upgraded to methane, it is primarily used as a natural gas substitute (Mertins & Wawer, 2022).

Table 1.1: Properties of Biogas, Biomethane, and Natural Gas (DOSH, 2016)

Gas composition	Biogas	Biomethane	Natural gas
Methane	50-75%	94-99.9%	93-98%
Carbon dioxide	20-45%	0.1-4%	1%
Nitrogen	<2%	< 3%	1%
Oxygen	<2%	< 1%	-
Hydrogen	< 1%	Traces	-
Hydrogen sulphide	20-20,000 ppm	<10 ppm	-
Ammonia	Traces	Traces	-
Ethane	-	-	< 3%
Propane	-	-	< 2%
Siloxane	Traces	-	-
Water	2-7%	-	-

Table 1.1 compares the composition of biogas, biomethane, and natural gas, highlighting the importance of cleaning and upgrading biogas to make it a viable substitute for natural gas. The presence of non-combustible gases in biogas varies depending on the different organic materials used in the digestate and operating conditions. Biogas cleaning involves the removal of minor constituents, primarily hydrogen sulphide and water vapor (5 - 10%). This is necessary, as they cause corrosion to mechanical appliances such as generators, metallic equipment like valves, engines, and pipes, as well as biogas storage facilities, thereby reducing their lifespan. Furthermore, the combustion of hydrogen sulphide produces sulphur oxide, a major air pollutant. Biogas upgrading, on the other hand, is the process of increasing the calorific value by concentrating methane to enhance energy density and, consequently, its quality (Adnan *et al*., 2019).

Various biogas upgrading techniques exist, including membrane separation, cryogenic separation, water scrubbing, chemical absorption, adsorption, and, most recently, biological reduction. They rely on the physical, chemical, and thermodynamic

variations of the gas properties to separate the gas constituents of biogas (Mutunga *et al*., 2022). The technologies differ in operational requirements and costs, efficiency, and energy needs. Consequently, the choice of technology relies on factors such as biogas composition, production scale, and end-user requirements. Despite advancements, biogas upgrading still encounters challenges, including variability in biogas composition, energy-intensive processes, initial and operational cost constraints, and a high dependence on process parameters that influence the stability of these systems (Golmakani *et al*., 2022).

Among these upgrading technologies, adsorption has emerged as a promising method due to its ability to selectively separate carbon dioxide from methane using solid adsorbents such as activated carbon, zeolites, and silica gels (Gbangbo *et al*., 2023). Within this category of technologies, thermal swing adsorption (TSA) has emerged as a promising approach, as it exploits the temperature-dependent adsorption characteristics of carbon dioxide on adsorbents. In TSA-based biogas upgrading, carbon dioxide is preferentially adsorbed at relatively low temperatures. Regeneration of the adsorbent is achieved by increasing the temperature to desorb the retained species, thereby producing a methane-enriched gas stream. The technique offers several advantages, including high carbon dioxide selectivity, reusability of adsorbents, and comparatively lower energy requirements than other conventional upgrading methods. While previous studies have examined the influence of key operating parameters, such as temperature, pressure, and gas flow rate, on adsorption performance, challenges persist in optimizing these variables simultaneously to enhance selectivity and overall system efficiency.

To address the interactions and trade-offs between operating parameters in the thermal swing adsorption process, multi-objective optimization can be effectively performed using the Response Surface Methodology (RSM). This approach provides a systematic statistical framework for understanding how factors such as regeneration temperature, adsorbent properties, and gas flow conditions collectively influence performance indicators such as methane purity and recovery. Using empirical models such as RSM allows these correlations to be evaluated using fewer experiments and without compromising the accuracy. The Box-Behnken design (BBD) in RSM is advantageous

as it reduces the number of experimental runs while considering the nonlinear interaction between the variables. This makes it an ideal tool in evaluating optimal operating conditions in dynamic processes such as the biogas upgrading process.

1.3 Status of Biogas as an Energy Source in Kenya

The Kenyan Government in collaboration with the private sector has continued to encourage the uptake of biogas as an energy source, primarily at the household level. The use of biogas in the country for cooking is projected to reach 0.8% and 0.07% for electricity generation of the renewable energy mix by 20230 (Bioenergy Strategy 2020-2027, 2020). Some of the challenges facing the development and uptake of biogas in the country include the acceptance problem where recharging of the systems is seen as dirt, inadequate support post installation, and limited technology awareness (Robinson *et al*., 2023).

Kenya is estimated to have 21,000 installed biogas digesters distributed across various counties (Bioenergy Strategy 2020-2027, 2020). Fixed-dome, floating-drum, and plastic tube digesters are the common technologies that have been adopted. Fixed-dome digesters are the most common being more durable and efficient. The scale of the biogas digesters varies depending on the energy need, available resources and economic conditions. Small-scale systems (1 - 10 m^3) utilizing livestock manure and kitchen waste are more common for household use to provide cooking and lighting energy. Institution systems such as schools and hospitals have medium-scale systems (10 - 50 m^3) using animal waste and food residues for large-scale cooking. Agro-processing plants and large farms have commercial digesters (50 - 500 m^3) using agricultural and organic waste for electricity generation (Mutahi *et al*., 2025). Simbi Roses of Ereka Holding Ltd. and P.J. Dave Flower Farms Ltd. reported biogas production from flower waste for electricity generation. One ton of flower waste produced 60 - 80 m^3 of biogas and consequently one m^3 of biogas produced 0.94 kWh of power (Chipo Mukonza, 2025).

Several studies have been carried out regarding biogas upgrading to enhance the calorific value and usability of biogas. They explored the potential of locally available material in developing sustainable solutions for the local context. A pilot-scale study

was conducted at Jomo Kenyatta University of Agriculture and Technology (JKUAT) to evaluate the performance of various low-cost adsorbents (Odero *et al*., 2025). Red soil, charcoal, clay soil, steel wool, iron shavings and wood ash are some of the adsorbents explored to increase the methane concentration in biogas. The highest methane concentration of 69.83% from an initial concentration of 58.47% was attained by combining various adsorbent. Another study explored the potential of combining adsorbents and water scrubbing in biogas upgrading (Njogu *et al*., 2015). This increased the methane concentration in biogas from 49 - 53% to 70 - 76%. While the methane concentrations were on the lower threshold, the study highlighted the potential of affordable local materials in biogas upgrading.

The utilization of geological materials abundant in Kenya such as the natural zeolite rocks as an adsorbent for upgrading biogas generated from cow dung and market waste has also been evaluated (Mbugua, 2021). The adsorbent reduced the levels of carbon dioxide and hydrogen sulphide in the biogas by 70% and 35% respectively. Another study optimized the biogas upgrading process parameters for combined adsorption and water scrubbing processes using the response surface methodology (Mugagga *et al*., 2023). Operating pressure, adsorbent height and liquid flow rate are some of the parameters evaluated. The optimal methane concentration of 84.71% was attained for configurations of 14 kPa gas pressure, 22.86 cm adsorbent height and 4.2 liters per minute water flow rate.

The country has a great potential in exploiting biogas as an energy source for both domestic and commercial use. The growing research interest in biogas upgrading with emphasis on low-cost and locally sourced materials is expected to enhance its sustainability. However, many conventional biogas upgrading techniques are energy-intensive and limiting for implementation in decentralized and rural settings. In addition, most studies do not evaluate the cyclic nature of the upgrading process.

1.4 Problem Statement

Biogas is a product of anaerobic digestion and is a feasible alternative source of energy. However, the high composition of carbon dioxide significantly reduces its energy density. Thermal swing adsorption is an energy-efficient technique for removing

carbon dioxide from gas mixtures. Its ease of integration with other renewable energy sources makes it particularly suitable for biogas upgrading. However, its application in this context has not been fully explored.

The performance of biogas upgrading using the thermal swing adsorption technique has primarily been evaluated using synthetically manufactured biogas, a mixture of pure methane and carbon dioxide gases, with limited applicability to biogas obtained from anaerobic digestion. This is crucial for establishing the influence of minor gas constituents in the biogas upgrading process. Furthermore, there is limited literature indicating the correlation between the system's process parameters and optimal configurations, given the complexity in their interrelation.

This study aimed to evaluate the relation between the various process variables, including adsorbent particle radius, purge-to-feed flow rate ratio, and regeneration temperature, to establish optimal values for effective performance. The use of numerical simulation tools was adopted due to their ability to predict conditions that would be difficult to replicate in experiments. Methane purity and recovery are crucial indicators of the system's performance. Increasing the methane flow rate during purging for bed regeneration enhances methane purity at the expense of methane recovery. This necessitated a multi-objective optimization approach to establish an optimal trade-off between methane purity and recovery.

1.5 Study Objectives

The main objective of this study was to numerically optimize the thermal swing adsorption process for biogas upgrading, using experimental data to inform and validate the model. To accomplish the main objective, the following specific objectives were pursued:

i. To develop and validate a numerical model for upgrading biogas obtained from anaerobic digestion.
ii. To evaluate the influence of adsorbent physicochemical properties on the biogas upgrading process.

iii. To investigate the influence of purge-to-feed flow rate ratio process parameter on the biogas upgrading process.
iv. To optimize the methane purity and recovery across the biogas upgrading system.

1.6 Justification

The increasing adoption of renewable energy sources, such as biogas, is essential for mitigating the environmental impacts of non-renewable energy, including greenhouse gas emissions and climate change. Biogas is a reliable energy source because it is self-replenishing, derived from naturally available organic materials, and can be produced continuously as long as waste feedstock is available, with minimal dependence on weather conditions. Moreover, promoting biogas technology supports the achievement of global Sustainable Development Goals (SDGs), particularly SDG 7 on affordable and clean energy and SDG 13 on climate action.

The adoption of biogas as an energy source plays a significant role in sustainable waste management. Anaerobic digestion converts organic waste materials such as agricultural residues, food waste, and animal manure into biogas through microbial processes, while the remaining digestate can be used as a soil amendment. Furthermore, many adsorbents used in biogas upgrading are derived from waste products, including coconut shells, maize cobs, and rice husks, helping to reduce harmful emissions that would otherwise result from uncontrolled decomposition.

In the long term, the adoption of biogas as an energy source can provide substantial health benefits by promoting proper management of organic waste and improving sanitation. By replacing traditional biomass and kerosene for cooking, biogas significantly reduces indoor air pollution, which in turn lowers the incidence of respiratory illnesses and creates healthier living environments in rural households. Beyond these health impacts, this transition also fosters cleaner, safer, and more dignified daily living conditions for communities.

In addition, the deployment of biogas upgrading technologies offers opportunities for carbon mitigation and carbon credit generation. By capturing and utilizing methane

from organic waste streams, this prevents the uncontrolled release of potent greenhouse gas into the atmosphere while reducing reliance on fossil fuels. The measurable reduction in greenhouse gas emissions can be quantified and verified under international carbon accounting standards, enabling project developers to earn carbon credits which enhance economic viability. This not only incentivizes the adoption of renewable energy technologies but also strengthens environmental and financial cases for sustainable biogas solutions, particularly in developing counties where energy access and climate mitigation are critical priorities.

Developing a compact, user-friendly biogas upgrading unit based on locally available resources is essential to making biogas a sustainable energy option for marginalized communities in Kenya. By improving biogas quality and reliability, such systems can broaden biogas applications, from cooking and heating to electricity generation. Wider adoption would not only reduce dependence on costly fossil fuels but also contribute to stimulate local economic activities, support small enterprises, and create jobs. Ultimately, this strengthens rural value chains and enhances household livelihoods.

In this study, a numerical model for biogas upgrading using biogas derived from anaerobic digestion was developed and optimized. The model provides a practical approach to overcoming the challenges of performing extensive experimental measurements for assessing the effects of various process parameters on system performance. Moreover, the optimized model allows for the identification of optimal trade-offs between methane purity and recovery under different operating conditions, providing valuable insights for process design and operation.

1.7 Thesis Structure

This thesis is organised in five themed chapters. The present chapter is **Chapter One**. Here, various renewable energy sources are introduced, and the classification of biomass used in biogas production is discussed. It also outlines the problem statement, states the research objectives, and justifies the significance of the research. In **Chapter Two**, a comprehensive literature review on separation and sorption biogas upgrading techniques, along with related numerical and experimental studies, is presented. Furthermore, the identified research gaps from previous studies are presented in this

chapter. **Chapter Three** focuses on the materials and methods. It highlights the material characterization techniques employed, model development in Aspen Adsorption, and the design and fabrication of the experimental setup. In **Chapter Four**, the results of tests on experimental and numerical models are presented and discussed. The results include experimental measurements, model validation, numerical modelling, and multi-objective optimization findings. **Chapter Five** presents key conclusions drawn from the research findings, while also outlining recommendations that provide opportunities for future research. Supplementary information is presented in the appendices.

CHAPTER TWO

LITERATURE REVIEW

2.1 Overview

In this chapter, various carbon dioxide capture technologies are discussed and reviewed in detail. The application of these concepts and theories in biogas upgrading is analyzed, and inconsistencies are identified. In addition, the numerical and experimental findings of various researchers on employing the thermal regeneration technique for biogas upgrading have been evaluated, and research gaps identified.

2.2 Biogas Upgrading Technologies

Several biogas upgrading approaches have been studied and implemented at both laboratory and industrial scales to promote biogas energy utilization. They are categorized based on the point of contaminant removal during the biogas production process as: during digestion and post-digestion (Mutunga *et al*., 2022). A different classification based on the contaminant being removed has also been adopted, as it represents process evolution with minimal external influence (Werkneh, 2022). The latter is adopted for this work, with a specific focus on carbon dioxide removal. Being the highest non-combustible gas by composition, and significantly affecting the average calorific value of biogas, has greatly contributed to the attention it has received (Rauch & Haloua, 2018).

Biogas upgrading techniques rely on physical, chemical, and thermodynamic variations in the properties of the gas during the separation of its components. Figure 2.1 illustrates the classification of primary biogas upgrading techniques into sorption (absorption and adsorption) and separation (membrane and cryogenic) methods (Adnan *et al*., 2019). Biological reduction processes, a technology that has recently been proposed, are also discussed in this review, although they are currently in the research and development, as well as pilot stages. The governing principles and current status of these technologies are presented, along with a more in-depth analysis of the sorption processes.

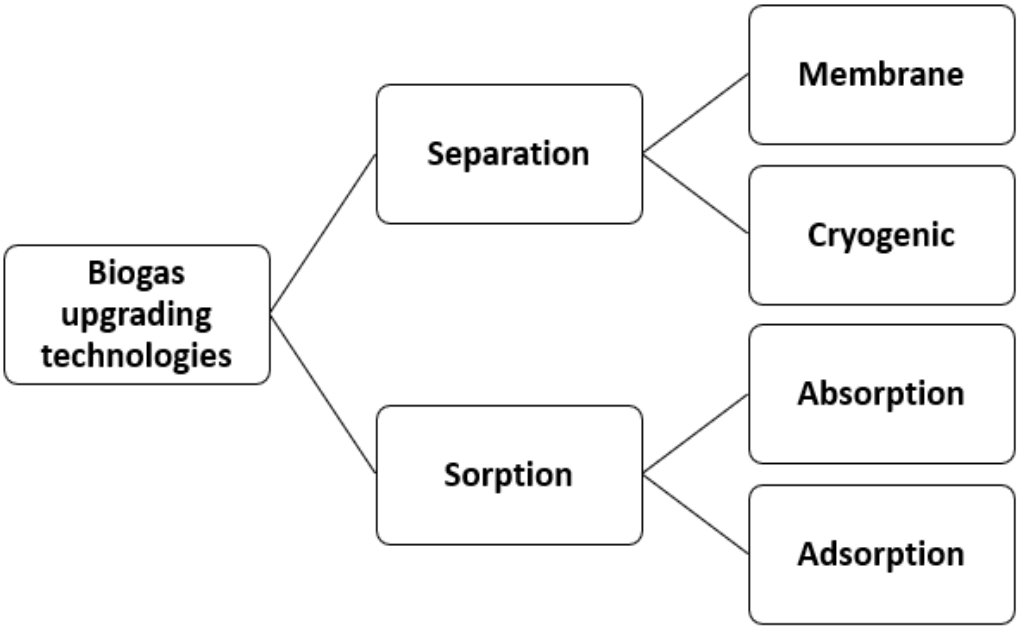

Figure 2.1: Technologies for Biogas Upgrading

Source: (Adnan et al., 2019)

2.2.1 Membrane Separation

Membrane technology for biogas upgrading has been strongly adopted, given that it is the core technology used in the natural gas industry to remove contaminants, with a market share of up to 10% (Baena-Moreno *et al*., 2020). Gas separation is based on the selective permeability properties of membrane materials, including polymeric materials (such as polyimide, polysulfone, and polyetherimide), inorganic/non-polymeric materials (zeolites, silica, and carbon molecular sieves), and composites of these. While carbon molecular sieves have demonstrated high permeability and selectivity, their brittle nature makes it challenging to scale up for industrial applications. Polymeric membranes are predominantly used due to their lower cost, high-pressure stability, and facile module fabrication (Gkotsis *et al*., 2023; Haider *et al*., 2016).

The ideal membrane for biogas upgrading should exhibit a high permeability difference between carbon dioxide and methane, and be capable of withstanding the high operating pressures of 5 to 20 bar. Figure 2.2 illustrates the process of biogas

upgrading using membrane technology (Baena-Moreno *et al*., 2020). Gas permeation occurs in two steps: sorption and diffusion. The sorption process involves the interaction between gas molecules and the membrane material, which depends on their chemical affinity. Subsequently, gas diffusion occurs depending on the molecular size of the gas. Carbon dioxide permeates through the membrane, with a kinetic diameter of 0.33 nm, while methane is retained in the mainstream flow channel, which has a larger kinetic diameter of 0.38 nm.

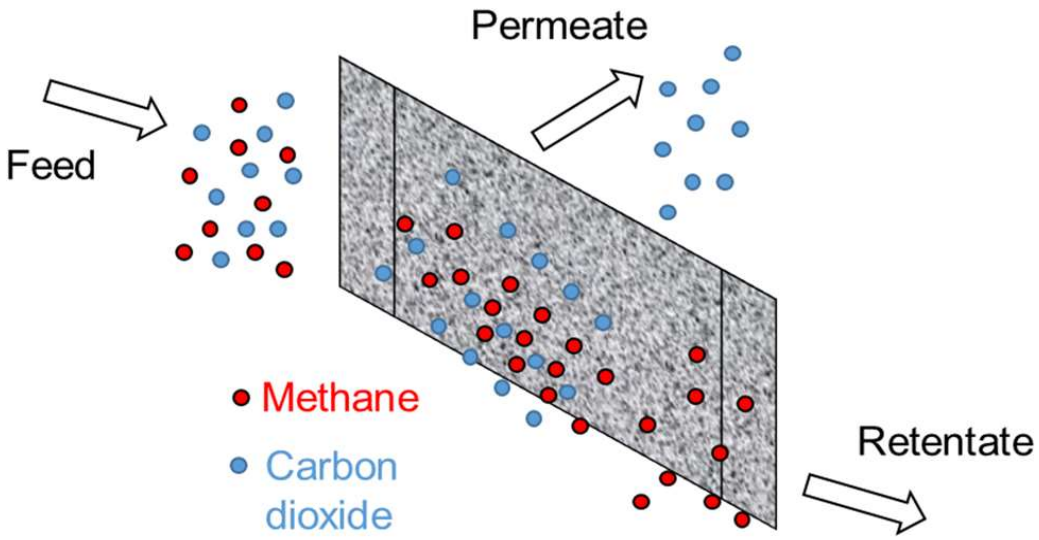

Figure 2.2: Membrane Configuration Scheme

Source: (X. Y. Chen et al., 2015)

The advantages associated with this technique include the ability to scale down the process without significant efficiency losses, in addition to a minimal demand for water and chemicals (Bauer *et al*., 2013). It is also an environmentally friendly technique with moderate energy consumption. Current methane purity achieved using this technique ranges between 92% and 96%, with <1% methane loss. This has been enhanced by using several layers of membranes with recirculation of the gas across the system up to optimal conditions (Gkotsis *et al*., 2023; Scholz, 2013).

Membrane separation technique, however, requires pre-treatment of the biogas as elements such as moisture contribute to the deterioration of the membrane, necessitating replacement. The frequent membrane replacements required are also a

drawback linked to this technique. The performance of this technology depends significantly on the system configurations implemented, including the number of pressure stages and loops utilized. Depending on the permeability of the membrane, this technique could also affect the flow characteristics of the biogas. To minimize methane loss during the upgrading process, compression of biogas is inevitable, which is associated with increased energy demands (Haider *et al*., 2016; Iovane *et al*., 2014).

The influence of methane concentration in the range of 50% to 80% was studied using a three-stage membrane of 0.001 μm in a biogas upgrading system, at a constant flow rate of 35 Nm^3/h (Buivydas *et al*., 2024). This was evaluated through an experimental configuration involving biogas compression to a pressure of 16 bar before being passed across the membrane. Increasing the methane concentration in the biogas resulted in a 19.3% increase in methane slip with the off-gas. This indicates that the membrane's selectivity at high methane concentrations is low, and releasing the off-gas into the atmosphere would have a negative environmental impact.

One approach to reducing methane concentration in the off-gas is to recirculate the gas. The influence of membrane area, selectivity, and permeability in upgrading biogas with a 60% methane concentration has been evaluated (Zito *et al*., 2022). Increasing the number of recirculation steps reduced the required membrane area and increased the overall purity of the system. Increasing the number of recycling steps from 2 to 10 across the membrane significantly reduced the membrane area from 580 to 200 m^2 required to attain a methane purity concentration of 98% and above. This, however, resulted in an increased methane loss on the permeate side, attributed to a reduction in the carbon dioxide driving force, and consequently, a lower flux through the membrane.

2.2.2 Cryogenic Technology

The contents of biogas liquefy under different temperature and pressure conditions, making it possible to separate them by compression and cooling. Figure 2.3 illustrates an overview of the biogas upgrading process employing the cryogenic technique. The biogas is first cleaned to remove impurities such as hydrogen sulphide, siloxanes, and particulates. This protects downstream cryogenic equipment and ensures adequate gas

separation. The biogas is then compressed to a pressure ranging between 5 and 10 bars before being cooled in stages using heat exchangers to gradually lower its temperature. At cryogenic temperatures of approximately $-78℃$, carbon dioxide condenses into a liquid or solid form, while methane remains in the gaseous state because of its boiling point of $-161.5℃$ that is much lower. The solid or liquid carbon dioxide is then separated from the high-purity methane (Naquash *et al*., 2022).

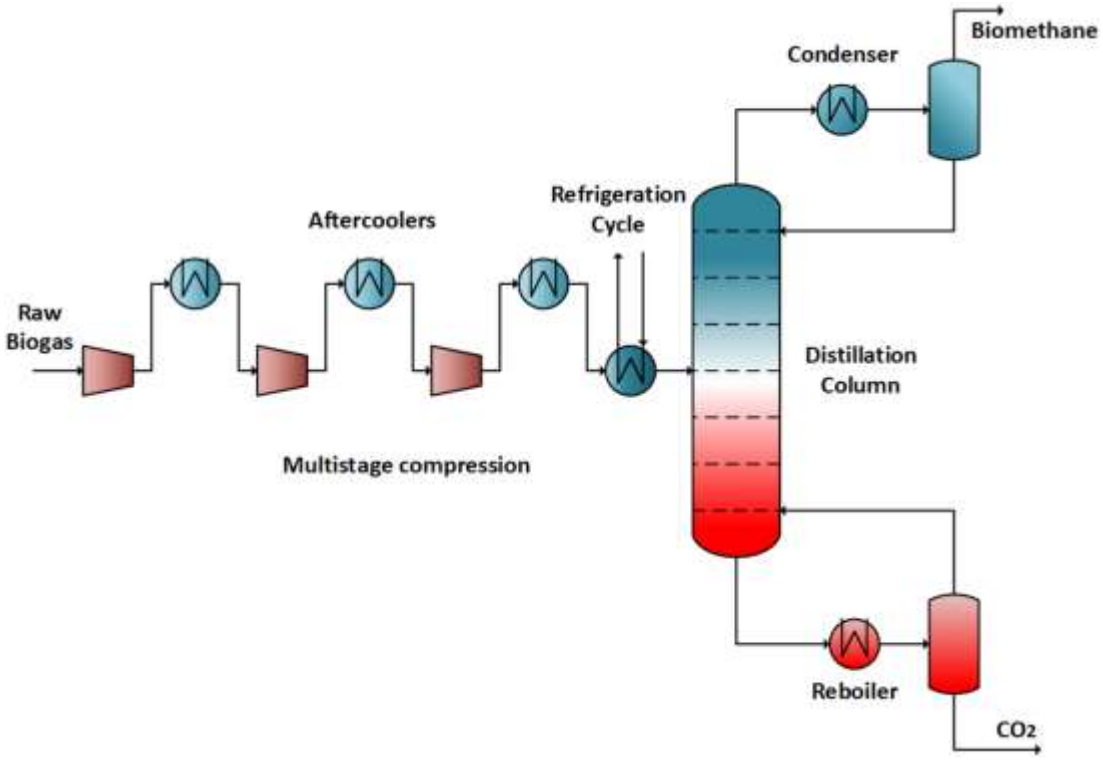

Figure 2.3: Cryogenic Distillation Process for Biogas Upgrading

Source: (Naquash et al., 2022)

The cryogenic technology can be categorized as either anti-sublimation technology or distillation-based technology. In the anti-sublimation process, carbon dioxide is directly converted from the vapor phase to the solid phase, bypassing the liquid phase. Methane is then extracted in the vapor phase and liquefied for end use. For the distillation process, both methane and carbon dioxide are separated and extracted in a liquefied form (Naeiji *et al*., 2022).

Process parameters are crucial to the biogas upgrading process employing the cryogenic technique. The biogas flow rate across the cryogenic system was identified to influence the methane composition at the outlet. A recent study by Naeiji *et al.* (Naeiji *et al*., 2022) noted that increasing the biogas flow rate from 22 to 27 kg.mol/h reduced the methane composition from 99% to 94.5%, assuming the other variables were held constant. This was primarily attributed to a decrease in residence time in the cryogenic system, which in turn decreased the efficiency of the separation process. Another study by Haddad *et al.* (Haddad *et al*., 2021) evaluated the influence of carbon dioxide concentration in biogas on its targeted removal from biogas by frost deposition. For a fixed biomethane concentration of 97.5% at the outlet, decreasing the carbon dioxide concentration of biogas from 35% to 20% required a longer operating time to achieve the set methane purity. Further research, evaluating several variables simultaneously, is needed to establish their interaction and overall influence on system performance.

The cryogenic purification technique has achieved a high methane purity of above 97%, with less than 2% methane loss. It is also environmentally friendly as it does not utilize chemicals that would negatively affect the ecosystem upon disposal. It, however, requires huge capital investment and operation costs, has complex operation configurations, and a high energy demand (Adnan *et al*., 2019).

2.2.3 Biological Reduction

Recently, carbon dioxide removal using biological approaches has been proposed. Biological reduction of carbon dioxide from biogas can be categorized based on the point of occurrence as either during or post-anaerobic digestion. The methanation process, as represented in Equation (2.1), entails the valorisation of carbon dioxide by capturing and converting it into methane through a reaction with hydrogen (Rainone *et al*., 2023).

$$4H_2 + CO_2 \rightarrow CH_4 + 2H_2O \qquad 2.1$$

Hydrogen is produced by splitting water into its elemental constituents using renewable electricity through the process of electrolysis, as shown in Equation (2.2). It is then injected into the digester and stirred to facilitate the reaction process.

$$2H_2O \rightarrow 2H_2 + O_2 \qquad 2.2$$

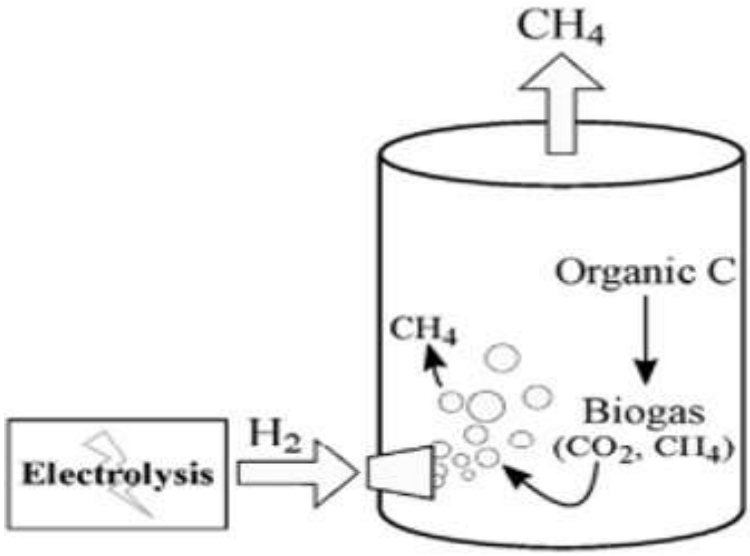

Figure 2.4: In-situ Biomethanation Process

Source: (Rainone et al., 2023)

The in-situ methanation process is considered complex, as it is essential that the added hydrogen does not interfere with the anaerobic process. A recent study utilized a venturi-based hydrogen ejector to evaluate the performance of the in-situ methanation process (Jensen *et al*., 2021). A maximum hydrogen conversion efficiency of 49% was attained, which increased with increased hydrogen injection and recirculation within the system. The hydrogen conversion process was primarily limited by low gas-liquid mass transfer, with up to 90% of the injected hydrogen leaving the biogas reactor unconverted.

The feasibility of ex-situ biological methanation process post anaerobic digestion to upgrade biogas to synthetic natural gas quality has been assessed (Fenske *et al*., 2023). It was established that maintaining a constant sulphur concentration during the process was crucial to prevent dilution by the product water. An optimal hydrogen-to-carbon

dioxide ratio of 3.9 enabled the sustainable conversion of carbon dioxide to methane. Favourable growth conditions for the hydrogenotrophic methanogens enabled attainment of a mean methane concentration of 98.2%.

The implementation of this technology during the anaerobic process makes it an environmentally friendly and cost-effective approach for biogas upgrading. This makes carbon dioxide bioconversion a viable alternative post-anaerobic digestion. However, its drawbacks include the high flammability of hydrogen, anaerobic conditions are required for biogas generation, and the negative impact that excessive mixing could have on biogas production and the design of the digester (Bardi *et al*., 2023). The technology is currently under research, with most prototypes being laboratory-scale.

2.2.4 Absorption Technique

The absorption technique is the most common, well-developed, and widely implemented approach in biogas upgrading, accounting for approximately 63% of the global market (Thrän *et al*., 2014). Depending on the governing principles, absorption can be classified into physical and chemical processes. Physical absorption is dependent on the physical properties of both the gas and the liquid, such as temperature, pressure, and solubility. Chemical absorption is an irreversible process and commonly uses amines and alkali solutions as the absorbent. It has a preference over physical absorption since carbon dioxide is more soluble in polyethylene glycol than in water. For the same upgrading capacity, the flow of the liquid phase can be lower, resulting in a smaller plant (Anneli & Arthur, 2014).

Figure 2.5 presents a schematic diagram of the biogas upgrading technique using the absorption technique. Biogas is injected at high pressures, ranging from 10 to 20 bars, through the bottom of the absorption column, with the absorbent flowing from the top. Packing material is filled in the column in an arbitrary pattern to increase contact time and surface area for mass transfer. The counterflow of the absorbent liquid and biogas has been identified to enhance the rate of mass transfer compared to the effect resulting from the use of packing material in the column to improve the surface area (Nayeem

et al., 2023). Furthermore, the counterflow configuration reduces the required compression work lowering the overall energy consumption.

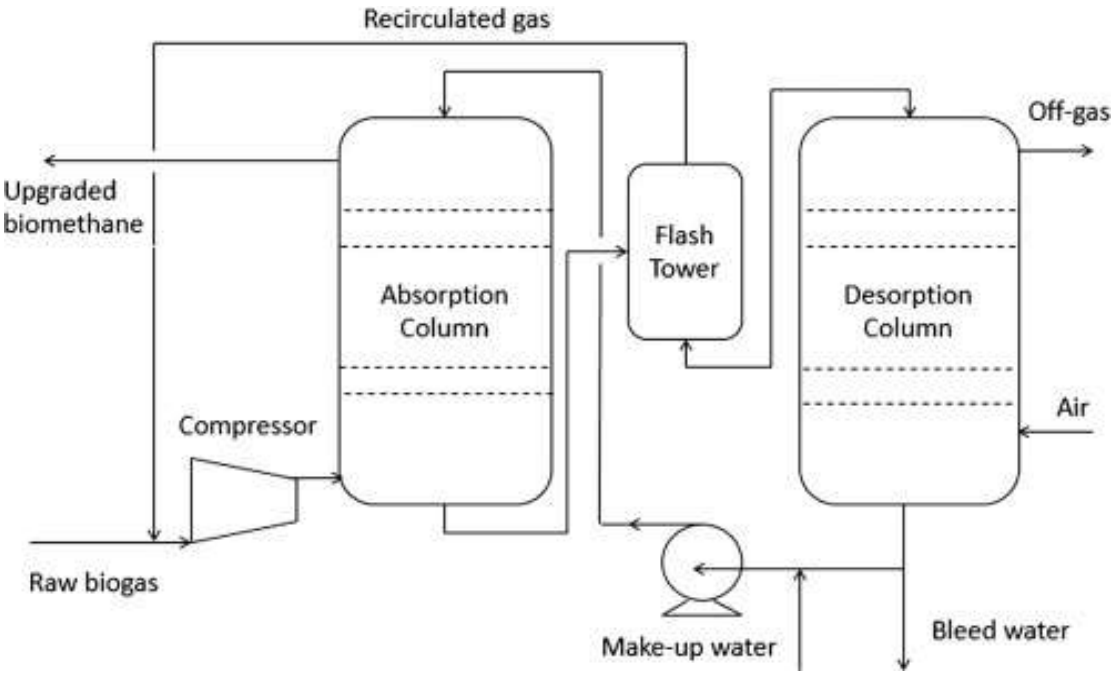

Figure 2.5: Biogas Upgrading via Water Scrubbing

Source: (Nayeem et al., 2023)

The absorbent liquid is regenerated using air in the desorption column to separate it from the absorbed carbon dioxide, before being recirculated back to the absorption column. The flash tower enables a partial reduction in pressure before the desorption process. The off-gas is primarily composed of carbon dioxide that has been absorbed in the absorbent liquid.

In absorption systems, regeneration is achieved by reversing the mass transfer driving force through changes in temperature, pressure, or solvent composition. Thermal regeneration is the most widely used approach in absorption, particularly in chemical absorption systems such as amine-based carbon dioxide removal (Kalsum, 2025). The rich solvent is heated in a regeneration column to break the chemical bonds, which reduces the gas solubility and releases the absorbed gas. Physical absorption systems such as water scrubbing, rely on pressure reduction or moderate heating for regeneration (Herdem *et al*., 2024). They however, exhibit lower energy demand

compared to chemical absorption but are characterized by lower regeneration completeness.

The influence of operating and physicochemical parameters on the performance of the high-pressure water scrubbing absorption technique for biogas upgrading has been studied (Wantz *et al*., 2022). While the packing material and liquid-to-gas ratio influenced the mass transfer kinetics, other variables, including pressure and temperature, affected the purity and recovery of methane. The water flow rate regeneration variable had the highest influence on the process. Desorption carried out at 0.1 bar yielded a methane purity of 99%, compared to desorption at 1 bar, which yielded a methane purity of 90%.

The effect of solution temperature and regeneration temperature variables on the biogas upgrading process, employing the chemical absorption technique, has also been evaluated (Augelletti *et al*., 2020). Increasing the solution temperature from 25℃ to 45℃ increased the carbon dioxide concentration in the outlet stream by 5%. This was attributed to the increased mass transfer rate from gas to liquid and reduced solution viscosity. Similarly, the regeneration process was favored by the high temperatures.

The absorption technique can achieve a very high methane purity of up to 99% while ensuring minimal methane loss of less than 2%. However, it has a high energy demand for compressor and pump operation, drying the methane upon upgrading, and regeneration of the absorbent. The high installation cost further limits its application in small-scale setups.

2.2.5 Adsorption Technique

The adsorption process is a mass transfer phenomenon where a molecule of a chemical species in the gas or liquid phase binds to the surface of a porous solid with which it comes into contact, due to the presence of attractive forces generated at the solid-fluid interface (Rainone *et al*., 2023). The fluid phase species is referred to as the adsorbate, while the solid phase species is known as the adsorbent. Figure 2.6 illustrates the adsorption mass transfer process. Depending on the nature of the forces involved in the attraction, the adsorption process can be categorized as either physisorption or

chemisorption. For a physisorption process, the contaminant is retained on the adsorbent through weak van der Waals forces, characterized by low binding energy. On the other hand, the chemisorption process involves interactions equivalent to either covalent or ionic chemical bonds, resulting in the dissociation of molecules.

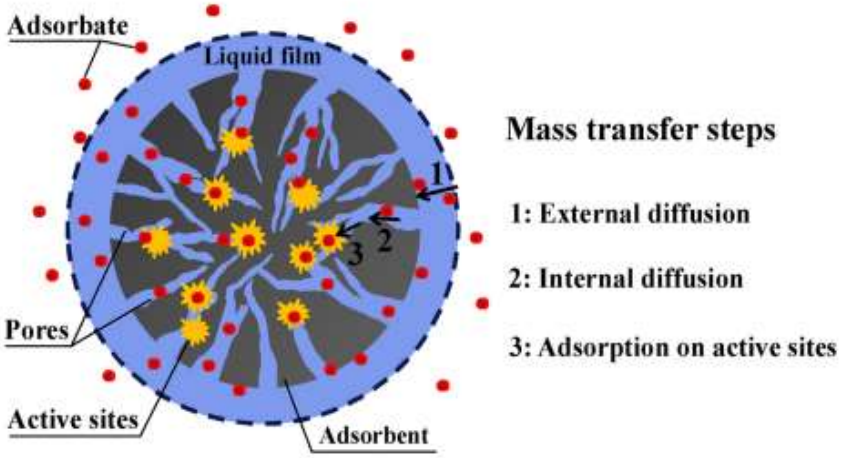

Figure 2.6: Adsorption Mass Transfer Process

Source: (Wang & Guo, 2020)

In the gas separation process, adsorption isotherms play a crucial role in determining the properties of the adsorbent. They are described as experimental relationships between the mass of the adsorbate per unit mass of the adsorbent and the partial pressure of the adsorbate, at fixed temperature and equilibrium conditions (Raganati *et al*., 2020). These properties provide insights into the suitability of using various materials as adsorbents. Figure 2.7 illustrates the classification of adsorption isotherms based on their concavity. Favourable isotherms should have a concave down shape, as they represent high adsorption capacity even at low partial pressures. Adsorption isotherms with exponential growth curve are considered unfavourable as they are characterized with a slow initial growth (Al-Ghouti & Da'ana, 2020).

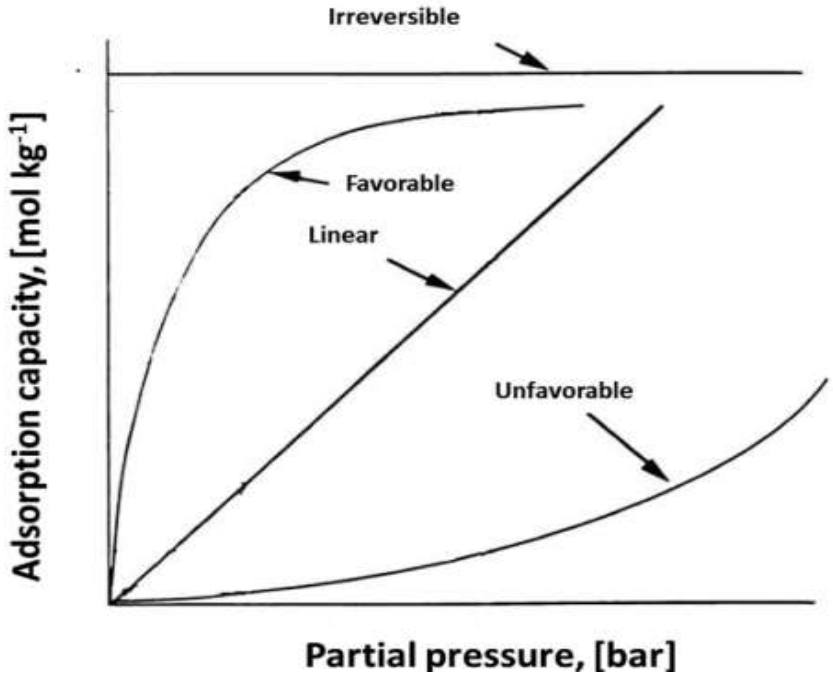

Figure 2.7: Classification of Adsorption Isotherms

Source: (Rainone et al., 2023)

2.3 Adsorbent Selection

The choice of adsorbent material in an adsorption process is crucial, as its properties significantly impact the performance of the gas separation process. In biogas upgrading, it is essential that the adsorbent material has a higher affinity and selectivity towards carbon dioxide compared to methane. This ensures that minimal methane is adsorbed to the adsorbent, translating to enhanced methane recovery and reducing methane losses or slip with carbon dioxide in the waste gas (Selim *et al*., 2024).

Adsorbents used in the carbon dioxide capture process can be categorized into two types: equilibrium adsorbents and kinetic adsorbents (Rainone *et al*., 2023). The former has a stronger interaction between the surface of the adsorbent and carbon dioxide, when compared to methane. They include activated carbon (Mutunga *et al*., 2024), zeolites (Boer *et al*., 2022), and silica gel (Grande *et al*., 2020). Kinetic adsorbents, on the other hand, can adsorb more carbon dioxide compared to methane because of their higher diffusional velocity through their pores. This is attributed to

the smaller kinetic diameter of carbon dioxide (3.4 Å) compared to methane (3.7 Å). Examples of kinetic adsorbents include molecular sieves (Rainone *et al*., 2021), porous solids with uniform structures, and titano-silicates (Zhou *et al*., 2017). Equilibrium adsorbents are preferred for the biogas upgrading processes due to their reversible adsorption forces, which enhance the regeneration process.

Carbonaceous adsorbents can be produced from natural biomass or waste material, thus lowering associated costs and increasing their sustainability (Rainone *et al*., 2023). Compared to zeolites, they also exhibit easier and more energy-efficient regeneration. Their use in biogas upgrading is particularly advantageous because carbonaceous material can simultaneously remove carbon dioxide and any traces of water vapour from biogas streams. In contrast, zeolites suffer the limitation of rapid and preferential adsorption of water vapour which suppresses carbon dioxide uptake. Although carbonaceous adsorbents are also capable of adsorbing hydrogen sulphide, upstream desulfurization of biogas is essential to avoid further competition of adsorption sites (McEwen *et al*., 2013).

Activated carbons have received considerable attention as adsorbents owing to their lower cost, higher thermal stability, and lower sensitivity to moisture (Zhou *et al*., 2017). They are mainly developed through the pyrolysis of different carbon-containing biomass. This process involves reducing the non-carbon elements, such as nitrogen, oxygen, and hydrogen, which have non-attractive surface properties. The activation process enhances the active sites and porosity of the material, resulting in a significantly increased surface area (Kong *et al*., 2013). Coal, peat, and biomass resources, such as rice husks, maize cobs, and coconut shells, are commonly used to produce activated carbon (Abuelnoor *et al*., 2021; Aljeboree *et al*., 2017). They have demonstrated good adsorption capacity for various applications, including gas separation.

The incorporation of plastic waste in the production of activated carbons used in biogas upgrading processes has recently been proposed (Pérez-Huertas *et al*., 2023). A recent study assessed the performance of a plastic-based activated carbon, activated using potassium carbonate in biogas upgrading (Solís *et al*., 2024). The adsorbent achieved

a carbon dioxide adsorption capacity of 130.2 mg/g at 273 K, along with a longer carbon dioxide breakthrough time of 55 seconds, compared to 32 seconds for methane. Similarly, polyacrylonitrile-based activated carbon attained a carbon dioxide adsorption capacity of 257 mg/g at 273 K, and demonstrated a good regeneration ability over repeated adsorption cycles (Kamran *et al*., 2020). While these adsorbents exhibit promising behaviour for biogas upgrading, the complex nature of the plastic waste and required pre-processing make the production process costly.

Biomass-based activated carbons are increasingly being used due to their sustainability and environmental friendliness. The use of activated carbon derived from pinewood attained a methane purity of above 95% when used as an adsorbent in biogas upgrading (Durán *et al*., 2022). This was attributed to its higher adsorption capacity for carbon dioxide (1.97 mol/kg) compared to methane (0.6 mol/kg). Another study used a 3D-printed activated carbon monolith for carbon dioxide capture with thermal regeneration, which underwent rapid and homogeneous heating during the regeneration step. The temperature rise of up to 150°C in less than 30 seconds allowed for effective regeneration (Verougstraete *et al*., 2022). A comparative analysis of activated carbons produced from maize waste and prepared at different activation times was done for biogas upgrading using the adsorption technique (Surra *et al*., 2022). The activated carbon produced from long activation times (3 h/2 h) had a higher surface area (820/630 m^2/g) and micropore volume (0.32/0.21 cm^3/g), which favours the biogas upgrading process. Additionally, it exhibited a higher adsorption capacity for carbon dioxide (130 mg/g) compared to methane (23 mg/g), making it ideal for biogas upgrading.

Coconut shell activated carbon (CSAC) has been found to have a larger number of pores developed during activation, resulting in a better adsorption capacity for gas separation compared to other forms of activated carbons (Rajasekaran *et al*., 2021). In a recent study, polydisperse CSACs with particle diameters ranging from 1.8 mm to 3.5 mm were utilized for the separation of pure component methane and carbon dioxide (Song *et al*., 2022). The authors achieved a carbon dioxide selectivity of 6.62 at a 50/50 gas volume ratio. Another study evaluated the performance of mixed CSAC pellets with a diameter range of 1 mm to 3 mm in the separation of pure equimolar

methane: carbon dioxide mixtures using the pressure swing adsorption technique (Abdeljaoued *et al*., 2018). The high selectivity of 3.6 towards carbon dioxide over methane, along with its stable adsorption performance over six successive cycles, demonstrates its suitability as an adsorbent for separating methane and carbon dioxide mixtures. While previous studies discussed above have evaluated the performance of CSAC polydisperse adsorption columns in biogas upgrading, there is a need to study the performance of monodisperse adsorption columns. Furthermore, a wider diameter range should be adopted to evaluate the influence of particle size on flow variables.

2.4 Adsorption Regeneration Techniques

An adsorption system features two steps, namely: i) an adsorption step and ii) a regeneration step. During the adsorption step, the target component of the gas mixture, such as carbon dioxide in biogas, is selectively retained on the surface of the adsorbent, and the purified gas exits the column. The efficiency of this process is governed by the physicochemical properties of the adsorbent, gas composition, flow rate, pressure and temperature. Once the adsorbent approaches saturation, the regeneration step restores its adsorption capacity by removing the adsorbed species. Effective regeneration ensures sustained cyclic operation, prolonged adsorbent life, maximum adsorption efficiency and optimized energy use.

Pressure and temperature are the primary gas properties that impact system regeneration performance. Figure 2.8 shows the major classification of adsorption techniques based on the different regeneration approaches adopted. The use of multiple adsorption columns has been proposed to ensure continuous operation and maintain a stable methane supply during regeneration (Lillia *et al*., 2018; Shen *et al*., 2018).

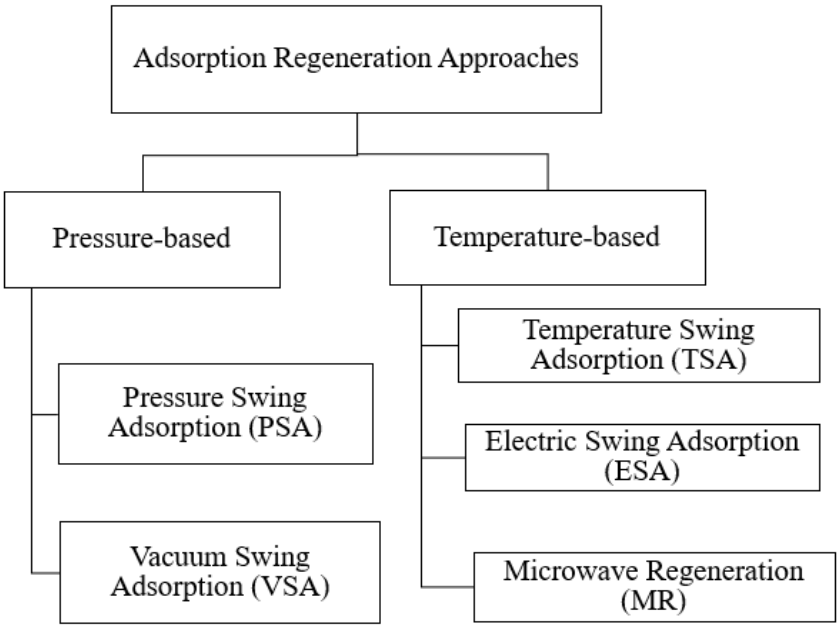

Figure 2.8: Classification of Adsorption Regeneration Techniques

Source: (Mutunga et al., 2022)

2.4.1 Pressure-Based Regeneration

Pressure-based regeneration of adsorbents for biogas upgrading is based on the theory that pressurized gases are attracted to solid surfaces, and reducing the pressure releases the gases. During the biogas upgrading process, the columns are often operated at high pressures of 4 to 10 bar to selectively retain carbon dioxide molecules on the adsorbent. The pressure-based technique has the advantage of equipment compactness; therefore, small, compact, and modular units can be easily fabricated for small-scale applications. The high energy requirement is the main challenge facing this approach.

Figure 2.9 illustrates the steps of a PSA cycle, which include adsorption, blowdown, purge, and pressurization. During the adsorption step, the target component such as carbon dioxide in biogas is preferentially retained on the adsorbent while the upgraded gas exits the column. The subsequent blowdown and purge steps remove the adsorbed species from the bed by reducing pressure and introducing a portion of the purified gas, respectively, restoring the adsorbents capacity. Pressurization step brings the bed

back to the operating pressure for the next adsorption cycle. Recent advances in PSA systems have introduced additional intermediate steps such as equalization, depressurization, and re-pressurization (Shen *et al*., 2018). In the extended cycles, gas is transferred between the beds during equalization to reduce pressure losses, while controlled depressurization and re-pressurization allows more complete desorption and improved utilization of the adsorbent. This is particularly beneficial in biogas upgrading as it optimizes methane recovery and reduces the total energy consumption.

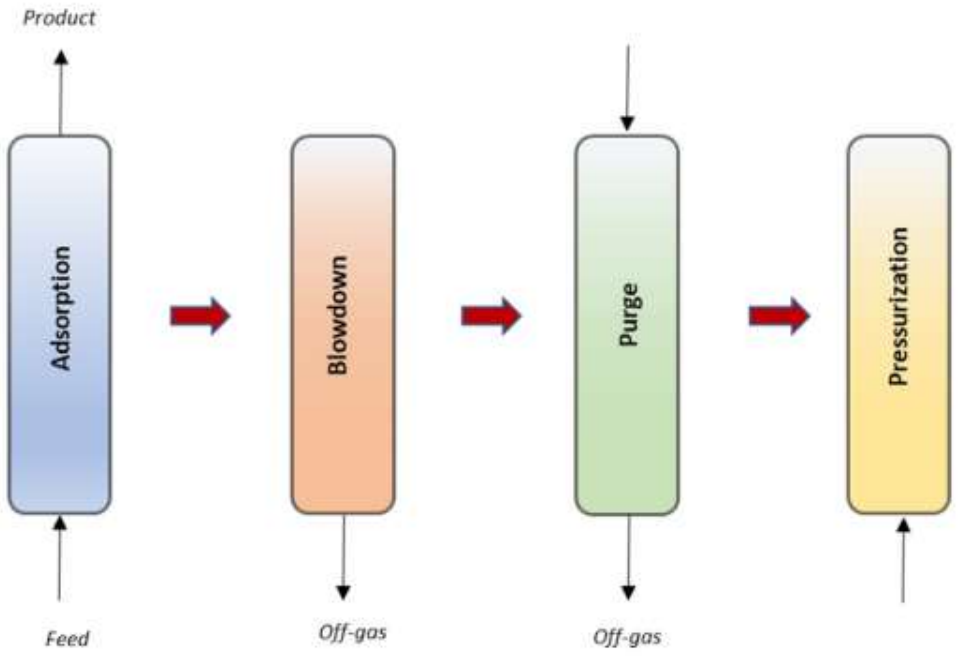

Figure 2.9: Schematic Representation of the PSA Cycle

Source: (Rainone et al., 2023)

A recent study compared the performance of zeolite 13X, activated carbon, and carbon molecular sieve in upgrading biogas using the PSA technique (Punpee *et al*., 2023). The highest methane purity of 98% was achieved when using zeolite as the adsorbent, due to its three times higher selectivity between carbon dioxide and methane compared to activated carbon and carbon molecular sieve, which achieved purity levels of 93% and 97%, respectively. While activated carbon had the highest carbon dioxide adsorption capacity, its relatively low selectivity for carbon dioxide over methane at high pressures resulted in lower methane purity.

The inlet biogas composition and length-to-diameter ratio are crucial variables to the PSA upgrading process. Increasing the carbon dioxide concentration in the feed gas from 20% to 40% was observed to reduce the methane purity by 7% (Abd *et al*., 2023). This was attributed to the faster diffusion of carbon dioxide molecules in the adsorption bed, resulting from a higher concentration gradient and limited active sites, which reduced the separation efficacy of the adsorption bed. In their other work, they also established that the presence of nitrogen in biogas (10%) increased the pressure drop across the adsorption column by 23.46%, and consequently decreased methane purity and recovery by 48.66% and 23%, respectively (Abd *et al*., 2023). This was attributed to the increased viscosity and density of the gas, resulting in a high friction factor between the gas molecules and the bed surface.

Vacuum Swing Adsorption (VSA) operates on similar principles to those of Pressure Swing Adsorption (PSA), with the primary difference being that the desorption process occurs under vacuum conditions. The high capital cost of equipment required to achieve deep vacuum levels has contributed to the adoption of a minimum desorption pressure of 0.1 bar when employing this technique. Recent studies combined both PSA and VPA principles, applying Vacuum Pressure Swing Adsorption (VPSA) principles in the biogas upgrading process (Tabar *et al*., 2022). The attained methane purity and recovery of 98.2 mol% and 73.8 mol%, respectively, were greatly influenced by the short adsorption time, low desorption pressure, and high purge-to-feed flow rate ratio. These techniques are limited by the high initial cost required to set up the various vessels, which can withstand extreme working pressures.

2.4.2 Temperature-Based Regeneration

Temperature-based regeneration for adsorption processes is a promising approach that could fully exploit biogas as a renewable energy source, provided that the energy is harnessed from other renewable energy sources, such as solar and wind. Compared to pressure swing adsorption, temperature swing adsorption is preferred due to reduced power requirements and system complexity (Rainone *et al*., 2023). Figure 2.10 illustrates the primary steps of a thermal swing adsorption process, which include adsorption, heating, purging, and cooling.

The thermal regeneration of adsorbents can be achieved by either direct or indirect heating. The conventional temperature swing adsorption process, classified as indirect heating involves passing a stream of hot steam or gas through an adsorption column during the desorption process (Keller *et al*., 2019). The increase in temperature results in desorption of the adsorbed species, carbon dioxide, which is driven away along with the purge gas current.

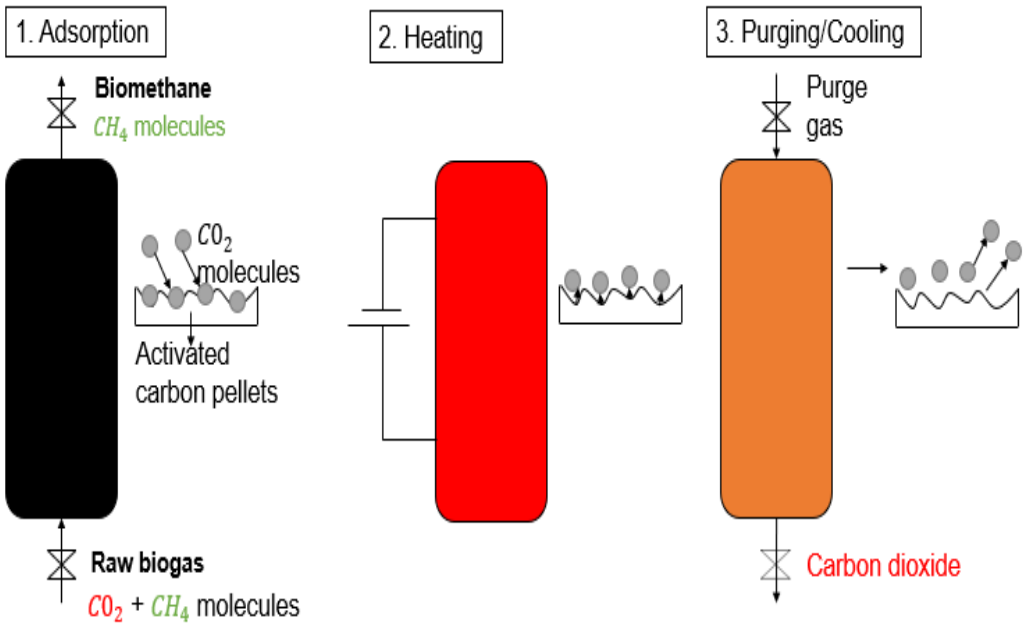

Figure 2.10: Thermal Swing Regeneration Cycle

Source: (Mutunga et al., 2022)

The direct heating of the adsorption column approach for the regeneration of biogas upgrading systems has also been proposed (Moon & Shim, 2006; Sonnleitner *et al*., 2018; Verougstraete *et al*., 2022). The use of heat pumps, microwave heating, electrical heating, and resistive heating are some approaches proposed. The heating and purge gas flow rates can be controlled separately, allowing higher adsorbate concentrations to be attained (Lee *et al*., 2023). While increased temperatures reduce the adsorption capacity of the adsorbent, favouring the desorption process, it is essential to consider the thermal resistance of the adsorbent to prevent its degradation.

The use of a heat pump for the regeneration process has been tested with energy requirements of 2.8 MJ/kg of methane (Vogtenhuber *et al*., 2018). This compares favourably in terms of energy savings to the use of conventional temperature swing adsorption systems, with a heat pump coefficient of performance exceeding 2. The prolonged heating and cooling periods required during the process contributed to the thermal aging of the adsorbents, negatively impacting process efficiency.

Electric Swing Adsorption (ESA) is considered a second-generation technology for carbon dioxide separation. High electric power enables faster heating of columns, thereby reducing the time required during the heating step. While copper, aluminium, and brass are some of the electrodes proposed for electric conductivity (indirect ESA), the use of adsorbents that are good conductors of electricity (direct ESA) has proved to increase the overall system efficiency. This is attributed to the reduced heat loss due to contact resistance between the electrode and the adsorbent. The employment of the ESA technique using a 3D printed monolith for biogas upgrading (30 v% carbon dioxide and 70 v% methane) successfully achieved a methane purity and recovery of up to 84.5% and 87.3%, respectively (Verougstraete *et al*., 2022). Similarly, a constant desorption efficiency of over 85% was attained using the ESA technique, a 20% increase when compared to the VSA approach (Moon & Shim, 2006).

Microwave regeneration technology utilizes electromagnetic energy that is converted into thermal energy in the adsorbent bed. Microwave energy is delivered directly to the adsorbent by varying the magnetic field, as opposed to conventional heat transfer processes such as conduction and convection, which require a medium (Klinbun *et al*., 2011). The feasibility of carbon dioxide capture using zeolite from a mixture containing nitrogen and helium, with microwave irradiation applied for regeneration, was investigated (Meloni *et al*., 2021). As a result of the direct heating, low purge gas flow rates were required during the purging step, making it economically viable. The repeatability in the carbon dioxide adsorption and desorption process represented minimal interference with the adsorbent adsorption properties. This is a feasible alternative for regeneration during the biogas upgrading process, given its environmental sustainability when electricity is harnessed from renewable energy

sources. While a regeneration efficiency of 100% was attained, the low energy efficiency of 75% limits its adoption for biogas upgrading.

Electrically-driven thermal swing adsorption (ETSA) is an emerging technique, given its simplicity and ease of integration with renewable electricity sources (Lee *et al*., 2023; Moinee *et al*., 2024). In direct heating ETSA, an electric current or potential is applied directly to the adsorption column, or to electrically conductive elements within the adsorption column, resulting in a change in the chemical and physical properties of the adsorbent that results in desorption. Some advantages of direct heating include a high heating efficiency of up to 60% (Zhao *et al*., 2018), and a high concentration of purged adsorbate of up to 80% (Grande *et al*., 2009). Additional benefits include precise temperature control and reduced thermal inertia. While ETSA has been applied for carbon dioxide separation from flue gases and other gas mixtures, its feasibility for biogas upgrading has not been fully explored.

2.5 Experimental and Numerical Studies on Biogas Upgrading

Experimental and numerical studies provide essential insights into biogas upgrading by evaluating process parameters, adsorbent behaviour, and system performance. Experiments help determine the effects of variables such as adsorption time, purge flow rate, and regeneration temperature on system performance, while numerical models simulate complex interactions and predict outcomes under varying conditions. When combined with optimization techniques such as RSM, these studies enable systematic tuning of process parameters to improve efficiency, energy use, and overall system performance.

2.5.1 Experimental Studies on Biogas Upgrading

Experimental studies on thermal swing adsorption have played a critical role in advancing adsorption-based biogas upgrading, particularly in understanding desorption behaviour, regeneration efficiency, and energy demand under cyclic thermal operation. TSA relies on temperature variation to regenerate the adsorbent, making the process highly sensitive to operating variables such as purge flow rate, regeneration temperature, and adsorbent physical properties.

The purge flow rate has been identified as a key parameter governing the desorption process and the overall TSA process. Mulu *et al.* (Mulu *et al*., 2021) reported a 70.5% reduction in carbon dioxide capture efficiency when the biogas flow rate was increased from 45 mL/min to 250 mL/min during adsorption using modified clay. This highlighted the strong influence of flow conditions on adsorbent utilization. Similarly, Verougstraete *et al.* (Verougstraete *et al*., 2022) observed that high purge flow rates during regeneration resulted in an earlier and higher carbon dioxide concentration peak in the waste. This was attributed to faster displacement of carbon dioxide from the adsorbent pores. While increased purge flow rates improved methane purity when methane was used a s purge gas, they significantly reduced methane recovery and diluted the waste gas stream. These findings underscore the need to optimize purge flow rate to achieve a balanced trade-off between methane purity and recovery in TSA systems.

Regeneration temperature is another critical variable in the desorption efficiency, as carbon dioxide physisorption decreases significantly at elevated temperatures. Experimental studies on electrically driven thermal swing adsorption have demonstrated the strong dependence of regeneration performance on heating voltage and electrification time. Verougstraete *et al.* (Verougstraete *et al*., 2022) showed that increasing electrification time from 15 seconds to 55 seconds raised the maximum regeneration temperature from 62.3℃ to 175.2℃, increasing the carbon dioxide concentration in the waste gas from 46.7% to 58%. However, this improvement was accompanied by a substantial increase in energy consumption, with a 10-second increase in electrification time resulting in an additional 110 J/g energy input, corresponding to a by 26% rise in total energy demand. This highlights that although higher temperatures favour desorption, optimization of regeneration temperature is essential to minimize energy consumption and limit adsorbent deterioration under repeated thermal cycling.

The physical properties of the adsorbent, particularly the particle size and mass, have also been shown to significantly influence the TSA performance. A previous study reported that decreasing adsorbent particle size enhanced carbon dioxide removal efficiency due to increased surface area and number of active adsorption sites.

Increasing adsorbent mass similarly improved carbon dioxide removal; however, excessive bed loading reduced effective adsorption capacity due to pore overlap and limited interaction between adsorbate molecules and active sites (Mulu *et al*., 2021). These effects are strongly coupled with flow variables such as gas flow rate and flow distribution, which govern residence time, mass transfer rates, and pressure drop within the adsorption column. Poor flow distribution limits access to active adsorption sites, thereby reducing overall upgrading efficiency.

The reviewed studies demonstrate that flow variables, regeneration temperature, and adsorbent physical properties are highly interdependent. This highlights that efficient biogas upgrading requires a balanced, system-level optimization that integrates adsorbent characterization, adsorption equilibrium behaviours, and thermally driven regeneration strategies. These insights provide an essential foundation for numerical modelling and process optimization.

2.5.2 Numerical Studies on Biogas Upgrading

Numerical modelling is a central tool in the study and optimization of adsorption-based biogas upgrading systems due to the complex and cyclic nature of adsorption processes such as pressure swing adsorption and thermal swing adsorption. These processes involve strongly coupled mass transfer, heat transfer, fluid flow, and adsorption-desorption equilibria that vary with time (Castley *et al*., 2022). Numerical analysis complements experimental studies and enables the formulation and solution of governing equations, allowing real systems to be represented in a simplified form.

Among the computational tools, Aspen Adsorption has been widely adopted for modelling cyclic adsorption processes in biogas upgrading due to its capability to simulate complex cycle steps and detailed adsorption and regeneration behaviour (Abd & Othman, 2022; Bahrun *et al*., 2025; Durán *et al*., 2022). Additional platforms such as MATLAB (Cutillo, 2024; Mendel *et al*., 2025), and gPROMS (Karimi *et al*., 2026) have been employed to solve custom dynamic models and to capture coupled heat and mass transfer effects with higher spatial resolution. These numerical tools enable the simultaneous evaluation of multiple interacting variables, including flow rate, pressure, temperature, cycle configuration and adsorbent properties, limited when

using an experimental approach. Numerical models provide a cost-effective and efficient framework for the development, evaluation, and optimization of adsorption-based biogas upgrading systems.

A critical aspect of numerical modelling is the accurate representation of adsorption equilibrium and adsorbent properties. Adsorption equilibrium in biogas upgrading studies is commonly described using Langmuir, Freundlich, and Langmuir-Freundlich isotherm models, each offering varying levels of complexity and applicability (Kong *et al*., 2013; Mulu *et al*., 2021). The Langmuir isotherm is mostly used to represent monolayer adsorption on homogeneous surfaces and has been adopted in PSA and TSA simulations due to its simplicity (Karimi *et al*., 2026). For heterogeneous adsorbents such as biomass-derived carbons such as activated carbon, the Freundlich and Langmuir-Freundlich models have been shown to provide improved agreement with experimental data by accounting for surface heterogeneity and non-uniform adsorption energies (Punpee *et al*., 2023). Incorporating these isotherms models into numerical simulations enhances the accuracy of predicted carbon dioxide uptake, methane purity and breakthrough behaviour.

In addition to equilibrium models, textural characterization of adsorbents plays a vital role in numerical studies. Surface area and pore structures are commonly determined using Brunauer-Emmett-Teller (BET) surface area analysis and the Barrett-Joyner-Halenda (BJH) method for pore size distribution (Rajasekaran *et al*., 2021). BET-derived surface area data are essential for estimating adsorption capacity, while BJH analysis provides insight into pore distribution which influences diffusion resistance and mass transfer rates within the adsorption bed (Masthan *et al*., 1992; McLaren *et al*., 2021). Incorporating these parameters in numerical studies has demonstrated improved prediction of adsorption kinetics and breakthrough curves, particularly for carbonaceous materials used in biogas upgrading.

Several numerical investigations have focused on the influence of flow-related variables on adsorption system performance. The purge gas flow rate during the desorption step has been identified as a key parameter affecting methane purity and recovery. Duran *et al.* (Durán *et al*., 2022) analyzed purge-to-feed flow rate ratios

between 0.67 and 1 in A PSA-based biogas upgrading system and reported an increase in methane purity from 94.4% to 97.1% and methane recovery from 46.9% to 63.0% with increasing purge intensity. Similarly, Shen *et al.* (Shen *et al*., 2018), using Aspen Adsorption to model a vacuum PSA system, investigated lower purge-to-feed ratios (0 - 0.2) and observed an increase in methane purity accompanied by a reduction in methane recovery. These opposing trends highlight the complex interactions between flow variables and other operating parameters, reinforcing the importance of numerical models capable of capturing multi-variable effects.

The impact of adsorbent particle size has also been examined through numerical modelling. Ballesteros *et al.* (Ballesteros *et al*., 2022) used Aspen Adsorption to analyse particle radii ranging from 0.1 to 2.4 mm in monolayer and bilayer PSA adsorption beds. Their results showed that larger particle sizes reduced pressure drop and improved gas floe distribution, leading to higher methane purity of up to 98%, compared to smaller particles with methane purity of 95%. These findings demonstrated the trade-off between adsorption kinetics and hydrodynamic performance, and emphasize the need to integrate adsorbent physical properties into numerical simulations.

A comparative summary of representative numerical studies on adsorption-based biogas upgrading, including adsorption techniques, isotherm models, adsorbent characterization methods, software platforms, and key findings, is presented in Table 2.1.

Table 2.1: Summary of Selected Numerical Studies on Biogas Upgrading

Author	Adsorption technique	Isotherm model	Adsorbent characterization	Software used	Key findings
Shen *et al.* (2018)	VPSA	Langmuir	BET, BJH	Aspen Adsorption	Increased purge improved methane purity but reduced methane recovery
Kottititum *et al.* (2020)	PSA	Langmuir	BET, BJH	Aspen Adsorption	Optimized cycle steps enhanced methane purity and energy efficiency
Abd and Othman (2022)	TSA and PSA	Langmuir-Freundlich	BET	Aspen Adsorption	Highlighted the role of heterogeneous adsorption in regeneration performance
Karimi *et al.* (2026)	VPSA	Langmuir	BET, BJH	gPROMS	High purge flow rates enhance methane purity at the expense of increased energy demand

2.5.3 Optimization Approaches for Biogas Upgrading

Optimization of biogas upgrading processes requires analytical frameworks capable of resolving complex, non-linear interactions among operating variables, material properties, and system design parameters. Key performance indicators, including methane purity and recovery, carbon dioxide and hydrogen sulphide removal efficiency, and energy consumption, are often governed by competing mechanisms. As a result, traditional one-factor-at-a-time experimental approaches are inadequate for capturing interaction effects and trade-offs. Consequently, advanced optimization techniques such as Response Surface Methodology, Analysis of Variance, Box-Behnken design (BBD), Taguchi methods, and Artificial Neural Networks have increasingly been applied in biogas upgrading research.

Among these techniques, the response surface methodology has gained widespread acceptance due to its ability to quantify variable interactions and identify optimal operating regions with a reduced number of experimental or numerical runs (Ahmad *et al*., 2024; Djimtoingar *et al*., 2022; Tan *et al*., 2023). RSM employs second-order polynomial models to relate system responses to multiple independent variables, enabling both prediction and optimization. ANOVA is an integral component of RSM

used to evaluate the statistical significance of model terms, assess model adequacy, and identify dominant parameters influencing system performance.

RSM-based optimization has extensively been applied to adsorption-based biogas upgrading systems, particularly pressure swing adsorption. Shen *et al.* (Shen *et al*., 2018) demonstrated that adsorption time, purge-to-feed flow rate ratio, and desorption pressure exert opposing effects on methane purity and methane recovery, and showed that RSM enabled simultaneous optimization of these competing objectives. Similarly, Seong *et al.* (Seong *et al*., 2024) applied RSM to evaluate the effects of column geometry, feed composition, and temperature, achieving above 99% methane purity. However, their use of simplified biogas composition of carbon dioxide and methane shows a common limitation in literature, since real biogas contains additional impurities that affect adsorption behaviour and reaction rates.

RSM has also been used in absorption-based biogas upgrading, offering methodological insights relevant to adsorption and TSA processes. Mugagga *et al.* (Mugagga *et al*., 2023) combined the Taguchi method with RSM to optimize a low-pressure water scrubbing system, where Taguchi screening was first used to identify influential variables, followed by RSM to resolve interaction effects and response curvature. This hybrid approach demonstrated improved optimization efficiency and robustness, particularly for systems involving multiple interacting variables. Within the RSM framework, the Box-Behnken design is especially attractive for adsorption-based systems. BBD requires fewer runs than full factorial or central composite designs and avoids extreme conditions that may be impractical or damaging to adsorbents. This characteristic is particularly important for TSA systems where excessive regeneration temperatures, heating voltage, or purge flow rates can accelerate adsorbent degradation and increase energy penalties.

Artificial neural networks have also been applied to biogas upgrading processes characterized by strong non-linearity and complex interactions. Hananpour Seyedlar *et al.(Hasanpour Seyedlar et al., 2024)* developed an ANN model to predict and optimize hydrogen sulphide mitigation in a full-scale anaerobic digestion system. The model demonstrated high predictive accuracy without the need for explicit mechanistic

equations. However, despite their strong interpolation and prediction capabilities, ANN models lack physical transparency and do not directly reveal variable interactions or process sensitivities. ANN are best positioned as complementary tools to support RSM-based optimization rather than replace statistically interpretable methods.

Despite the extensive application of RSM, Taguchi, and ANN methods to PSA and absorption-based systems, optimization studies focused on TSA remain limited. TSA introduces additional interacting variables such as regeneration temperature, heating voltage, electrification time, purge flow rate and adsorbent thermal properties that often exert opposing effects on methane purity, methane recovery and energy consumption. Combined application of RSM, ANOVA and BBD provide a rigorous and transparent framework for optimizing TSA-based biogas upgrading processes.

2.6 Summary of the Research Gaps

From the literature review, it is evident that upgraded biogas is a promising alternative energy source to fossil fuels. Activated carbon was found to be a suitable adsorbent for the thermal swing regeneration technique. Various process parameters, including particle radius, gas flow rate, regenerating pressure, and temperature, have been shown to influence the methane purity and recovery. Studies on various optimization techniques indicated that the Response Surface Methodology is an efficient and effective tool. It allows for relatively fewer experiments to be conducted, but with reasonably accurate results. The review indicated an adequate amount of literature on the optimization of these process variables for the pressure-based regeneration technique. However, their combined influence on thermal swing regeneration techniques has not been explored as per the articles reviewed in this write-up.

The identified research gaps from the literature review can be summarized as follows;

i. Existing studies on the biogas upgrading process have mainly focused on pressure-based regeneration of adsorption columns/beds, with limited investigation employing the temperature-based regeneration technique.

ii. There are limited studies employing the thermal swing adsorption technique to upgrade biogas obtained from the anaerobic digestion of organic waste, with the majority of studies using synthetic biogas, which comprises a mixture of pure methane and carbon dioxide.
iii. While the application of temperature-based regeneration of adsorbent columns has been studied for carbon dioxide capture from stack flue gas, there is limited data on its feasibility for biogas upgrading applications.
iv. There is a scarcity of validated numerical simulation models employing temperature-based regeneration techniques in the biogas upgrading process.
v. The majority of numerical studies focused on parametric analysis, with limited studies evaluating their correlation and optimization. The available optimization studies are limited to maximizing single outputs, rather than multi-objective optimization.

This research was conducted to address the aforementioned gaps, aiming to optimize the performance of a thermal swing adsorber for biogas upgrading. The detailed methodology applied is presented in the next chapter.

CHAPTER THREE

METHODOLOGY

3.1 Overview

This chapter outlines the materials and methods utilized to achieve specific objectives. Figure 3.1 presents the methodology outline adopted for this study. Both the experimental and numerical study approaches were used. The experimental study involved comprehensive adsorbent characterization, prototype development, and its analysis. The numerical model was developed using the Aspen Adsorption software and validated using experimental data from the fabricated model for similar operating conditions. The response surface methodology employed in the process optimization is also discussed.

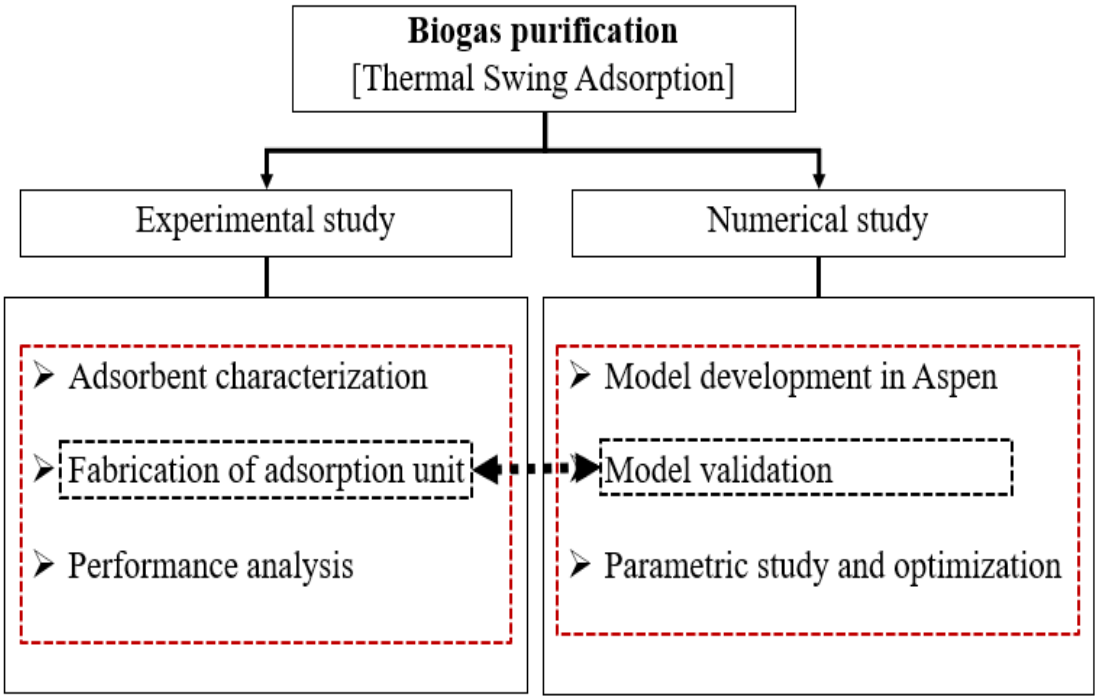

Figure 3.1: Methodology Outline

3.2 Activated Carbon Characterization

Kenya generates substantial quantities of coconut waste, particularly in the coastal counties such as Kilifi and Lamu where coconut processing for food and oil is a major economic activity (Muriuki *et al*., 2024). The coconut shells, often discarded, possess high lignocellulosic content and fixed carbon, making it suitable for use in production of activated carbon adsorbents. The characterization of adsorbents is crucial in the biogas upgrading process because it affects the efficiency and effectiveness of carbon dioxide capture. The procedures used to determine key properties of the adsorbent such as surface area, pore size and distribution, adsorption capacity, and regenerability are discussed below.

3.2.1 Nitrogen Adsorption Isotherms

Activated carbon pellets derived from coconut shells, as shown in Figure 3.2, were supplied by Repuls International in India and used as adsorbents. They were produced by carbonizing coconut shells at an average temperature of 450℃ within an inert atmosphere. The pellets then underwent physical activation using steam. The purpose of this activation process was to eliminate any volatile matter and enlarge the pores of the adsorbent.

Figure 3.2: Activated Carbon Pellets

Nitrogen adsorption tests have been recognized as effective in characterizing porous materials with sufficient microporosity to warrant the use of carbon dioxide for

determining surface area, pore size, and total pore volume (Abdulsalam *et al*., 2019; Thommes *et al*., 2015). The Brunauer-Emmett-Teller (BET) model presented in Equation (3.1) was used to determine the physical properties based on the nitrogen adsorption isotherms at − 203 ℃ based on ISO standard 9277 (Rouquerol *et al*., 2014).

$$\frac{P}{V(P_0 - P)} = \frac{C - 1}{V_m C}\frac{P}{P_0} + \frac{1}{V_m C} \qquad 3.1$$

where P is the equilibrium pressure of the adsorbed gas; P_0 is the saturated vapor pressure of the adsorbed gas; V is the actual (multi-layer) adsorption volume of the sample (cm^3/g), V_m is the single-layer saturated adsorption volume per unit mass, (cm^3/g), C is the BET constant related to the enthalpy of adsorption. The constant C represents the strength of interaction between the adsorbate and the adsorbent. Adsorbents with a high BET constant represent better selectivity and adsorption capacity, making them suitable for the biogas upgrading process.

A sample of 0.1731 g of activated carbon was degassed at 150℃ for six hours using a Micromeritics FlowPrep 060 (accuracy ± 10℃) unit to remove moisture and impurities before conducting adsorption measurements. The Micromeritics TriStar II plus 3030 (accuracy ± 0.25℃) was utilized for the analysis. Nitrogen adsorption-desorption isotherms were measured in the relative pressure (P/P_0) range of 0.0001 to 0.99. The surface area, pore diameter, and pore volume were assessed based on the obtained isotherms.

The relationship between the amount of adsorbed gas in the multilayer stage and the relative pressure in the adsorption isotherm was characterized using the linearized BET equation (Thommes *et al*., 2015). The Barrett–Joyner–Halenda (BJH) model, as described by Equation (3.2), was used to determine the pore size distribution of the adsorbent (Masthan *et al*., 1992). It employs the modified Kelvin equation, represented by Equation (3.3), to relate the amount of adsorbate removed from the pores of the material to the pore size as the relative pressure decreases. This approach estimates the mesopores and macropores, but it is known to underestimate pores smaller than 10 nm (McLaren *et al*., 2021).

$$v_n = R_n(\Delta V)_n - R_n \Delta t_n - \sum_{i=1}^{n-1} c_i A_i \qquad 3.2$$

where v_n is the volume (cm^3/g) of the pores involved in the n^{th} desorption step and is given in terms of the volume of nitrogen, ΔV is the volume (cm^3/g) exuded from the porous material, R_n and c_i coefficients depend on the average pore size and average thickness (nm) of the physically adsorbed multilayer, Δt_n is the decrease in thickness (nm) of the multilayer as a result of the n^{th} desorption step and A_i is the surface area (m^2/g) of the set of pores involved in the i^{th} desorption step.

$$RT \ln \frac{P_D}{P_0} = -\frac{2\gamma V_L}{r_P - t_D} \qquad 3.3$$

where P_D/P_0 is the relative pressure of desorption, γ and V_L are surface tension (N/m) and molar volume of bulk liquid (m^3/mol) respectively, and t_D is the adsorption film thickness (nm) at the relative pressures of P_D/P_0, with R and T being the gas constant (J/(mol.K)) and temperature (K) respectively.

3.2.2 CO2 and CH4 Adsorption Isotherms

Adsorption isotherms play a crucial role in the adsorption process, as they represent the relationship between the adsorbate and the adsorbent. The static volume method, whose setup is shown in Figure 3.3, was used to obtain the adsorption equilibrium data of carbon dioxide and methane on activated carbon (Nam *et al.*, 2005). Temperature and pressure were the two state variables considered. The exothermic nature of the adsorption process makes temperature a crucial variable to be considered. In addition, temperature is the main variable in the thermal regeneration process considered in this study. The adsorbent was activated at 100°C under vacuum conditions for 1 hour prior to the experiment to eliminate any moisture or contaminant.

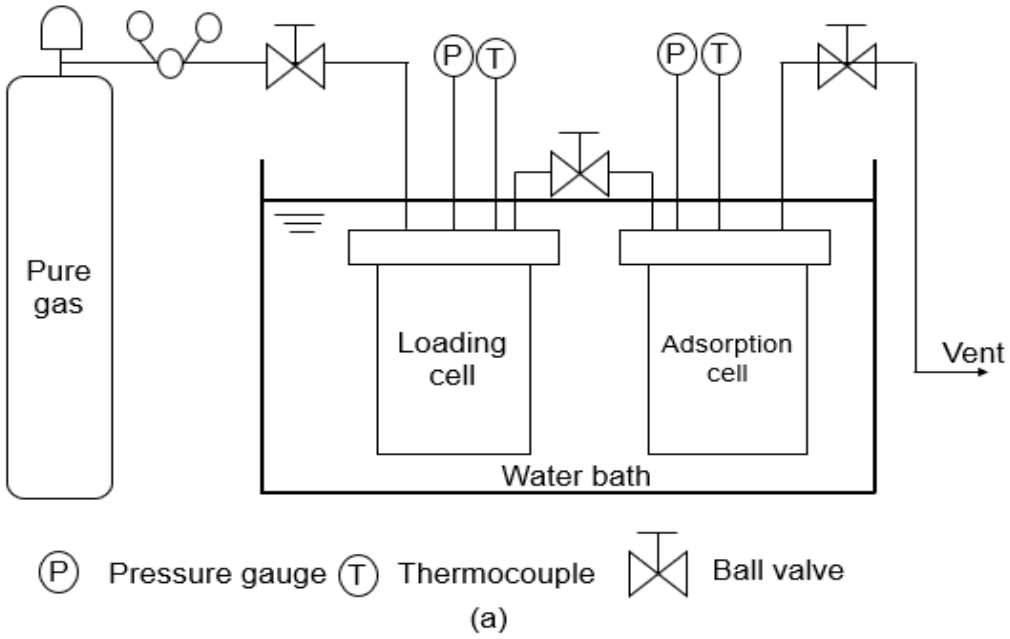

(b)

Figure 3.3: Static Volume Method (a) Schematic Setup (b) Pictorial Setup

Regulating the volume of gas introduced in the adsorption column is also significant to ensure adequate filling of the adsorption pores and mass balance accuracy, while minimizing axial dispersion effect. The amount of gas in the system was determined based on the equation of state. Pressure and temperature were measured using a pressure gauge (0 to 20 bar, $\pm$ 0.5 bar) and K-type thermocouples (-200℃ to 1200℃,

$\pm$ 0.01℃) respectively. The volumes of the adsorption and loading cells were 520 and 522 cm^3, respectively. During the experiments, the adsorption and loading cells were immersed in a water bath for 30 minutes to maintain the specified temperature. A vacuum pump (0 to 20 slpm) was then used to remove gaseous impurities from the loading and adsorption cells (Nam *et al*., 2005).

Pure carbon dioxide and methane gases with purities exceeding 99.99%, supplied by the British Oxygen Company (BOC) Kenya, were used in the experiments. Each gas was introduced into the loading cell, and its pressure and temperature were measured once the cell volume stabilized. Stability was considered to be attained when there was no significant change in the system pressure, indicating that adsorption had reached equilibrium. The valve between the loading and adsorption cell was then opened, allowing the gas to contact the adsorbent. The pressure and temperature were measured after equilibrium was achieved, and the number of moles remaining in each cell was calculated. The adsorption equilibrium state was considered to occur when the respective temperature and pressure of the cells were constant. This was attained within an average of 5 minutes. The amount adsorbed was calculated using the mass balance equation presented in Equation (3.4) (Nam *et al*., 2005).

$$\frac{PV}{ZRT}\Big|_{l_1} + \frac{PV}{ZRT}\Big|_{a_1} = \frac{PV}{ZRT}\Big|_{l_2} + \frac{PV}{ZRT}\Big|_{a_2} + qM \qquad 3.4$$

where subscripts l, a, 1, and 2 represent the loading cell, adsorption cell, state before adsorption equilibrium, and after adsorption equilibrium, respectively. Z is the compressibility factor, q is the amount of gas adsorbed (mmol/g), M is the mass of the adsorbent (g), R is the universal gas constant (J/(mol. K)), P is the gas pressure (N/m^2), V is the gas volume (m^3), and T is the gas temperature (K).

Equilibrium sorption temperatures of 30, 50, and 80°C, which were influenced by the adsorbent regeneration temperature range of up to 60°C, were considered in determining the isotherms (Mutunga *et al*., 2024). Each experiment was conducted in triplicate under identical conditions to ensure repeatability. Appendices I and II present preliminary results of carbon dioxide and methane adsorption isotherm fittings on the Langmuir, Freundlich, and Langmuir-Freundlich models. The Langmuir–Freundlich

model, expressed in Equation (3.5), was used to fit the experimental data (Azizian *et al*., 2007).

$$q^* = \frac{q_{m,i} b_i P_i^n}{1 + b_i P_i^n} \tag{3.5}$$

where, q^* and $q_{m,i}$ are the adsorption capacity (mmol/g) and saturated adsorption capacity (mmol/g) of the component i on the adsorbent, respectively. P is the partial pressure of the adsorbate (Pa). b_i and n represent the affinity constants of the Langmuir–Freundlich model.

3.2.3 Proximate Analysis

The ISO 11722, 1171, and 562 standards were used to determine moisture, ash, and volatile matter, respectively. The Thermogravimetric Analyzer 701 equipment (accuracy ±2%, LECO Corporation, USA) was employed for the analysis. The weight of the empty crucible pan was zeroed before conducting the tests. A sample mass of activated carbon was then placed into the empty crucible pan using a spatula, and its weight was measured. The sample was analyzed at temperatures of up to 1,200 °C for 5 hours. This process was repeated three times to ensure the repeatability of the test samples.

3.2.4 SEM and EDS Analysis

Scanning electron microscopy (SEM) analysis was conducted to examine the surface morphology and development of the activated carbon pellet using a field-emission scanning electron microscope (ZEISS Sigma 300 VP). The SEM micrographs were captured under conventional secondary electron imaging conditions at an accelerating voltage of 5 kV. The elemental composition of the activated carbon pellets was analyzed with an energy-dispersive X-ray spectroscopy (EDS) detector (Oxford Instruments X-act PentaFET Precision). A magnification range of 10,000 to 20,000x and an accelerating voltage of 20 kV were applied.

3.3 Design and Development of Experimental Setup

Figure 3.4(a) illustrates a schematic diagram of the biogas upgrading system, which includes the biogas, pre-cleaning system, adsorption columns/beds, and the electrical control unit. The pre-cleaning system consisted of a desulphurizer and silica gel pellets, which were used to remove hydrogen sulfide and water vapor, respectively. A pictorial view of the laboratory-scale biogas upgrading system, as presented in Figure 3.4(b), was fabricated and assembled at the JKUAT mechanical engineering workshops. Biogas obtained from the anaerobic digestion of animal waste was used in the experiment and was supplied by the Institute of Energy and Environmental Technology Center at JKUAT. Table 3.1 presents the parameters of the adsorbent and the adsorption column used to conduct the experimental study. The specifications are based on design criteria for a laboratory-scale adsorption column (Shen *et al*., 2018).

Table 3.1: Parameters of Adsorbent and Adsorption Column

Parameter	SI unit	Value
Bed height	m	1
Internal bed diameter	m	0.06
Wall thickness	m	0.002
Average particle radius	m	0.002
Adsorbent density	kg/m^3	1,000
Bed wall density	kg/m^3	7,800
Adsorbent specific heat capacity	kJ/kg. K	1.213
Adsorbent thermal conductivity	W/m. K	0.119

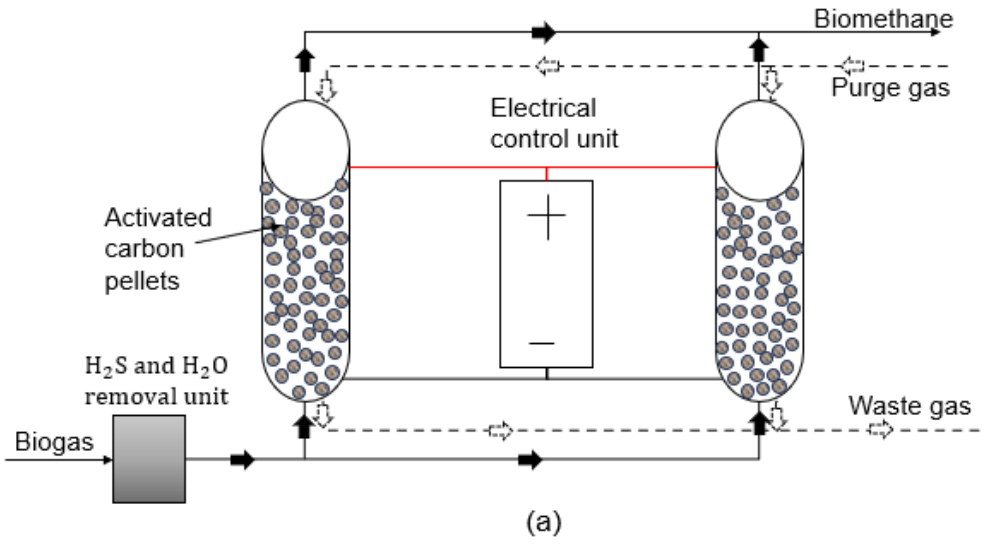

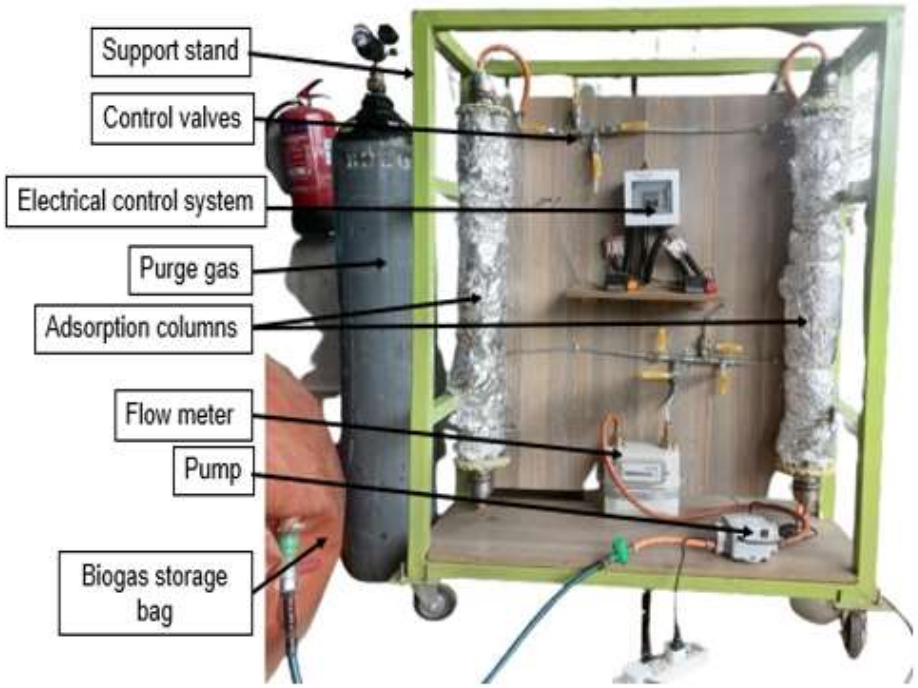

Figure 3.4: Experimental Setup (a) Schematic Illustration (b) Pictorial View

3.3.1 Adsorption Column Design

The adsorption column consists of a cylindrical stainless-steel pipe with a bed height of 1 m and an internal diameter of 0.06 m. This sizing was based on design criteria for laboratory-scale adsorption columns (Shen *et al*., 2018). Stainless steel grade $G304$ material was chosen for the adsorption column due to its high temperature tolerance and excellent corrosion resistance (Piechota, 2021).

The gas piping connecting the gas pressure pump (0 to 20 slpm), flow meter (4 m^3/h, accuracy $\pm$ 3%), and the adsorption column consisted of flexible gas piping with a diameter of 3.2 mm to minimize dead volumes (Nam *et al*., 2005). The adsorption columns were connected to the flexible gas pipe using stainless steel weld-neck flanges, as shown in Figure 3.5. This flange design was selected because it can withstand high temperatures and pressures, making it ideal for systems with multiple repeat bends. Rubber gaskets, 3 mm thick, were placed between the flanges to provide

a strong seal and prevent gas leakages. The bolted nature of the flanges provided for the ease of replacement of the adsorbent at the end of its lifespan.

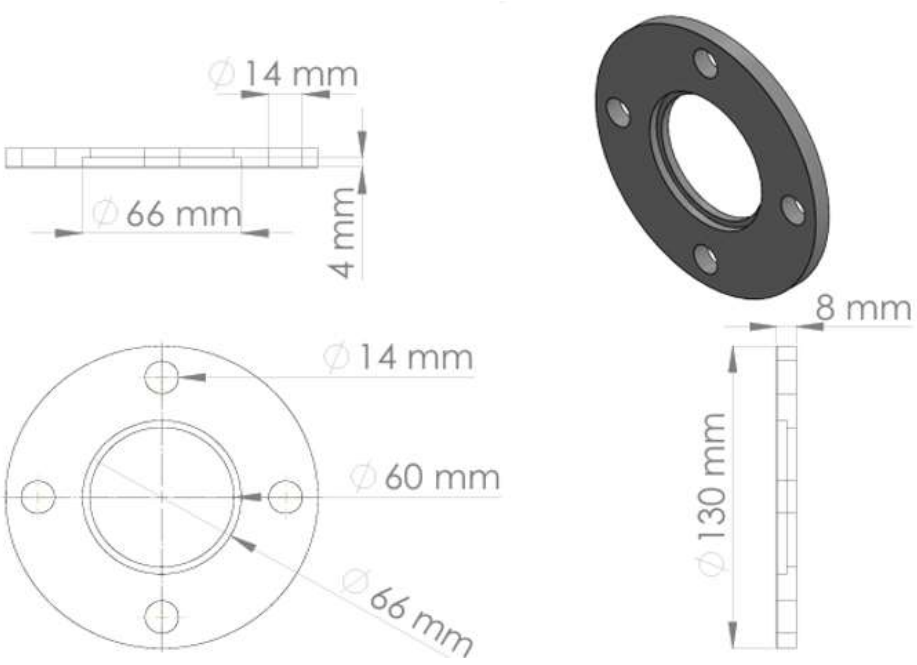

Figure 3.5: Flange Design

Figure 3.6 shows a conical reducer, designed to gradually decrease the cross-sectional area of the column to match that of the flexible gas pipe, thereby minimizing pressure losses. The concentric design of the reducer ensured a minimal pressure drop. It was welded to one of the flanges and connected to the flexible gas pipe on the other end. Its design was based on the design of adsorption columns (Bassey *et al*., 2024).

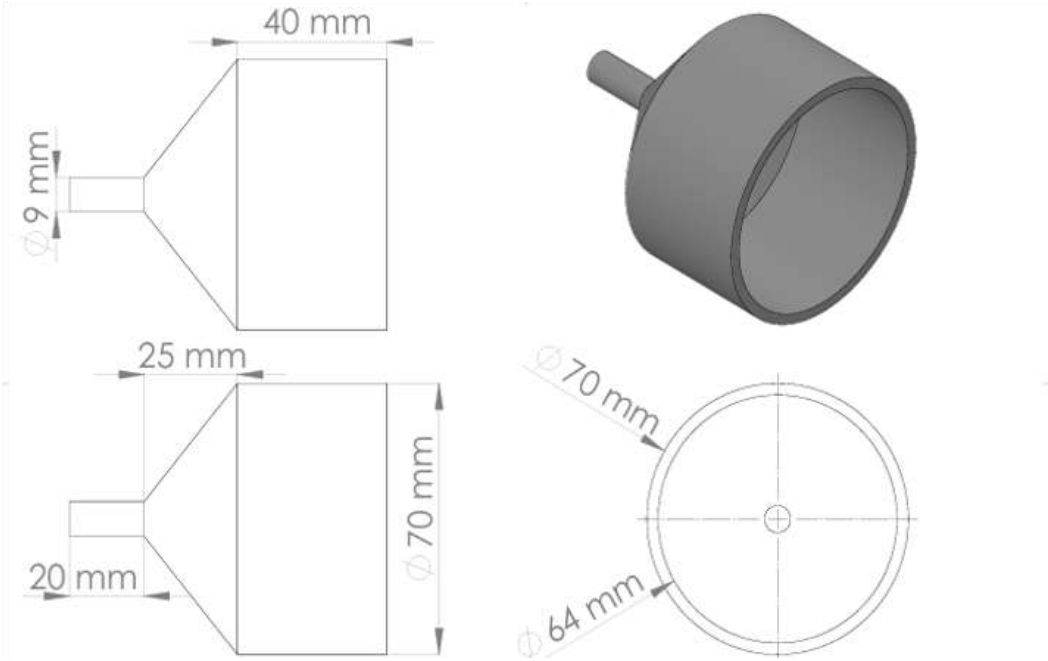

Figure 3.6: Column Reducer Design

The components of the housing of the biogas upgrading system (1 m length, 0.3 m width, 1.4 m height) are shown in Figure 3.7. It consists of hollow mild steel tubes with a square cross-section, welded together to form the support stand. The high strength-to-weight ratio of mild steel, along with its cost-effectiveness, makes it an ideal material for the stand fabrication. In addition, mild steel is readily available locally and can be fabricated using conventional machining and welding techniques. The stand was painted to prevent corrosion. Instruments and other electrical components were mounted on a fiber board. Four caster wheels were added to the stand to improve its mobility.

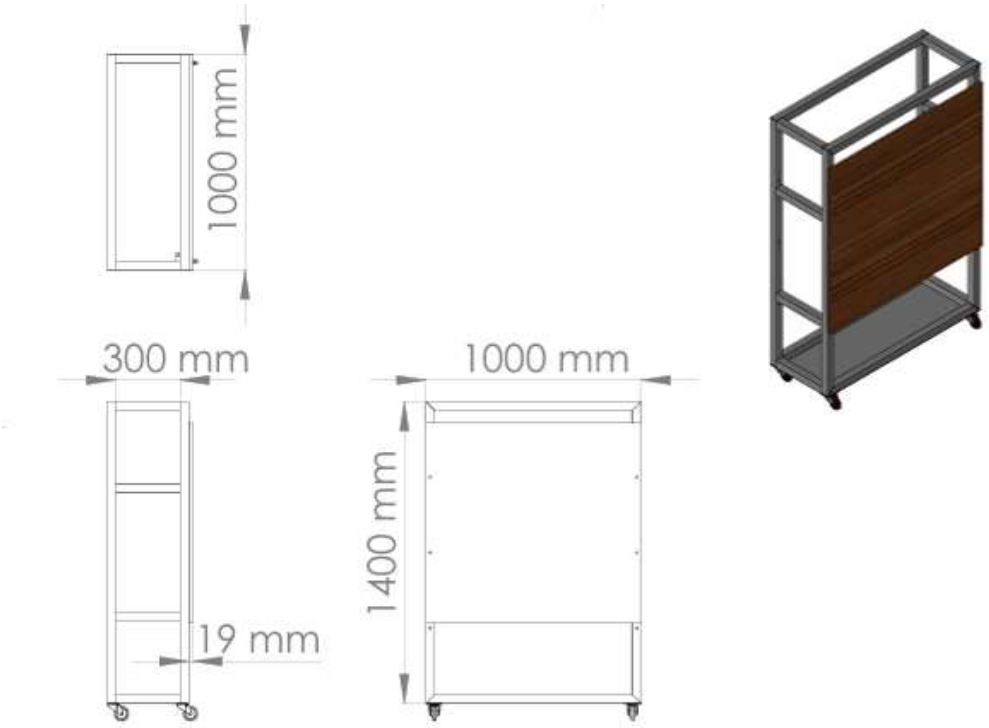

Figure 3.7: Support Stand Design

3.3.2 Heat Energy Requirements

This section outlines the design considerations for meeting the energy needs to heat the adsorption column during the regeneration process, controlling temperature, and ensuring thermal insulation.

a) Adsorption Column Heating System

The design considerations for meeting the energy requirements of heating the adsorption column during bed regeneration are discussed below. The total heat required was calculated by considering the energy needed to heat the adsorbent and the heat loss due to convection and conduction heat transfer. Equation (3.6) represents the energy required to heat the bed to the desired temperature (Rohsenow *et al*., 1998).

$$Q_{adsorbent} = mC_p\Delta T \qquad 3.6$$

where m is the mass of the adsorbent (kg), C_p is the adsorbent's specific heat capacity (J/(kg · K)) and ΔT is the maximum change in temperature (K).

Based on Joule's effect, energy requirements were calculated using Equation (3.7).

$$Q_{supply} = I^2 R.t \tag{3.7}$$

where Q is the heat energy supplied (J), I is the electric current (A), R is the electrical resistance (Ω), and t is the time (seconds).

Radial heat transfer was assumed, as the adsorption column length (1 m) is significantly greater than the column diameter (0.06 m). Heat loss due to conduction and convection was based on Fourier's law, as presented in Equation (3.8) (Dubi & Ventra, 2009).

$$Q_{loss} = \frac{\Delta T}{R_t} \tag{3.8}$$

where R_t is the total thermal resistance (K/W) due to convection and conduction, determined by Equations (3.9) to (3.11) (Guo *et al*., 2010).

$$R_{t,total} = R_{t,conv.} + R_{t,cond.} \tag{3.9}$$

$$R_{t,cond} = \frac{\ln \frac{r_2}{r_1}}{2\pi Lk} \tag{3.10}$$

$$R_{t,conv.} = \frac{1}{2\pi r_2 Lh} \tag{3.11}$$

where L, k, and h are the length of the adsorption column (m), thermal conductivity of stainless steel (W/ (m.K)), and convective heat transfer (W/ (m^2.K)), respectively.

The total time required to heat the adsorbent was calculated using Equation (3.12).

$$t = \frac{Q_{total}}{P} \tag{3.12}$$

where t is the total time (seconds), P is the power (W), and $\boldsymbol{Q_{total}}$ is the total heat energy (J).

Table 3.2 shows the calculated design values.

Table 3.2: Calculated Design Values for the Bed Heating System

Parameter	Value
$Q_{adsorbent}$ (J)	617,422
Q_{loss} (W)	305
Q_{total} (W)	3,800
Heater rating (W)	2160
Time (seconds)	180

b) Temperature Control

Figure 3.8 shows the wiring diagram of the temperature control system, which includes a Proportional-Integral-Derivative (PID) (0 to 1300℃) controller, model REX-C100 (accuracy $\pm$ 2%), supported by a solid-state relay (SSR). The controller monitored the temperature and adjusted the power output of the heating elements accordingly to maintain the desired temperature range. The SSR provided electrical isolation between the control circuitry of the PID controller and the load circuit. This protected the controller from electrical surges caused by the load, reducing interference while ensuring the safety of the control system.

Three K-type thermocouples (-200℃ to 1200℃, $\pm$ 0.01 ℃) were placed at 30 cm, 50 cm, and 70 cm from the feed end, and connected to the PID, to measure the temperature variations inside the bed. Three equally spaced band heaters, each rated at 720 W, were positioned at 10 cm, 50 cm, and 90 cm to heat the adsorption column.

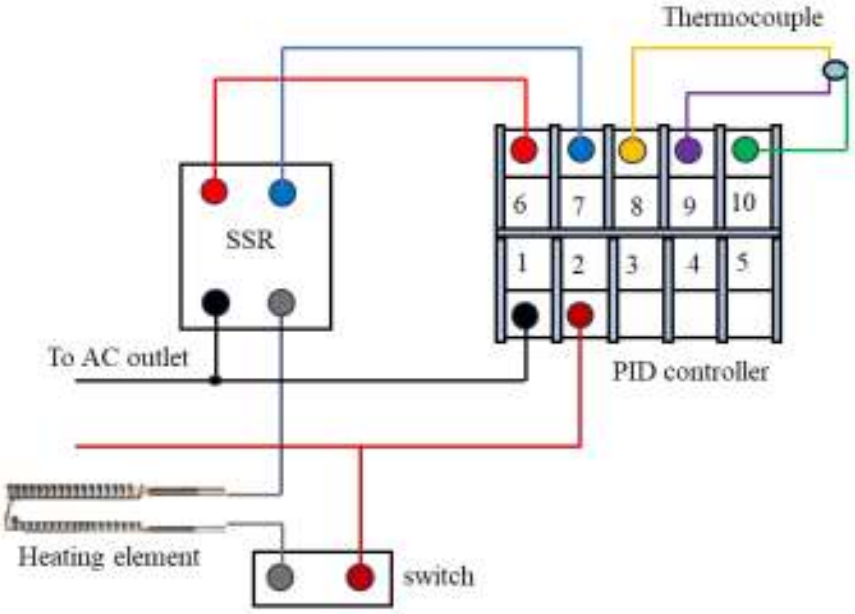

Figure 3.8: Temperature Control Wiring Diagram

c) Thermal Insulation

The adsorption column was insulated during breakthrough experiments to validate the simulation model. This is crucial as the adsorption process is exothermic. Equation (3.13), based on Fourier's law, represents the heat transfer rate for radial conduction across a cylindrical wall and convection heat loss due to air flow. A thermal conductivity of 15 W/m. K was adopted for stainless steel (k_1). Fiberglass wool was used as the insulation material, with a thermal conductivity (k_2) of 0.25 W/m. K. Having a critical radius of 17.5 mm, an insulation thickness of 30 mm was selected to minimize heat loss to the surroundings.

$$\dot{Q}_{with\ insulation} = \frac{T_2 - T_1}{\frac{1}{2\pi L k_1}\left(\ln\frac{r_2}{r_1}\right) + \frac{1}{2\pi L k_2}\left(\ln\frac{r_3}{r_2}\right) + \frac{1}{2\pi r_3 L h}} \qquad 3.13$$

where T_1, T_2, r_1, r_2, r_3, k, L, and h are the temperature of the outer wall, inner wall temperature, inner radius, outer radius of the cylinder, outer radius of the cylinder with insulation, thermal conductivity of the conducting material, the length of the adsorption column, and the convective heat transfer coefficient, respectively.

3.4 Experimental Procedure

The biogas used for the experiments was obtained from the anaerobic digestion of cattle dung and organic waste, mixed with water in a 1:1 ratio in a fixed dome biogas plant. The gas was passed through a desulfurizer and silica pellets for pretreatment, effectively removing hydrogen sulphide and water vapour, respectively, before being stored in a 5 m^3 gas bag. The biogas was primarily composed of carbon dioxide (23.04% v/v), methane (63.27% v/v), nitrogen (10.28% v/v), and oxygen (3.41% v/v), as determined by gas chromatography analysis. The activated carbon pellets and adsorption columns were preconditioned by heating at a temperature of 110°C for one hour to remove moisture and impurities before carrying out the experiments. The adsorbent, weighing approximately 1.7 kg, was then packed into each of the adsorption columns.

3.4.1 Breakthrough Experiments

Breakthrough experiments were conducted to study the main adsorbate concentration at the outlet of the adsorption column. The breakthrough curves were determined based on the carbon dioxide volumetric concentration at the outlet. This involved passing biogas across the adsorption column to establish how long it took before carbon dioxide molecules could be detected in the product gas. The other biogas constituents were assumed to have minimal adsorption capacity on the adsorbent compared to carbon dioxide.

A 20-kW biogas pressure pump (0 to 20 slpm, GreenLeaf Renewable Energy Ltd.) was used to maintain a mean biogas flow rate into the adsorption column. Three flow rates of 5, 12, and 20 standard litres per minute (SLPM) (minimum, average, and maximum flow rates, respectively) were preset by the manufacturer to analyze the transient behaviour of the adsorption bed. A G2.5 mass flow meter (accuracy $\pm$ (3%) was used to measure the gas flow rate before it entered the adsorption column. The desired gas flow rate was set using the flow regulator and valves supplying the biogas to the adsorption column, which were then opened.

The gas composition at the column outlet was monitored using a GASTiger 2000 gas analyser (0.025 to 4 m^3/h, accuracy ±3%). The concentration of carbon dioxide was recorded every 30 seconds until the outlet concentration reached the inlet concentration, indicating saturation of the adsorbent. The biogas flow into the adsorption column was then stopped, and the bed was regenerated for subsequent experiments. The adsorption column was purged with the product gas, primarily composed of methane, flowing counter-current to the feed flow at a maximum flow rate of 20 standard litres per minute (slpm). This decreased the time required for adsorbent regeneration until a carbon dioxide concentration of less than 1% v/v was attained in the waste gas (Ribeiro *et al*., 2014). The adsorption column was then allowed to cool to ambient conditions before subsequent experiments were carried out. The experiments were repeated three times under the same conditions, for the different flow rates to ensure repeatability.

3.4.2 Dynamic Experiments

The thermal swing adsorption cycle, consisting of feed, blowdown, heating, purging, and cooling steps, was adopted for the biogas upgrading process (Zhao *et al*., 2018). The preconditioned activated carbon pellets were filled in the adsorption column, ensuring uniform packing. The band heaters mounted on the adsorption columns were then connected to the power supply terminals for resistive heating up to 60℃. Biogas was introduced in the adsorption column at a flow rate of 12 slpm, and the outlet carbon dioxide concentration was recorded every 30 seconds. The biogas inlet valve was closed when 1 % v/v of carbon dioxide could be detected at the outlet.

To regenerate the bed, all the gas valves were closed, and the power supply to the adsorption column was connected. The column temperature was then monitored using K-type thermocouples to ensure uniform heating at various regeneration temperatures of 40°C, 45°C, 50°C, 55°C, and 60 °C. The time taken to achieve the set regeneration temperature was also recorded to evaluate the total cycle time. The electrification process was controlled using a proportional–integral–derivative temperature controller. A solid-state relay was used to provide electrical isolation to the band

heaters when the desired temperature was achieved. A light indicator was included to indicate the end of the heating step.

The waste valve was then opened to desorb the carbon dioxide from the adsorption column. The column was then purged with part of the product gas flowing counter-current to the feed flow, at a maximum flow rate of 20 slpm. The carbon dioxide concentration of the waste gas and column temperature were monitored using a GASTiger 2000 gas analyser and thermocouples, respectively, every 30 seconds until the concentration was less than 1% v/v. The bed was then allowed to cool to the average ambient temperature of 30℃, before subsequent experiments were carried out. Each experiment was performed in triplicate under identical conditions to ensure repeatability.

3.5 Energy Efficiency Analysis

The energy required to increase the energy density of biogas through upgrading varies across different technologies. Equation (3.14) expresses the energy efficiency equation used to compare these technologies (Rotunno *et al*., 2017; Sun *et al*., 2015). The total energy used during the various upgrading steps, that is, adsorption (pressure pump), electrification/heating (band heaters), and purging (pressure pump), was measured using a wattmeter (Intertek, Power Meter KWE-PM01-US, accuracy $\pm$ 3%). The parasitic loads from the system control unit were also taken into consideration. The energy contents of raw biogas and product gas, primarily composed of methane, were theoretically established based on the volume of gas passed through the adsorption column and the product gas collected (Swedish Gas Technology Centre Ltd (SGC), 2012).

$$\eta = \frac{Energy_{upgraded\ gas}}{Energy_{raw\ gas} + Energy_{upgrading}} \qquad 3.14$$

3.6 Uncertainty Analysis

Uncertainty analysis is crucial for assessing the performance of a system and obtaining reliable experimental data. It helps avoid errors and inaccuracies of measuring

instruments, errors under different working conditions, the improper planning of an experiment, manmade errors, and errors under different working conditions. The measuring equipment and instruments must be calibrated to prevent errors caused by wear and tear. The instrument uncertainty was calculated using Equation (3.15), which considers both systematic and random errors (Drosg, 2009). Appendix III shows pictorial representation of some of the measuring equipment.

$$\sigma_i = \sqrt{B_i^2 + P_i^2} \qquad 3.15$$

where B_i represents the systematic uncertainty, and P_i random uncertainty.

The standard uncertainty, which measures the spread or dispersion of data points in a set of measurements, was evaluated using Equation (3.16) (Drosg, 2009). Three sets of experiments were conducted for each biogas upgrading cycle at different regeneration temperatures.

$$\sigma_i = \sqrt{\frac{\sum_{i=1}^{n}(x_i - \bar{x})^2}{n-1}} \qquad 3.16$$

Where *n* represents the number of data points with values x_i, and $\bar{x}$ represents the mean value of the distribution.

The instrument uncertainties determined in this study are listed in Table 3.3. The total uncertainty of the equipment and the standard uncertainty of the measured column temperature were 5% and 2%, respectively.

Table 3.3: Instrument Used in Data Acquisition and Corresponding Uncertainty

Instrument	Parameter	Accuracy	Resolution	Capacity	Unit	Uncertainty
Thermocouple	Temperature	±0.5 %	0.5	1,100	℃	±0.5%
Mass flow meter	Gas flow rate	±3 %	0.025	4	m^3/h	±3%
Gas analyser	CO_2 concentration	±3 %	0.01	50	mg/m^3	±3%
Power meter	Energy density	±3 %	0.001	9,999	kWh	±3%

3.7 Numerical Simulations

Aspen Adsorption software (version 11) was used to simulate the breakthrough and dynamic experiments of the biogas upgrading process. The feed gas was considered to consist of 23% mol carbon dioxide and 77% mol methane at a temperature of 30℃. Figure 3.9 depicts the schematic setup of the cyclic thermal swing adsorption process.

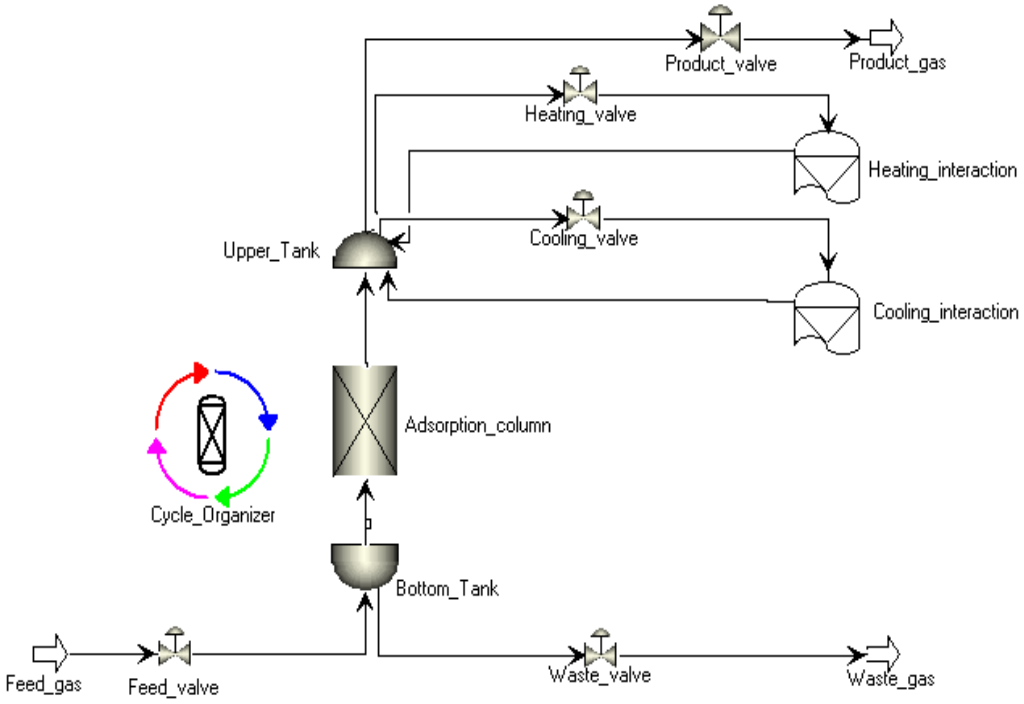

Figure 3.9: One-bed Thermal Swing Adsorption Model in Aspen Adsorption

The thermal swing adsorption model included a combination of mass, momentum, and energy equations, along with adsorption equilibrium and kinetics models. They were informed by the initial and boundary conditions to define the adsorption and desorption behaviours. The partial differential equations were discretized using the Upwind Differential Scheme 1 method in the spatial coordinate with 20 nodes per adsorption bed. The number of nodes was determined from a grid-independent evaluation that considered variation in the performance indicators and the total computation time. The subsequent differential algebraic equations obtained where then solved by the implicit Euler integration method together with the Newton Nonlinear Solver.

The adsorption process was conducted in a bed with a single layer of activated carbon as the adsorbent material. Table 3.4 presents detailed specifications of the bed and adsorbent used to develop the numerical model. The thermodynamic properties of biogas, including density and specific heat capacity, were determined by Aspen Adsorption software based on the specified gas composition. The thermal swing adsorption process is a cyclic, dynamic process; therefore, the cyclic steady state was used to determine the process status in place of the steady-state configuration. The cyclic state configuration ensured that the algebraic and differential variables of the thermal swing adsorption process had the same values at the end of a cycle and the beginning of the consequent cycle.

In developing the mathematical model of the thermal swing adsorption process, the following main assumptions were made:

- The gas mixture behaved as an ideal gas.
- The porosity of the bed was assumed to be constant.
- The radial dispersion for both concentration and temperature gradients was assumed to be negligible because the column radius was relatively small compared to the length, ensuring radial gradients equilibrate quickly.
- The fluid dynamics followed the axial dispersion plug flow model in the bed.
- The properties of the adsorbent throughout the bed remained constant.
- The Langmuir-Freundlich model, as presented in Equation 3.5, described the competitive adsorption behavior.
- The lumped linear driving force (LDF) kinetic model presented the mass transfer rate, where the diffusion described the mass transfer coefficient in the film, macropore, and micropores.
- The mass transfer coefficient was constant, and the adsorption process was non-isothermal with gas and solid conduction.
- Ergun's equation was used to model pressure drop along the bed.
- The heat capacities of the adsorbent and the adsorbate phase were assumed to be constant.
- The heat of adsorption was assumed to be constant for both carbon dioxide and methane.

Table 3.4: Numerical Model Specifications of the Bed and Adsorbent

Parameter	Symbol	Value	Unit
Bed height	H_b	1	m
Internal bed diameter	D_b	0.06	m
Wall thickness	W_t	0.002	m
Inter-particle voidage	ε_b	0.41	m^3void/m^3bed
Intra-particle voidage	ε_p	0.42	m^3void/m^3bed
Particle radius	r_p	0.002	m
Adsorbent density	ρ_s	1000	kg/m^3
CH_4 mass transfer coefficient	MTC_{CH_4}	0.375	1/s
CO_2 mass transfer coefficient	MTC_{CO_2}	0.058	1/s
Adsorbent specific heat capacity	Cp_s	3.5	kJ/kg.K
Adsorbent thermal conductivity	k_s	0.119	W/m.K
Gas phase heat conductivity	k_g	0.0344	W/m.K
Wall density	ρ_w	7800	kg/m^3
Adsorbent shape factor	ψ	0.83	-

3.4.1 Governing Equations

The different models used in this study and the calculated constants are discussed below (Verdade, 2020).

a) Mass Balance

Equation (3.17) presents the four main terms accounted for in the material balance along the adsorption bed: axial dispersion contribution, convection, gas phase accumulation, and adsorbed phase accumulation (AspenTech, 2009).

$$-\varepsilon_b D_{ax,i}\frac{\delta^2 C_i}{\delta z^2}+\frac{\delta\left(v_g C_i\right)}{\delta z}+\left[\varepsilon_b+[1-\varepsilon_b]\varepsilon_p\right]\frac{\delta C_i}{\delta t}+\rho_p(1-\varepsilon_b)\frac{\delta q_i}{\delta t}=0 \qquad 3.17$$

where ε_b is the bed voidage, ε_p is the particle voidage, C_i is the gas phase concentration of component i (mol/m^3), and v_g is the superficial gas velocity (m/s).

Axial dispersion coefficient D_{ax} was given by Equation (3.18) below.

$$D_{ax}=2v_i r_p\left(\frac{20}{Re.Sc}+\frac{1}{2}\right);Re=\frac{2r_p v_g \rho_g}{(1-\varepsilon_i)\mu};Sc=\frac{\mu}{\rho_g D};D=\frac{2.66\times10^{-5}T^{\frac{3}{2}}}{PM_{AB}^{0.5}\sigma_{AB}^2\Omega_D} \qquad 3.18$$

where v_i is the gas velocity of component i (m/s), r_p is the adsorbent particle radius (m), Re is the Reynold's number, Sc is the Schmidt number, ρ_g is the gas phase molar density (mol/m^3), ε_i is the total porosity, μ is bulk gas phase mixture viscosity (kg/(m.s)), D is the mass diffusivity (m^2/s), T is the absolute temperature (K), P is the pressure (bar), M_{AB} is the reduced molecular weight of the gas pair A (methane) and B (carbon dioxide) (kg/mol), σ_{AB} is the characteristic length of the gas pair (nm), and Ω_D is the dimensionless collision integral, a function of temperature and intermolecular force.

The mass transfer driving force due to solid phase loading and gas phase concentration was modelled as a single linear driving force coefficient, presented in Equation (3.19) (Shen *et al*., 2018). Values of the mass transfer coefficient (MTC) were estimated by considering resistances in the external fluid film and the macropore of the particle, thereby accounting for both molecular and Knudsen diffusion.

$$\frac{\partial q_i}{\partial t} = MTC_i(q_i^* - q_i) \qquad 3.19$$

where q_i^* is the equilibrium adsorbent loading of the component i (mol/kg), and MTC_i is the mass transfer coefficient of the component i. The estimated mass transfer values for methane and carbon dioxide are presented in Table 3.4.

b) Momentum Balance

The pressure drop through the adsorbent bed was estimated by the Ergun equation, Equation (3.20), as it accounts for both laminar and turbulent flow (Bennett *et al*., 1986). Furthermore, it takes into account the effect of particle size on the flow.

$$\frac{\partial p}{\partial z} = -\left(\frac{150 \times 10^{-5}\mu_g(1-\varepsilon_b)^2}{\left(2r_p\varphi\right)^2{\varepsilon_b}^3}v_g + \frac{1.75 \times 10^{-5}M_w\rho_g(1-\varepsilon_b)}{\left(2r_p\varphi\right)^2{\varepsilon_b}^3}v_g^2\right) \qquad 3.20$$

where φ is the shape factor of the particle, M_w is the molecular weight of the gas (kg/mol)

c) Energy Balance

The energy balance between the gas and solid phases was considered and discussed below.

i. Gas Phase Energy Balance

The energy balance of the gas phase in the bed, presented by Equation (3.21), considered the axial thermal conduction, the convection, P-V work compression, thermal accumulation in the gas phase, heat transfer between gas and solid, and heat transfer between gas and the internal wall of the adsorber (AspenTech, 2009).

$$-k_g\varepsilon_b\frac{\delta^2 T_g}{\delta z^2}+C_{vg}v_g\rho_g\frac{\delta T_g}{\delta z}+P\frac{\delta v_g}{dz}+C_{vg}\rho_g\left(\varepsilon_b+[1-\varepsilon_b]\varepsilon_p\right)\frac{\delta T_g}{\delta t}+HTCa_p\left(T_g-T_s\right)+a_{HX}Q_{HX}=0 \quad 3.21$$

where k_g is the gas phase thermal conductivity (W/(m.K)), C_{vg} is the specific heat capacity of the gas (J/(kg.K)), a_p is the specific surface area of the particles (m^2/m^3), a_{HX} is the heat exchanger surface area per unit volume (m^2/m^3), and Q_{HX} is the heat exchange rate (W/m^3).

The heat transfer coefficient (HTC), Equation (3.22), was estimated by the software based on the Colburn j-factor correlation (Malinowski *et al*., 1994).

$$HTC = jC_{pg}v_g\rho_g Pr^{-\frac{2}{3}} \quad 3.22$$

where C_{pg} is fluid phase heat capacity (J/kg/K), ρ_g is fluid-phase density (kg/m^3), v_g is fluid phase velocity (m/s), Pr is the dimensionless Prandtl number. The j-factor and Prandtl number were determined based on Equations (3.23) and (3.24), respectively (AspenTech, 2020).

$$Pr = {\mu C_{vg}}\Big/{k_g} \quad 3.23$$

j was modelled as;

$$j = 1.66Re^{-0.51} \text{for Re} < 190, \text{otherwise } j = 0.983Re^{-0.41} \quad 3.24$$

ii. Solid Phase Energy Balance

The solid energy balance on the adsorbent, presented in Equation (3.25), considered the axial thermal conduction, thermal accumulation in the solid phase, thermal accumulation by the enthalpy of adsorption, and heat transfer between the gas and the solid (AspenTech, 2009).

$$-k_s \frac{\delta^2 T_s}{\delta z^2} + \rho_s C_{ps} \frac{\delta T_s}{\delta t} + \rho_s \sum_{i=1}^{n} \left(\Delta H_i \frac{\delta q_i}{\delta t} \right) - HTCa_p \left(T_g - T_s \right) = 0 \qquad 3.25$$

where the specific particle surface per unit volume of bed is; $a_p = (1 - \varepsilon_i) \frac{3}{r_p}$, k_s is the solid thermal conductivity (W/(m.K)), ρ_s is the adsorbent density (kg/m^3), ΔH_i is the isostatic heat of adsorption of component i (kJ/mol), T_g is the temperature of the gas mixture (K), T_s is the temperature of the adsorbent (K), and n represents the number of heterogeneous chemical reactions happening in the solid phase, contributing to the heat generation.

The heat of the adsorbed phase for each component was given by Equation (3.26) (AspenTech, 2020).

$$H_k = \rho_s C_{pak} \omega_i \frac{\delta T_s}{\delta t} \qquad 3.26$$

where H_k is the heat accumulation in the solid phase (W/m^3), C_{pak} is the heat capacity of the adsorbed phase component in J/(kg. K), and ω_k is the mass fraction of i in the solid phase.

The wall energy balance presented by Equation (3.27) considers the axial thermal conduction along the wall, thermal accumulation in the wall material, heat transfer between gas and wall, and heat transfer between the wall and the surrounding environment (Verdade, 2020).

$$-k_w \frac{\delta^2 T_w}{\delta z^2} + C_{pw} \rho_w \frac{\delta T_w}{\delta t} - h_w \frac{4 D_B}{(D_B + W_r)^2 - {D_B}^2} \left(T_g - T_w \right) + h_b \frac{4 (D_B + W_r)^2}{(D_B + W_r)^2 - {D_B}^2} (T_w - T_{env}) = 0 \qquad 3.27$$

where k_w is the thermal conductivity of the wall (W/(m.K)), T_w is the temperature of the wall (K), D_B is the diameter of the adsorption column (m), W_r is the wall thickness (m), and T_{env} is the external environment temperature (K).

iii. Heat Transfer Model

The heat transfer process was generally governed by Equation (3.28) (Aspen, 2020). A jacket heat exchanger was used to heat and cool the bed.

$$Q = UA\Delta T_{lm} \tag{3.28}$$

Where Q is the heat transfer rate (W), U is the overall heat transfer coefficient ($\mathrm{W/m^2K}$), A is the heat transfer area ($\mathrm{m^2}$), and ΔT_{lm} is the log mean temperature difference, determined by Equation (3.29) (Rohsenow *et al*., 1998).

$$\Delta T_{lm} = \frac{\Delta T_1 - \Delta T_2}{\ln \frac{\Delta T_1}{\Delta T_2}} \tag{3.29}$$

$$\Delta T_1 = \Delta T_{jacket,in} - \Delta T_{gas,in}$$

$$\Delta T_2 = \Delta T_{jacket,out} - \Delta T_{gas,out}$$

The overall heat transfer coefficient U incorporates resistances to the heat transfer system as shown in Equation (3.30) (AspenTech, 2009).

$$\frac{1}{U} = \frac{1}{h_{jacket}} + \frac{t_{wall}}{k_{wall}} + \frac{1}{h_{column}} \tag{3.30}$$

where h_{jacket} is the heat transfer coefficient of the jacket fluid ($\mathrm{W/m^2K}$), t_{wall} is the thickness of the wall separating the jacket fluid and the adsorbent (m), k_{wall} is the thermal conductivity of the wall material (W/m. K), and h_{column} is the effective heat transfer coefficient in the adsorbent bed, including the gas phase and adsorbent particles ($\mathrm{W/m^2K}$).

3.4.2 Initial and Boundary Conditions

The initial conditions of the adsorption column, describing the state of the system at the start of the cycle, for $0 < z < L$ and $t = 0$ are presented in Equations (3.31) to (3.35) below (Aspen, 2020). Table 3.5 defines the properties of the various streams of the developed simulation model. The boundary conditions for the multiple steps, which influence the system throughout the cyclic process, are presented in Table 3.6.

$$y_i|_{t=0} = 0 \tag{3.31}$$

$$n_i|_{t=0} = 0 \tag{3.32}$$

$$T_{gas}|_{t=0} = T_{gas,0} \tag{3.33}$$

$$T_{solid}|_{t=0} = T_{solid,0} \tag{3.34}$$

$$T_{wall}|_{t=0} = T_{wall,0} \tag{3.35}$$

where $\boldsymbol{y_i}$ is the mole concentration of component i in the gas phase, $\boldsymbol{n_i}$ is the amount of moles of component i adsorbed on the solid surface of the adsorbent, and $\boldsymbol{T_{gas}}$, $\boldsymbol{T_{solid}}$, and $\boldsymbol{T_{wall}}$ are the temperatures of the gas, solid/adsorbent, and wall respectively.

Table 3.5: Numerical Model Streams Definition

Stream	**Composition** ($\%_{vol}$)	**Temperature** (℃)	**Flowrate** (mol/s)	**Pressure** (bar)
Feed	77CH_4:23 CO_2	30	0.024	1.2
Product	99CH_4:1 CO_2	30	variable	1.15
Purge	99CH_4:1 CO_2	30	variable	1.2
Waste	variable	variable	variable	1.0

Table 3.6: TSA Process Boundary Conditions

Step	Z=0	Z=L
Adsorption	$C_i(t,0) = C_i^{feed}(t)$	$\frac{\partial C_i}{\partial z}(t,L) = 0$
	$T(t,0) = T^{feed}(t)$	$\frac{\partial T_g}{\partial z}(t,L) = 0$
Blowdown	$\frac{\partial C_i}{\partial z}(t,0) = 0$	$\frac{\partial C_i}{\partial z}(t,L) = 0$
	$\frac{\partial T_g}{\partial z}(t,0) = 0$	$\frac{\partial T_g}{\partial z}(t,L) = 0$
Heating	$\frac{\partial C_i}{\partial z}(t,0) = 0$	$\frac{\partial C_i}{\partial z}(t,L) = 0$
	$\frac{\partial T_g}{\partial z}(t,0) = 0; \frac{\partial T_g}{\partial r}(t,0) = 0$	$\frac{\partial T_g}{\partial z}(t,L) = 0;$ $-k_{eff}\frac{\partial T_g}{\partial r}\|_{r=R} = h_{hx}(T - T_{steam})$ $T_{gas} = T_{adsorbent} = T$
Purge	$\frac{\partial C_i}{\partial z}(t,0) = 0$	$\boldsymbol{C_i(t,L) = C_i^{purge}(t)}$
	$\frac{\partial T_g}{\partial z}(t,0) = 0$	$T(t,L) = T^{purge}(t)$
Cooling	$\frac{\partial C_i}{\partial z}(t,0) = 0$	$\frac{\partial C_i}{\partial z}(t,L) = 0$
	$T(t,0) = T^{coolant}(t)$	$\frac{\partial T_g}{\partial z}(t,L) = 0$
		$-k_{eff}\frac{\partial T_g}{\partial r}\|_{r=R} = h_{hx}(T - T_{water})$ $T_{gas} = T_{adsorbent} = T$

3.6.1 Simulation Procedure

The five-step cyclic configuration adopted for the dynamic biogas upgrading process is discussed below.

1. Adsorption: Upon defining the various stream configurations and boundary conditions in the developed model, the process was initialized. The feed valve was then opened to allow for biogas flow across the adsorption column. The product valve was open, and the waste valve was closed. The adsorbed carbon dioxide accumulated on the adsorbent, and the product consisted primarily of methane. The adsorption step duration was 90 seconds, based on the recommended 30% to 60% range of the breakthrough time (Li *et al*., 2011; Shen *et al*., 2018).
2. Blowdown: The waste valve was then opened and all other valves closed to allow for counter-current blowdown of adsorbed carbon dioxide. The blowdown step duration was 20 seconds, sufficient to reduce the adsorption

column to atmospheric pressure of 1 bar. Furthermore, this allowed for depressurization of the adsorption column and a slight decrease in temperature due to adiabatic expansion during depressurization.

3. Heating: The adsorption column was then heated using steam via a heat exchanger to desorb carbon dioxide from the adsorbent completely. During this step, the feed and product valves were closed, with the waste valve open, to minimize the significant increase in bed pressure and ensure the thermal stability of the adsorbent. The heating step duration was varied for the different regeneration temperatures under investigation. The waste stream contained a high concentration of carbon dioxide and a fraction of methane.
4. Purging: The counter-current purging step involved passing a fraction of the product gas through the adsorption column to enhance adequate desorption and facilitate the removal of residual adsorbed carbon dioxide. Counter-current purging has been identified as a method to achieve higher product purity, as most of the adsorbate is concentrated at the lower end of the adsorption column (Yin *et al*., 2015). The product and waste gas valves were opened during this step, and all other valves were closed. The fraction of product methane used during the purging step was varied to evaluate its influence on the performance indicators.
5. Cooling: The bed was then cooled using water via a heat exchanger to return the system to the initial operating temperature of 30℃, for the subsequent cycle. The duration of the cooling step varied for the different regeneration temperatures considered, with the highest regeneration temperature considered having the longest cooling time.

3.6.2 Convergence Criteria

The dynamic simulations were carried out until a cyclic steady state (CSS) was achieved to ensure the stability of the process performance indicators. Equation (3.36) represents the relative tolerance (δ) (Shen *et al.*, 2018). In this study, a relative tolerance of $\delta = 1 \times 10^{-5}$ was set for both the thermal and concentration profiles of successive cycles. The CSS convergence was achieved after 45 simulation cycles.

$$\int_0^L n_i\,\delta z|_{(nc-1)th\ cycle} - \int_0^L n_i\,\delta z|_{(nc)th\ cycle} < \delta \qquad 3.36$$

Where nc is the number of cycles.

3.6.3 Parametric Study

A parametric study was conducted to systematically analyze the sensitivity of the biogas upgrading model to variations in key operating parameters. The parameters examined were particle radius, regenerating temperature, and purge-to-feed flow rate ratio (P/F). These variables play a critical role in the thermal swing adsorption process, as they directly influence methane purity and recovery. Systematic evaluation of the selected parameters allowed the model behaviour to be assessed under varying operating conditions and enable clear identification of their individual effects on methane purity and recovery.

Objective two sort to establish the relationship between particle size, bed voidage, and biogas upgrading performance. A monolayer particle radius range of 1 mm to 9 mm was selected for this study, based on the reviewed literature (Gan *et al*., 2017; Valverde *et al*., 2024; Wasefi *et al*., 2022). The mean bed voidage was varied for each particle radius based on the correlation established for cylindrical particles, as presented in Equation (3.37) (Benyahia & O'Neill, 2005).

$$\varepsilon_m = 0.373 + \frac{1.703}{\left(\frac{d_t}{d_p} + 0.611\right)^2} \qquad 3.37$$

where ε_m is the bed voidage, d_t is the column diameter and d_p is the particle diameter.

Figure 3.10 presents the variation in bed voidage against particle size in a 6 cm diameter column. An increase in bed voidage was observed with an increase in particle radius. Particles with smaller radii pack more efficiently, thereby enhancing the adsorption surface area. On the other hand, a large particle radius results in a higher bed voidage, leading to reduced pressure drop and minimal flow resistance.

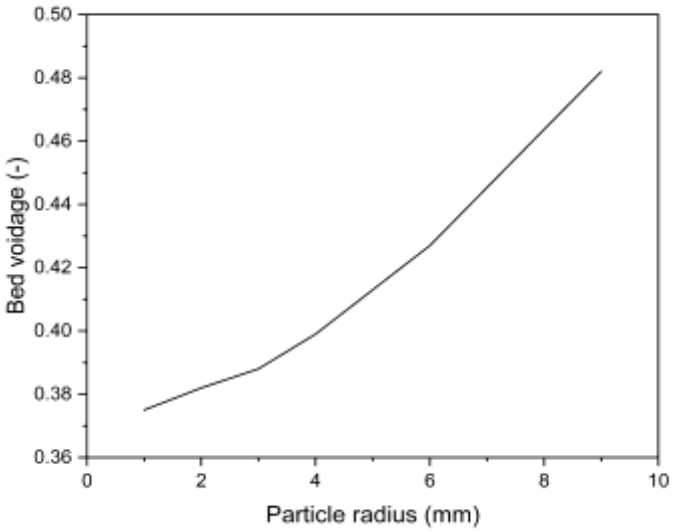

Figure 3.10: Variation of Bed Voidage against Particle Radius

For each simulation run, a specific particle radius and its corresponding bed voidage were set in the model. The thermal swing adsorption model was then executed under these conditions to simulate the biogas upgrading process. This process was repeated systematically for all combinations of particle radius and bed voidage.

Objective three sought to establish the relationship between the purge-to-feed flow rate ratio and the biogas upgrading process. The fraction of purge gas used during desorption has been identified to influence both the product purity and recovery significantly (Shah *et al.*, 2021). An opposing trend between methane purity and recovery was observed as the purge-to-feed flow rate ratio increased. This makes it a crucial variable as the biogas upgrading process aims to maximize both the methane purity and recovery. A purge-to-feed flow rate ratio range of 0.1 to 0.7 was adopted for this study based on a literature review (Durán *et al.*, 2022; Shen *et al.*, 2018). It is essential to comprehend how the purge-to-feed flow rate variable affects temperature variation along the bed during regeneration, and consequently, the process performance indicators.

The regeneration temperature plays a critical role in both the overall performance of the biogas upgrading process and the energy consumed. An ideal regeneration

temperature should allow for complete desorption of the adsorption bed while minimizing energy requirements. In this study, the effect of regeneration temperature was systematically evaluated for both Objective 2, which focused on particle size and bed voidage, and Objective 3, which examined the purge-to-feed flow rate ratio. For the simulation runs, the steam regeneration temperature in the heat exchanger was varied at 77, 127, 177, and 227°C. These values correspond to the experimental resistive heating bed temperatures of 45, 50, 55, and 60°C, respectively, ensuring consistency between experimental and simulation conditions. This approach allowed a comprehensive assessment of how regeneration temperature interacts with particle radius, bed voidage, and purge-to-feed flow rate ratio to influence the biogas upgrading process.

3.6.4 Performance Indicators

The dynamic results of the biogas upgrading process are converted into performance indicators in the steady state. Methane purity and recovery performance indicators, presented by Equations (3.38) and (3.39), respectively, represented the outcome of varying these operating conditions (Abd *et al*., 2023). All other cyclic configurations were held constant for all the experiments.

$$CH_4\ purity(\%) = \frac{n_{CH_4}\ in\ the\ product\ stream}{n_{CH_4+CO_2}\ in\ the\ product\ stream} x100 \qquad 3.38$$

$$CH_4\ recovery(\%) = \frac{n_{CH_4}\ in\ the\ product\ stream}{n_{CH_4}\ in\ the\ feed\ stream} x100 \qquad 3.39$$

Where n is the number of moles.

3.7 Validation of Numerical Model

The developed numerical model was validated using experimental data. Quantitative analysis was performed using the Average Standard Deviation (ASD) and Mean Absolute Percentage Error (MAPE), as calculated by Equations (3.40) and (3.41), respectively, to compare the experimental and simulated data. This approach was used

in other studies to validate simulation models (Baena-Moreno *et al*., 2023; Sakiewicz *et al*., 2020).

$$ASD = \sqrt{\frac{\sum(x - mean)^2}{n}} \tag{3.40}$$

$$MAPE = \frac{1}{n}\sum_{i=1}^{N}\left|\frac{A_i - P_i}{A_i}\right| \tag{3.41}$$

3.8 Optimization Approach

The response surface methodology is a suitable optimization tool for the design of experiments (DOE), yielding fewer experiments with reasonably accurate results. In addition, the technique allows for multi-objective optimization (Njuguna, 2024). Figure 3.11 presents the flow chart adopted in this study. The Box-Behnken design, as described by the Design of ExpertTM, was selected to model the interaction effect of particle size, regenerating temperature, and purge-to-feed flow rate ratio on the performance of the biogas upgrading process. It is commonly used to optimize three or more process parameters, employs a factorial design, but with fewer runs compared to a full factorial design (Mutunga *et al*., 2025). This was achieved by combining three orthogonal arrays, where each factor is examined at three levels: low, medium, and high. The number of experimental runs required was determined based on Equation (3.42).

$$N = 2k(k - 1) + C_0 \tag{3.42}$$

where C_0 is the number of central points, k is the number of input variables, and N is the number of runs.

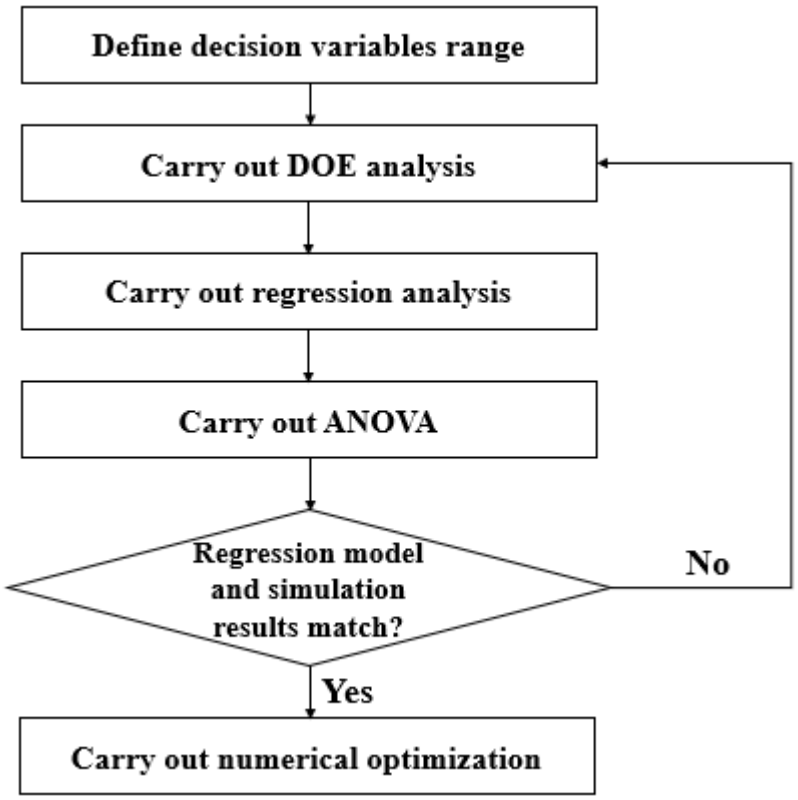

Figure 3.11: Response Surface Methodology Flow Chart

Source: (Mutunga et al., 2025)

Based on the preliminary evaluation of the studied parameters, the identified range of the independent variables is presented in Table 3.7. The responses to the 15 runs were obtained using the validated model in Aspen Adsorption. Simulation results of each set of conditions were input into the Box-Behnken model to generate a polynomial quadratic regression equation presented by Equation (3.43) (Polat & Sayan, 2019). The equation describes the effect of these parameters on the process indicators and identifies optimal points.

$$Y = b_0 + \sum_{i=1}^{n} b_i x_i + \sum_{i=1}^{n} b_{ii} {x_i}^2 + \sum_{i=1}^{n-1} \sum_{i=j}^{n} b_{ij} x_i x_j + \emptyset \qquad 3.43$$

where Y is the output response, b_0, b_i, b_{ii}, and b_{ij} are constant, linear, quadratic, and interaction coefficients, respectively, x is the decision parameter, n is the number of input variables, and ϕ is a statistical error.

Table 3.7: Range of Independent Variables

Parameter	Unit	Value
Particle radius (A)	mm	1 - 9
Regenerating temperature (B)	℃	77 - 227
Purge/Feed flow rate ratio (C)	-	0.1 - 0.7

Analysis of variance (ANOVA) was performed to assess the statistical significance of the process parameters, their interaction, and the adequacy of the fitted model in predicting the responses. Statistical metrics, including the degree of freedom (df), the sum of squares (SS), contribution percentage, F value, and p-value, as presented in Equations (3.44) to (3.49), were used to evaluate the significance of the model. F-value is described as the ratio that compares the variability explained by the model to the unexplained/error variability, as shown in Equation (3.44). Similarly, the model was considered significant for a p-value less than 0.05 (Müller *et al*., 2022).

$$F\ value = \frac{MS_{model}}{MS_{error}} \tag{3.44}$$

$$MS_{model} = \frac{SS_{regression}}{dF_{regression}} \tag{3.45}$$

$$MS_{error} = \frac{SS_{residual}}{dF_{residual}} \tag{3.46}$$

$$SS_{regression} = SS_{total} - SS_{error} \tag{3.47}$$

$$SS_{total} = \sum_{i=1}^{n} (y_i - \bar{y})^2 \tag{3.48}$$

$$SS_{error} = \sum_{i=1}^{n} (y_i - \hat{y}_i)^2 \tag{3.49}$$

where SS and dF are the sum of squares and degree of freedom, respectively. y_i is the observed response for the ith observation, $\bar{y}$ is the mean of all observed responses, and $\hat{y}_i$ is the predicted response based on the model.

A higher % contribution, calculated based on Equation (3.50), indicated that the factor had a greater influence on the response.

$$\%\ contribution = \frac{SS_{factor}}{SS_{total}} \times 100 \tag{3.50}$$

where SS_{factor} and SS_{total} are the total variation in a response and the sum of squares for each factor or interaction, respectively.

The coefficient of determination (R^2), Equation (3.51), represents the proportion of variation in the response variable explained by the model. The value of R^2 is usually between 0 and 1. The adjusted R^2, described by Equation (3.52), is a modification of R^2, that accounts for the number of terms in the model. It adjusts R^2 by penalizing for additional terms that do not significantly improve the model fit, making it useful for comparing models with different numbers of predictors. A regression model having a value of R^2_{adj} larger than 0.9 is considered a highly accurate model for predicting the response output (Njuguna *et al*., 2023). A model is also regarded as accurate if a value of less than 0.2 exists between the predicted coefficient of determination, $R^2_{predicted}$, and R^2_{adj} (Njuguna *et al*., 2023).

$$R^2 = 1 - \frac{SS_{error}}{SS_{total}} \tag{3.51}$$

$$R^2_{adj} = 1 - \frac{(1 - R^2)(n - 1)}{n - k - 1} \tag{3.52}$$

where n and k are the total number of observations and predictors, respectively.

Upon satisfactory comparison between the regression model and the simulation results, multi-objective optimization was carried out to maximize the response outputs. The optimal results were then compared with those obtained through simulation using

the developed model in Aspen Adsorption. This validated the optimized model configuration.

CHAPTER FOUR

RESULTS AND DISCUSSIONS

4.1 Overview

This chapter presents results obtained from the experimental study and numerical simulation of the biogas upgrading framework presented in the previous chapter. The properties of activated carbon adsorbents are presented and discussed. The developed numerical model was validated using experimental results. Findings of the parametric study and optimization process are also presented and discussed.

4.2 Experimental Study

The experimental measurements analyzed included the properties of the adsorbent material and the analysis of both carbon dioxide and temperature profiles during the cyclic biogas upgrading process. Additionally, the cycle time and energy requirements for various cyclic configurations were evaluated and discussed.

4.3 Adsorbent Properties

The nitrogen adsorption–desorption isotherms of the activated carbon pellets are shown in Figure 4.1. The sudden increase in the adsorption curve up to a relative pressure of 0.1 represents saturation and single-layer adsorption. In contrast, the near-linear middle section, with a relative pressure range of 0.1 to 0.9, indicates a gradual increase in multilayer adsorption, suggesting the presence of mesopores. The presence of macropores is indicated by the sharp rise in the relative pressure in the range of 0.9 to 1.

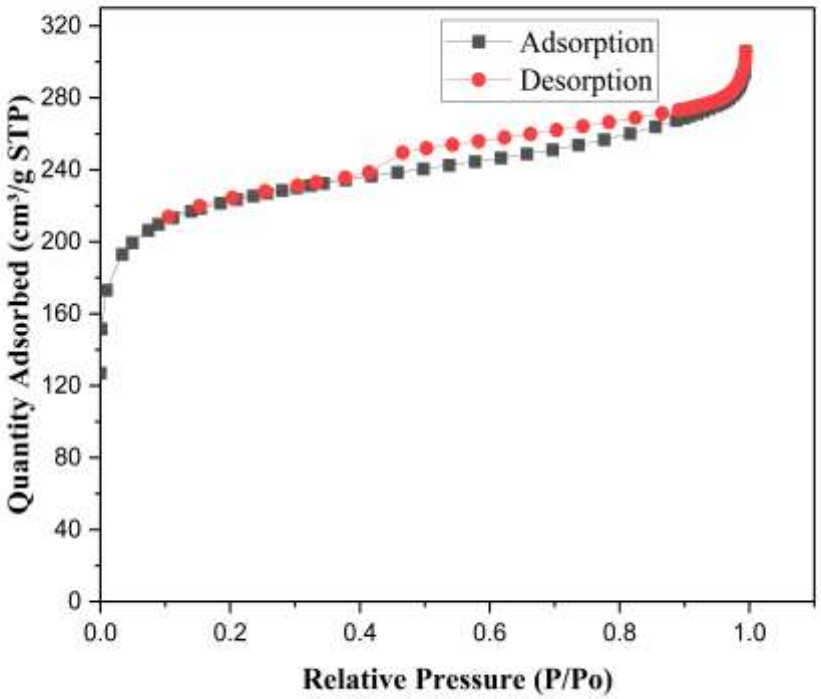

Figure 4.1: Nitrogen Adsorption–Desorption Isotherm on Adsorbent

At the interval range of 0.43 to 0.9 relative pressure, the desorption isotherm is closely separated from the adsorption isotherm owing to the cavitation phenomena. The type H4 hysteresis loop between the adsorption and desorption curves at this interval is attributed to pore networks consisting of micropores and mesopores that were not filled with pore condensate. Wider hysteresis loops are observed in activated carbon with larger pore diameters, indicating the presence of more mesopores (Thommes *et al*., 2015).

The isotherms were categorized as type IV isotherms and type II(b) in the updated classification based on the International Union of Pure and Applied Chemistry (IUPAC) 2015 classification standards for adsorption–desorption isotherms and hysteresis loops shown in Appendix IV (Rouquerol *et al*., 2014; Thommes *et al*., 2015). They represent the physisorption of gas on the adsorbent, resulting from unrestricted monolayer–multilayer adsorption, and the coexistence of micropores and mesopores (Satayeva *et al*., 2018). Similar isotherms were obtained for activated

carbons derived from rice husks and waste sugarcane bagasse in related studies from the literature (Gholami *et al*., 2022; McLaren *et al*., 2021; Song *et al*., 2021).

Table 4.1 lists the measured pore widths, surface areas, and pore volumes of the activated carbon pellets. The BET method for the surface area analysis of the adsorbent, recommended for type II and IV(a) isotherms, indicated a total surface area of 794 m^2/g. This was attributed to the presence of a large distribution of pores ranging across micropores, mesopores, and macropores (McLaren *et al*., 2021). The obtained total surface area was within the range of 500 to 850 m^2/g obtained for coconut-shell activated carbon (Dungani *et al*., 2022; Higai *et al*., 2021).

Table 4.1: BET, t-Plot, and BJH Data for Activated Carbon

Parameter	Value
BET surface area (m^2/g)	794
BET adsorption average pore width (nm)	2.1
t-plot micropore surface area (m^2/g)	571
t-plot mesopore/macropore surface area (m^2/g)	222
% t-plot micropore area compared with total	72
t-plot micropore volume (cm^3/g)	0.246
Single-point adsorption total pore volume (cm^3/g)	0.426
BJH adsorption average pore width (4 V/A) (nm)	4.9
BJH adsorption cumulative surface area of pores between 1.7 and 300 nm (m^2/g)	139.7
BJH adsorption cumulative volume of pores between 1.7 and 300 nm (cm^3/g)	0.174

Based on the BJH analysis, the cumulative surface area was 139.7 m^2/g and the cumulative volume was 0.174 cm^3/g, considering pore width in the range of 1.7 to 300 nm. The cumulative surface area represented 18% of the BET surface area. This indicated that the larger surface area was associated with pores outside the width range of 1.7 to 300 nm. Furthermore, t-plot analysis, which provides a better insight into the microporous structure of activated carbon, indicated that 72% of the apparent surface area of the activated carbon was due to the presence of micropores (pores smaller than 2 nm). The total pore volume of 0.426 cm^3/g obtained from this study compared well with that of other coconut shell-derived activated carbons from the literature review, which reported 0.425 cm^3/g (Song *et al*., 2021).

The measured pore distribution, ranging between 1.7 and 300 nm, is shown in Figure 4.2. The average pore size as determined by the BJH method was 4.9 nm. In contrast, the BET analysis showed a smaller average pore width of 2.1 nm. This was consistent with the t-plot analysis, which indicated that 72% of the surface area was associated with micropores. The deviation when compared with the BJH method was because the BJH method significantly underestimates the pore size for narrow mesopores (for pore diameter <∼ 10 nm, the pore size is underestimated by ∼20% to 30%) and considers adsorption and desorption in the relative pressure range of 0.4 to 0.967 *(Thommes et al., 2015)*. This makes the BET analysis a more reliable technique for determining pore width and surface area, and the BJH approach for pore volume analysis.

The data obtained from the proximate analysis of the activated carbon is summarized in Table 4.2. The results met the SNI 06-3730-1995 standard for activated carbon, which requires a maximum volatile matter content of 25%, a maximum moisture content of 15%, and a minimum fixed carbon content of 65%. This was consistent with the results obtained for a coconut shell-derived activated carbon by Aziz *et al.* (Aziz *et al*., 2020).

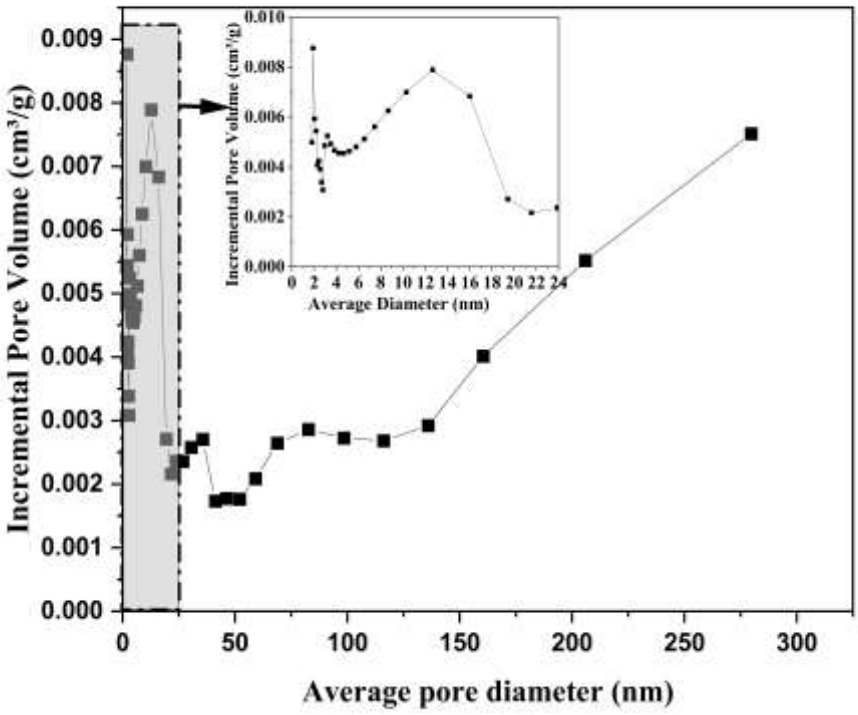

Figure 4.2: BJH Incremental Pore Volume as a Function of Average Pore Width

Table 4.2: Proximate Analysis of Activated Carbon Pellets

Analysis	Air-dried basis (adb) (wt. %)	Std. Deviation
Moisture content	8.68±0.15	0.1583
Ash content	13.63±0.12	0.3357
Volatile matter	12.92±0.33	0.1265
Fixed carbon	64.77±0.15	0.3670

The percentage of volatile matter indicates the amount of substance that evaporates at the treatment temperature, with high levels attributed to low adsorption properties. Similarly, a low moisture content is desirable in activated carbon to minimize clogging and ensure pore formation (Saputra *et al*., 2020). A high ash content is undesirable as it reduces the mechanical strength of activated carbon. Furthermore, it indicates a high mineral composition in the adsorbent, which covers the pores and reduces the adsorption on its surface. The fixed carbon content is influenced by the fraction of volatile matter, moisture content, and ash content of the activated carbon.

SEM analysis was utilized to evaluate the surface morphology of the activated carbon. As shown in Figure 4.3(a), at a magnification of 20,000x, prominent elliptical-shaped pores were evident on the activated carbon. The porous structure indicated that most of the organic volatiles had evolved, resulting in the formation of ruptured surfaces. The pores were shallow, relatively uniform in size, and evenly distributed. Previous studies obtained similar results for coconut shell-activated carbon (Dungani *et al*., 2022).

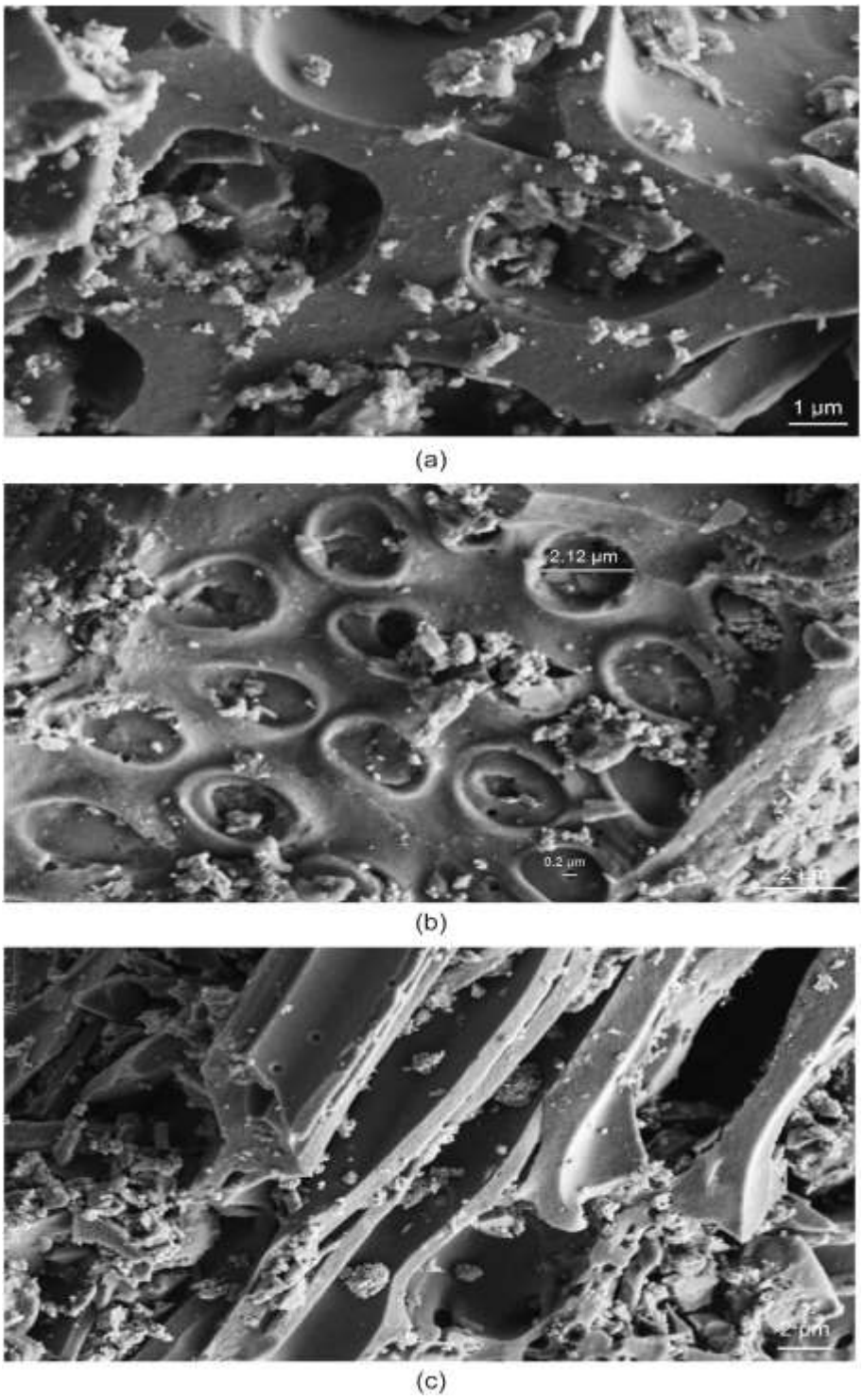

Figure 4.3: SEM Image of CSAC Pellet Sample (a) Magnification 20 K and (b) Magnification 15 K, and (c) Powder Sample

A mixed porous morphology was observed in Figure 4.3 (b) at a magnification of 15 K. The pore width ranged between 0.2 and 2 μm, representing the presence of

mesopores and macropores. Large channels consistent with plant-derived activated carbon were evident in the powder sample micrograph shown in Figure 4.3 (c) (Vivo-Vilches *et al*., 2017). The presence of pores in activated carbon pellets is crucial because they increase the surface area and pore volume, which enhances the adsorption process. The SEM micrographs supported the results obtained from the pore structure analysis using the nitrogen adsorption–desorption isotherms.

The results of the EDS analysis, revealing the composition of the elements present in the activated carbon pellets, are presented in Figure 4.4. Additional sample spectra are presented in Appendix V, and were used to determine the average activated carbon composition. The results revealed that the adsorbent was primarily composed of carbon, oxygen, and calcium, with average contents of 78.87%, 13.98%, and 4.93%, respectively. Other minor elements included sodium, silicon, chlorine, and potassium. High carbon and oxygen compositions are expected for a well-carbonized coconut shell material (Shukla *et al*., 2020; Tsai & Jiang, 2018). The presence of potassium and calcium is crucial for the removal of sulphur compounds from biogas (Papurello *et al*., 2019).

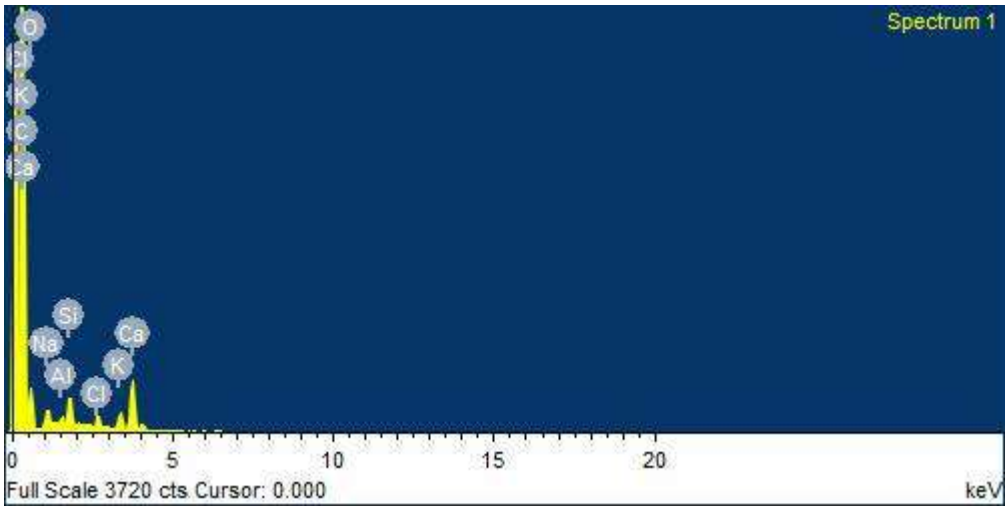

Figure 4.4: EDS Analysis Spectra of CSAC Sample

The fitting parameters of the Langmuir–Freundlich model for methane and carbon dioxide on activated carbon are listed in Table 4.3. A higher maximum adsorption capacity for carbon dioxide of 8.798 × 10^{-3} kmol/kg compared to 6.187 × 10^{-3}

kmol/kg for methane favoured the gas separation process. Similarly, the higher carbon dioxide affinity constant, b_0, of 4.26×10^{-3} compared to 6.55×10^{-4} for methane, represented a higher interaction between the adsorbent and the adsorbate. The heterogeneity index, n, of less than 1 for both methane and carbon dioxide represented a surface with diverse pore structures, consistent with the obtained SEM results. The higher heat of adsorption, ΔH, of 20.96 kJ/mol for carbon dioxide, compared to 14.71 kJ/mol for methane, indicated a stronger adsorbent-adsorbate interaction. Comparing the RSS values between the experimental and fitted data, both methane and carbon dioxide showed RSS values above 0.99. This indicated that the Langmuir–Freundlich model accurately fitted the experimental data within the temperature and pressure range considered in this study.

Table 4.3: CH4 and CO2 Fitting Parameters on Langmuir–Freundlich Model

Adsorbate	**CH_4**	**CO_2**
$q_{m,i}$ (kmol·kg^{-1})	6.187×10^{-3}	8.798×10^{-3}
b_0 (bar^{-1})	6.55×10^{-4}	4.26×10^{-3}
n	7.6151×10^{-1}	7.207×10^{-1}
$\Delta H(kJ.mol^{-1})$	14.71	20.96
RSS	0.9998	0.9969

Figure 4.5 shows the adsorption isotherms of methane and carbon dioxide on the activated carbon. A good agreement was observed between the experimental data and the Langmuir–Freundlich fitting curve. Carbon dioxide had a 45% higher maximum adsorption capacity than methane at saturation. A similar trend was noted at various pressure levels ranging from 6 to 12 bars. This is a beneficial attribute, as more carbon dioxide molecules are adsorbed onto the adsorbent than methane molecules during the biogas upgrading process. A decrease in maximum adsorption capacities for both methane and carbon dioxide was observed as the temperature increased from 30 to 80°C. This was attributed to the exothermic nature of the adsorption process, where high temperatures do not favour the adsorption process. (Zheng *et al*., 2019).

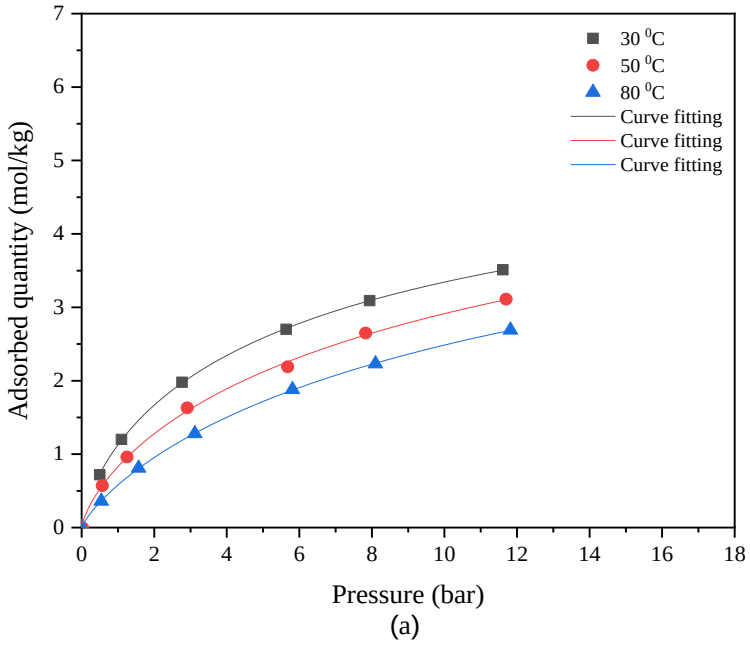

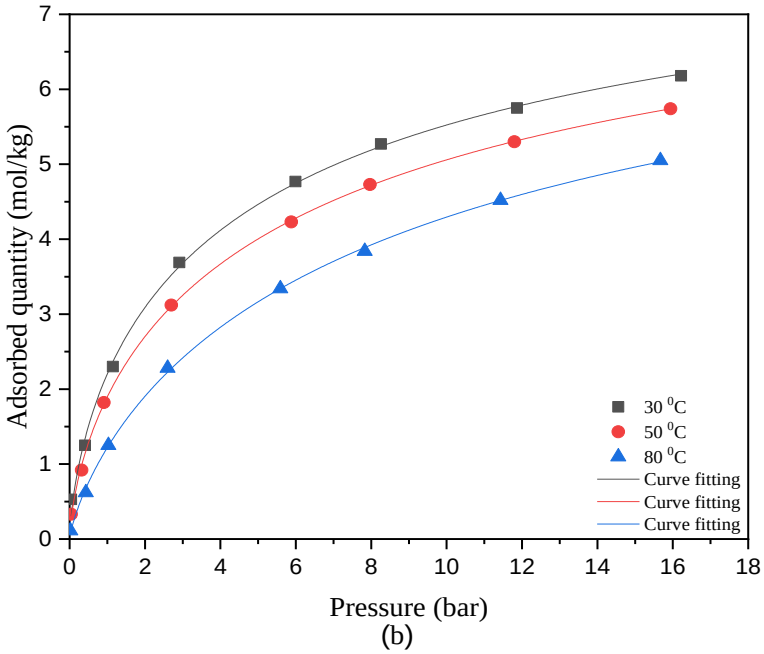

Figure 4.5: Adsorption Isotherms of (a) CH4 and (b) CO2 on Activated Carbon

4.3.1 Cyclic Process Performance

a) CO_2 Concentration Profiles

Figure 4.6 (a) shows the variations in carbon dioxide concentration in the waste gas during the thermal swing adsorption process, for the regeneration without heating at a bed temperature of 40°C. A negligible carbon dioxide concentration was recorded during the first 390 seconds, representing the adsorption step as the waste valve was closed. A sudden rise in carbon dioxide concentration was observed during the purging step, as carbon dioxide molecules that had been adsorbed were desorbed from the column. A carbon dioxide volumetric concentration peak of 23%, similar to the concentration in biogas, was recorded. The low carbon dioxide concentration in the waste gas was attributed to incomplete desorption of the adsorbent. Similar observations were made for low-temperature regeneration processes (Gao *et al*., 2024; Yu *et al*., 2023).

For the subsequent regenerations with heating at regeneration temperatures of 45, 50, 55, and 60℃, an increase in the peak waste carbon dioxide concentration was observed, as shown in Figures 4.6(b), (c), (d), and (e), respectively. A carbon dioxide concentration of 39% was obtained during regeneration at 60°C. This is consistent with observations of Rainone *et al.* (Rainone *et al*., 2021) in the separation of a methane and carbon dioxide mixture using the adsorption technique. A decrease in total purge/desorption time from 900 seconds to 540 seconds for a regeneration temperature of 40℃ to 60℃ was observed. This indicated that high regeneration temperatures enhance the desorption of carbon dioxide from the activated carbon pellets by increasing the kinetic energy of the molecules and reducing their adsorption affinity.

The decrease in carbon dioxide concentration during purging was attributed to the dilution effect of the purge gas as it passed through the column during this step. Purge gas has also been observed to dilute the carbon dioxide concentration, which limits its direct use in the food, beverage, and medical industries, where high purity levels of 99.99% are required (Verougstraete *et al*., 2022).

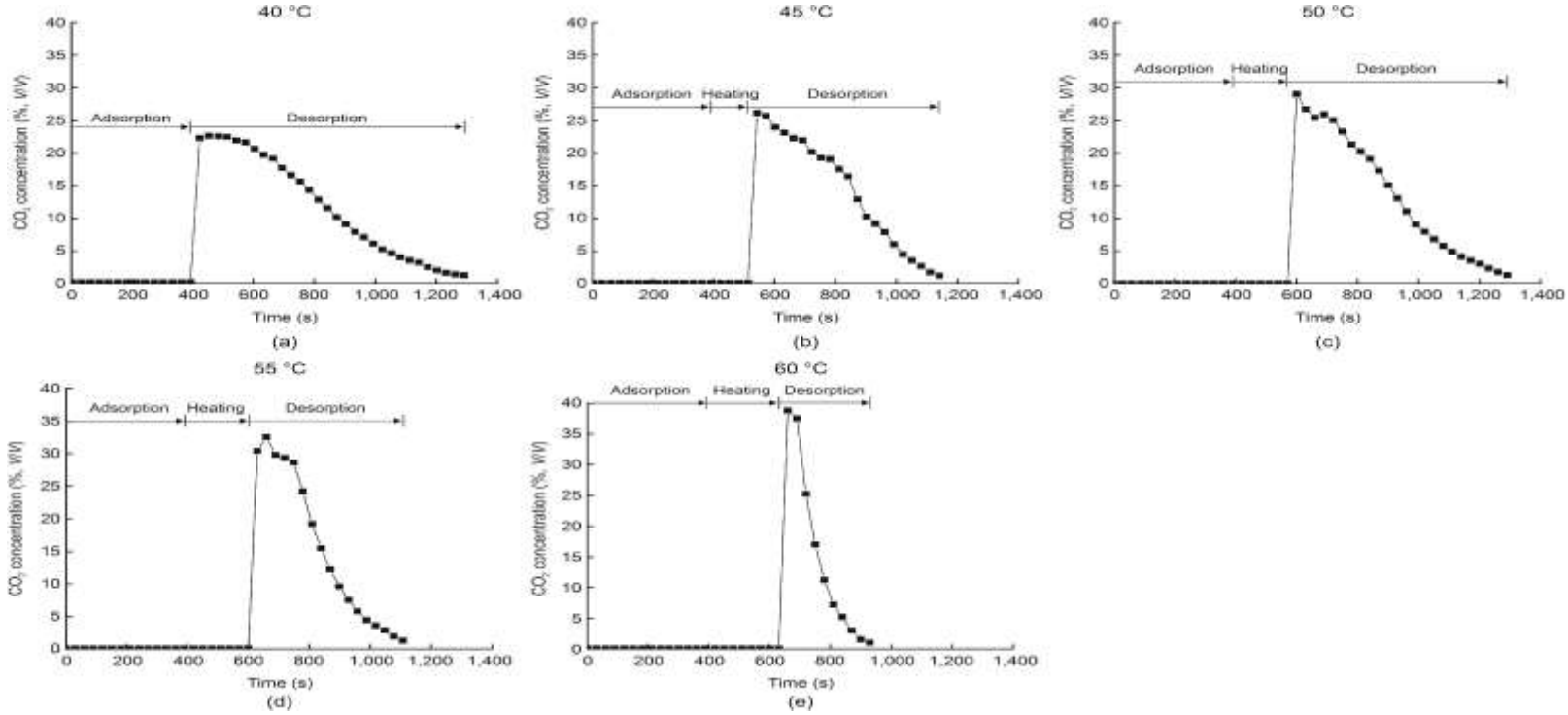

Figure 4.6: Influence of Regeneration Heating on Waste CO2 Concentration

b) Temperature Profile

Starting at an ambient temperature of 30℃ (±1 ℃), there was a rise in temperature in the columns during the adsorption step of up to 40℃, as illustrated in Figure 4.7(a). This exothermic process was mainly attributed to the adsorption of carbon dioxide molecules onto the pores of the activated carbon pellets, which have a 50% higher heat of adsorption compared to methane (Abdulsalam *et al*., 2019; He *et al*., 2021). The subsequent temperature increase from 29℃ to 30℃ at 900 seconds was attributed to heat transfer between the column and the surrounding environment. The absence of active heating the column tends towards thermal equilibrium with the surrounding. The slight temperature gain is also attributed to residual heat stored in the column wall and the adsorbent.

For bed regeneration with heating, an increase in heating time was observed at higher regeneration temperatures. The temperature increased during the heating phase until the target regeneration temperature was attained and decreased during the subsequent purge and cooling steps. At a regeneration temperature of 45℃, as shown in Figure 4.7(b), the heating time was 120 seconds, which doubled to 240 seconds for a regeneration temperature of 60℃, as shown in Figure 4.7(e).

During the heating step, the temperature remained nearly constant for the initial 60 seconds before a steady increase was observed, as illustrated in Figures 4.7(b), (c), (d), and (e). This initial temperature plateau was attributed to the structural configuration of the resistive band heaters and the thermal properties of the system components. Upon energizing the band heaters, electrical energy was first dissipated as resistive heat within the heating element and subsequently conducted through the heater casing to the column wall, that has a finite thermal conductivity. As a result, a significant portion of the supplied energy was absorbed by the column wall and used to overcome the thermal inertia of the adsorption bed. This resulted in a delayed temperature rise in the adsorption column. Once sufficient heat had been transferred through the column wall and distributed within the adsorbent, a steady temperature increase was observed.

During the desorption step, the temperature gradient increased with increasing regeneration temperature. This was ascribed to a significant deviation from the ambient temperature. However, a decrease in the temperature gradient was expected as the column temperature approached the ambient temperature. In addition to blowing out the adsorbed carbon dioxide molecules, the purging step contributed to cooling the column for subsequent cyclic steps. Natural heat transfer to the environment enhanced the cooling process.

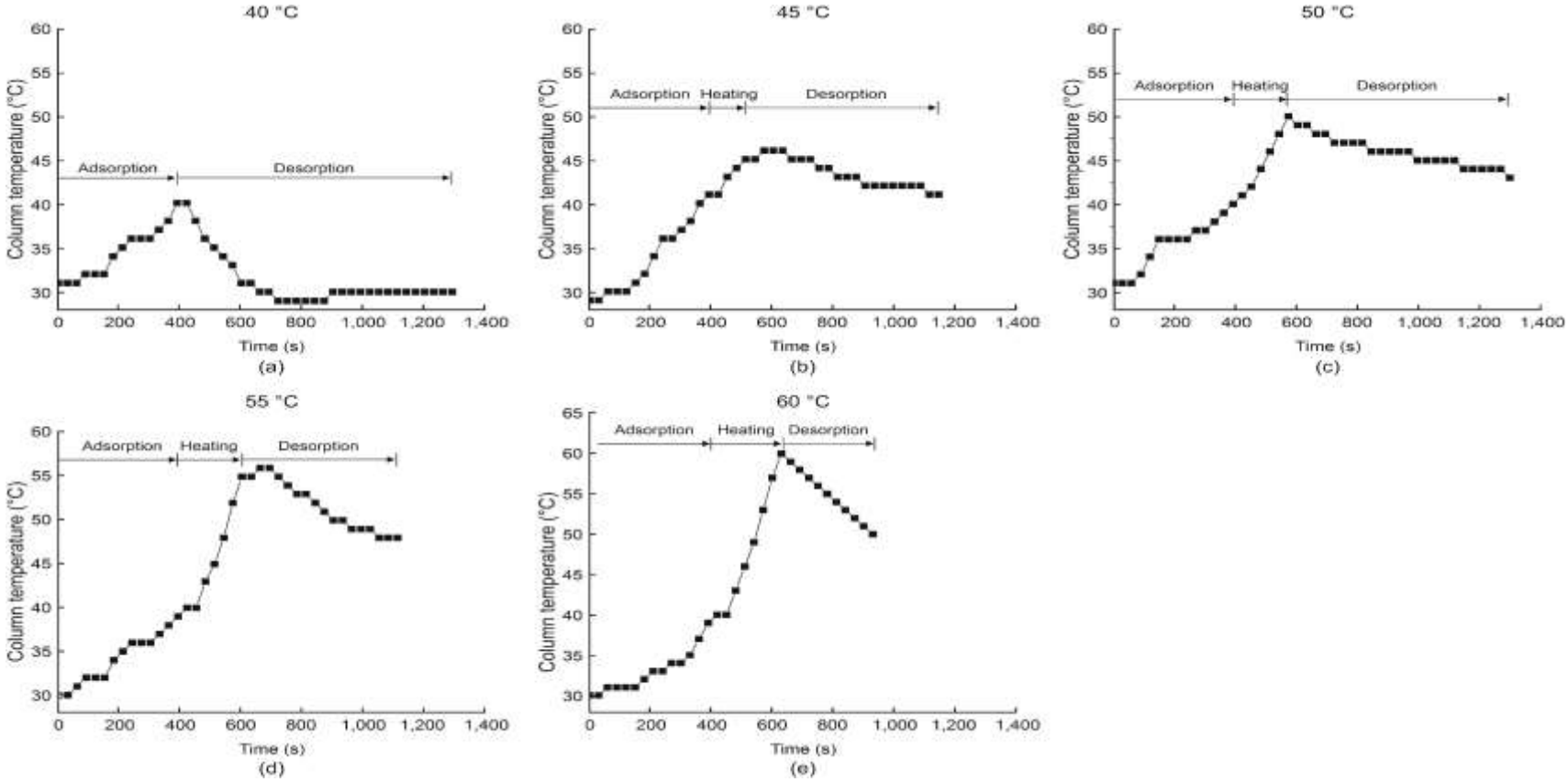

Figure 4.7: Influence of Regeneration Heating on Column Temperature

4.3.2 Cycle Time

Evaluating the total time required for a biogas upgrading cycle is essential in establishing the economic feasibility of the adopted technology. The cooling time was not considered in this analysis, being 5 times more than the total cycle time. However, it is essential to note that if the column is not allowed to cool thoroughly, this will reduce the carbon dioxide adsorption process in subsequent cycles, as high temperatures do not favour its adsorption.

Table 4.4 lists the duration of the various steps in the biogas upgrading process at various regeneration temperatures studied. Regeneration without heating the column cycle had the longest total cycle time of 1,290 seconds, with the adsorbent regeneration time accounting for 70% of the total time. For the highest regeneration temperature of 60℃ it had the shortest cycle time, and subsequently, the highest peak in carbon dioxide concentration in the waste gas of 39% v/v. The total adsorbent regeneration time decreased to 58%, indicating that thermal regeneration significantly reduced the total desorption time, and consequently, the total cycle time. This is crucial for enhancing the overall efficiency of biogas upgrading.

The regeneration temperature of 50℃ represented a critical point where the regeneration cycle time reached its maximum among the studied conditions. At this temperature, the increased heating duration to 180 seconds represented additional energy requirements to raise the adsorbent temperature above 45℃. This, however, represented a limited increase in the desorption efficiency as the purging time was 600 seconds with a total cycle time of 1170 seconds. Compared to lower regeneration temperatures, the increased heating demand was not sufficient to compensate for improved purge efficiency. The desorption kinetics were not yet strong enough to substantially reduce the purge duration. This shows that at this temperature represents an inefficient operating point in which increased thermal input does not translate into proportional improvement in the regeneration performance for this configuration.

Table 4.4: Cycle Time for Various Regeneration Temperatures

Regeneration/Final purge temperature (℃)	Adsorption time (s)	Heating time (s)	Purge time (s)	Total cycle time (s)
40/30	390	0	900	1,290
45/41	390	120	630	1,140
50/44	390	180	600	1,170
55/48	390	210	540	1,140
60/50	390	240	300	930

4.4.1 Energy Analysis

Electricity consumption in small-scale biogas upgrading systems (0 to 100 Nm^3/h) has been established to be higher when compared with that of conventional systems (>100 Nm^3/h) (Bauer *et al*., 2013). During the adsorption/feed step, for every 0.069 m^3 of biogas that passed through the column at 12 slpm, 0.054 m^3 of methane was collected. Given that the average energy densities of biogas and methane are 6.46 and 9.94 kWh/m^3, respectively, the energies of biogas and upgraded methane were 0.45 and 0.53 kWh, respectively (Swedish Gas Technology Centre Ltd (SGC), 2012).

Table 4.5 presents the energy requirements for the various processes, including adsorption (pressure pump), heating (band heaters), and purging (pressure pump), along with their respective energy efficiencies. Parasitic energy requirements, such as control and standby power, were also considered in the evaluation process.

Table 4.5: Cycle Energy Requirements for Various Regeneration Temperatures

Regeneration temperature (℃)	Adsorption energy requirements (kWh)	Heating energy requirements (kWh)	Purge energy requirements (kWh)	Parasitic energy requirements (kWh)	Total energy requirements (kWh)	Energy efficiency (%)
45	0.001	0.075	0.004	0.0004	0.0804	99
50	0.001	0.11	0.003	0.0006	0.1146	93
55	0.001	0.13	0.003	0.0007	0.1347	91
60	0.001	0.15	0.002	0.0008	0.1538	87

A decreasing trend in energy efficiency was observed as the regeneration temperature increased. At a maximum regeneration temperature of 60°C, an energy efficiency of 87% was achieved. Although system energy efficiency decreased with increasing regeneration temperature, it enhanced adsorbent recovery for subsequent biogas upgrading cycles. The energy efficiency of the developed small-scale biogas

upgrading system (0.69 Nm^3/h) compared favourably with that of conventional biogas upgrading systems (>100 Nm^3/h) employing water scrubbing technology, which has an energy efficiency range of 87.3% to 89.8% (Rotunno *et al.*, 2017). This demonstrates that the thermal regeneration of adsorption systems for biogas upgrading is a promising technology that can be adopted in water-deficient regions.

4.5 Validation of the Numerical Model

The biogas upgrading numerical model was validated by comparing the simulation results obtained from the study with the experimental results. Both the breakthrough and cyclic biogas upgrading configurations were analyzed.

4.5.1 Breakthrough Curves

Breakthrough curves represent the concentration of adsorbate at the outlet of an adsorption column as a function of time (Chen *et al*. 2015b). The breakthrough point represents the time when carbon dioxide concentration in the product gas abruptly rises, which is crucial in determining the duration of the adsorption step for cyclic configuration. The breakthrough results of the developed simulation model were validated using experimental data. Figure 4.8 shows the carbon dioxide breakthrough curves for feed flow rates of 5, 12, and 20 slpm. The lowest flow rate of 5 slpm had a longer breakthrough time of 810 seconds compared to 180 seconds for the highest flow rate of 20 slpm. At the average flow rate of 12 slpm, the breakthrough time was 390 seconds. Both experimental and simulation studies have shown a decrease in breakthrough time with an increase in flow rate.

A low biogas flow rate results in a prolonged breakthrough time, which in turn leads to a longer cycle time and inadequate utilization of the adsorbent. On the other hand, high flow rates reduce the contact time between the adsorbate and the adsorbent, particularly when the adsorption of the adsorbate is dominated by microporous diffusion. The obtained results correspond to the breakthrough results obtained using silica gel in the pressure swing adsorption technique for biogas upgrading (Shen *et al*., 2018).

A good agreement was observed in the breakthrough points of both the experimental and simulation studies, with a 2% mean absolute percentage error. The slight deviation was attributed to general assumptions adopted during the simulation study. In particular, the presence of other minor gases in the biogas used during the experimental study, which was assumed to be negligible in the simulation study, contributed to the deviation. The validated model was then used to study the transient behaviour of the adsorption bed. Subsequent studies adopted a feed flow rate of 12 slpm.

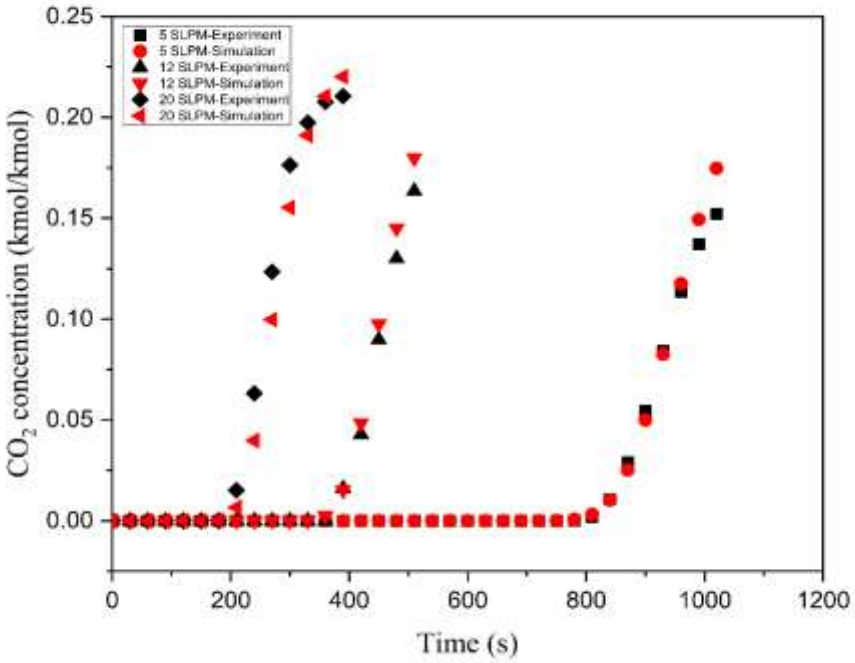

Figure 4.8: Simulation and Experimental Breakthrough Curves

4.5.2 Cyclic Experiments

A comparative study was conducted between the experimental and simulation performance of the cyclic biogas upgrading process, where regeneration was carried out without heating the bed. The main processes considered were the adsorption and desorption steps. Figure 4.9 illustrates variations in temperature at the center of the adsorption column and carbon dioxide concentration profile at the waste valve for both the adsorption and desorption processes. The initial rise in temperature to 34℃ over

the first 100 seconds was attributed to the exothermic nature of gas adsorption, particularly carbon dioxide adsorption on the activated carbon pellets. As adsorption progressed, a slight temperature decrease, attributed to axial heat dispersion and convection cooling caused by incoming feed gas at ambient temperature was observed.

During the desorption step, a sudden increase in carbon dioxide concentration was initially observed in the waste valve. This was attributed to opening the waste valve, which resulted in a sudden pressure decrease in the bed, allowing for rapid desorption of carbon dioxide. Since the desorption process involved purging with part of the product gas obtained during the adsorption step, this diluted the waste gas, resulting in a decrease in carbon dioxide concentration over time. Additionally, the methane cooled the bed, resulting in a reduction in temperature during the desorption step.

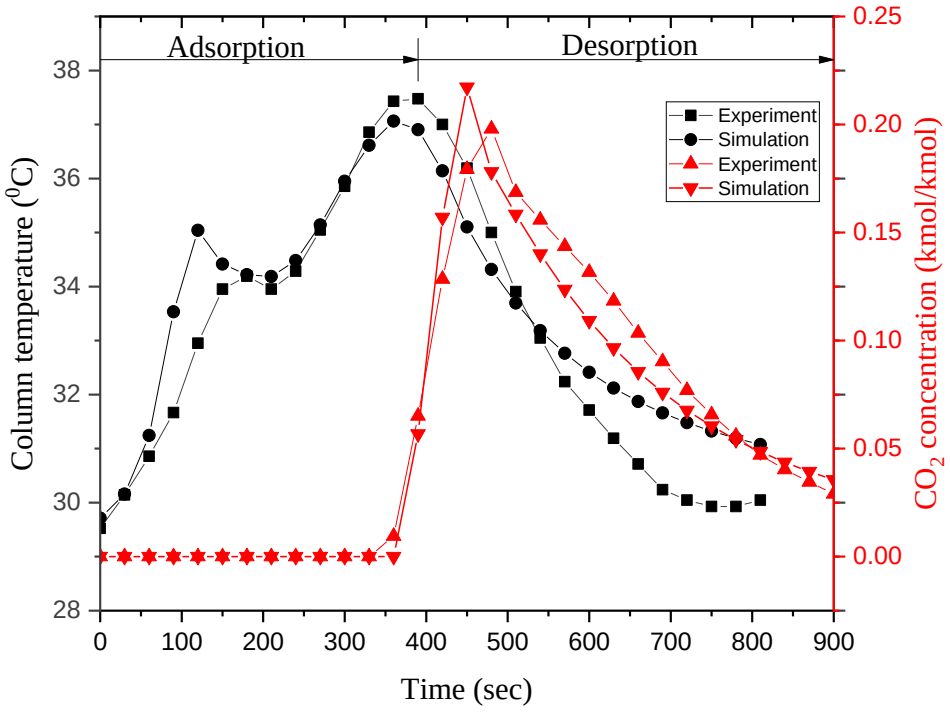

Figure 4.9: Simulation and Experimental Cyclic Curves

4.6 Parametric Study

This section investigated the influence of particle size, regenerating temperature, and purge-to-feed flow rate ratio on the biogas upgrading process, evaluated through simulation studies. Upon attaining cyclic steady state, the performance indicators were established.

4.6.1 Effect of Particle Size

The particle size significantly influences the gas flow resistance and, consequently, the performance of a packed bed in gas separation (Ballesteros *et al*., 2022). The effect of the adsorbent particle radius on the methane purity and recovery is presented in Figure 4.10. At a constant purge-to-feed flow rate ratio of 0.1, the adopted range of particle radius considered for this study, of 1 to 9 mm, presented a less than 1% decrease in methane purity for increased particle radius, as shown in Figure 4.10(a). The high surface area-to-volume ratio for smaller particle radii favoured the carbon dioxide adsorption process, resulting in increased methane purity.

The subsequent increase in the heat exchanger steam temperature from 77 to 227℃ increased the methane purity from 78% to 79%. Low regeneration temperatures result in slower desorption kinetics and, consequently, incomplete desorption of carbon dioxide from the bed, leading to lower methane purity.

Figure 4.10(b) illustrates the effect of particle radius on methane recovery at varying regeneration temperatures. A 1% average increase in methane recovery is observed with increased particle radius from 1 to 9 mm for all regeneration temperatures of 77, 127, 177, and 227℃. This trend was attributed to the improved gas flow distribution in the column when larger particles of the adsorbent were used, which enhanced effective adsorbent-adsorbate contact within the bed. A decrease in methane recovery with increasing regeneration temperature was also observed. The highest recovery of 73.5% was achieved at a regeneration temperature of 77℃ and progressively decreased with increased temperature of up to 227℃. The decrease in methane recovery at higher regeneration temperatures is attributed to increased methane desorption during the regeneration step as more methane is lost in the purge stream. Although the larger

particle radius of 9 mm partially mitigated recovery losses by improving flow characteristics, the influence of regeneration temperature was more dominant. This indicated that the particle radius has a secondary influence in enhancing methane recovery, compared to the regeneration temperature.

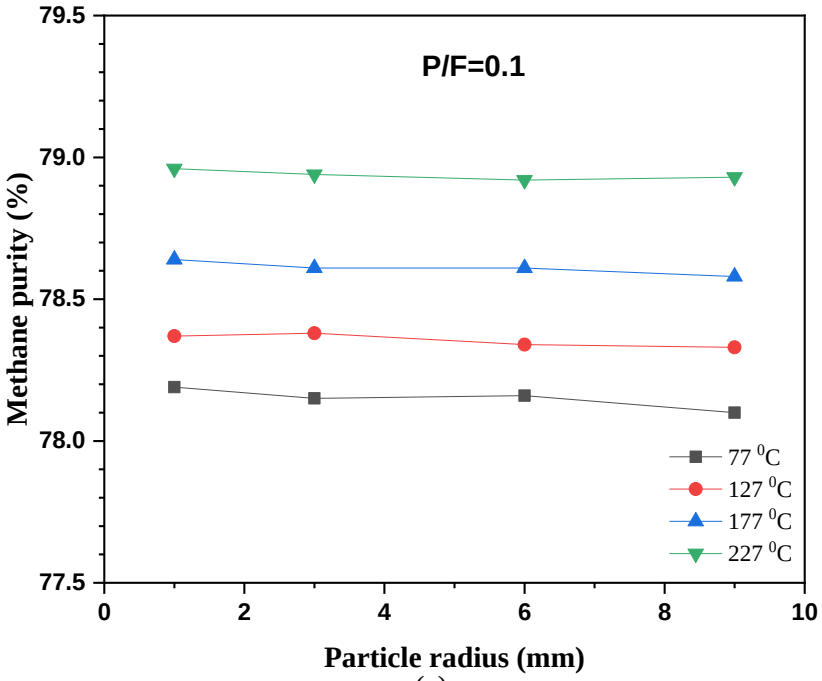

(a)

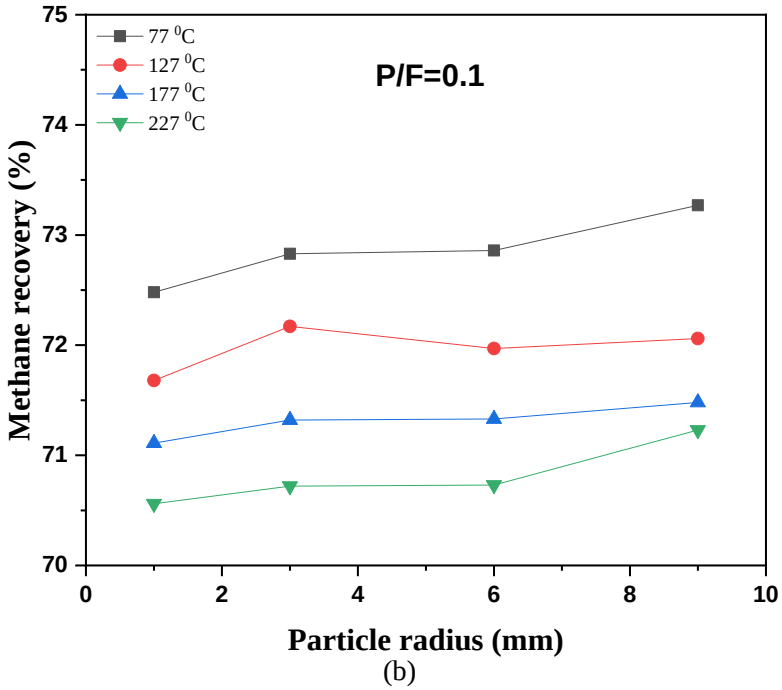

(b)

Figure 4.10: Effect of Particle Radius on CH_4 a) Purity and b) Recovery

4.6.2 Effect of Purge to Feed Flow Rate Ratio

The purge step is crucial in the cyclic biogas upgrading process, as it influences the purity and recovery in the product stream. Using part of the product gas for purging reduces column contamination by keeping unwanted gases from entering the system. However, using excessive product gas for purging has a negative impact on methane recovery. The effect of using a fraction of the product gas during the purge step at varying purge-to-feed flow rate ratios and regenerating temperatures was assessed. Figure 4.11 illustrates the impact of the purge-to-feed flow rate ratio on methane purity and recovery. An increase in methane purity from 78% to 88% was observed with an increase in the purge-to-feed flow rate ratio, ranging from 0.1 to 0.7, as shown in Figure 4.11(a). Higher regeneration temperatures increased the desorption rate by providing more energy for adsorbate molecules to be desorbed from the adsorbent surface. In addition, the capacity to overcome mass transfer resistance was enhanced by high purge flow rates, which allowed for efficient bed regeneration and resulted in improved methane purity.

A linear reduction in methane recovery, from 74% to 8%, was observed with an increased purge-to-feed flow rate ratio in the range of 0.1 to 0.7 for regeneration temperatures 77,127, 177, and 227℃, as shown in Figure 4.11(b). The lowest purge-to-feed flow rate ratio of 0.1 at a regeneration temperature of 77℃ yielded the highest product recovery of 74%, while the highest purge-to-feed flow rate ratio considered, 0.7, and a regeneration temperature of 227 ℃ , resulted in a product recovery of 8%. The increase in the amount of gas used during purging, accompanied by an increase in the purge-to-feed flow rate ratio, was attributed to the rapid decrease in product recovery. Variations in regeneration temperatures had no significant influence on the product recovery. The opposing trend between methane purity and recovery for increased purge to feed flow rate ratio was also observed, where inert gas was used to purge the adsorption bed (Canevesi & Grande, 2023; Durán *et al*., 2022). This necessitates process optimization to establish a good trade-off between methane purity and recovery.

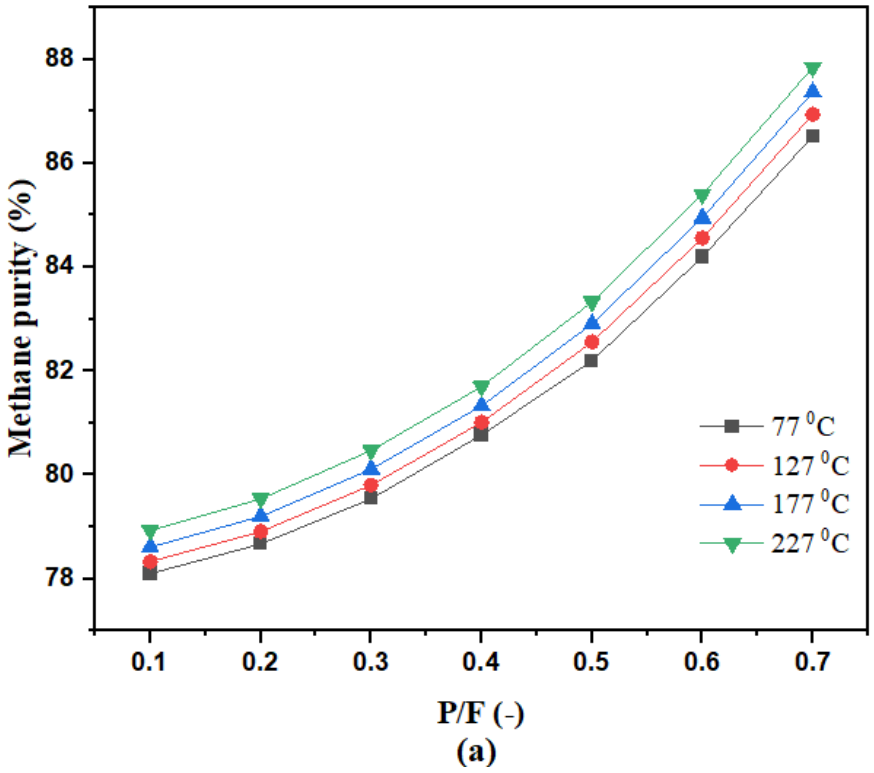

(a)

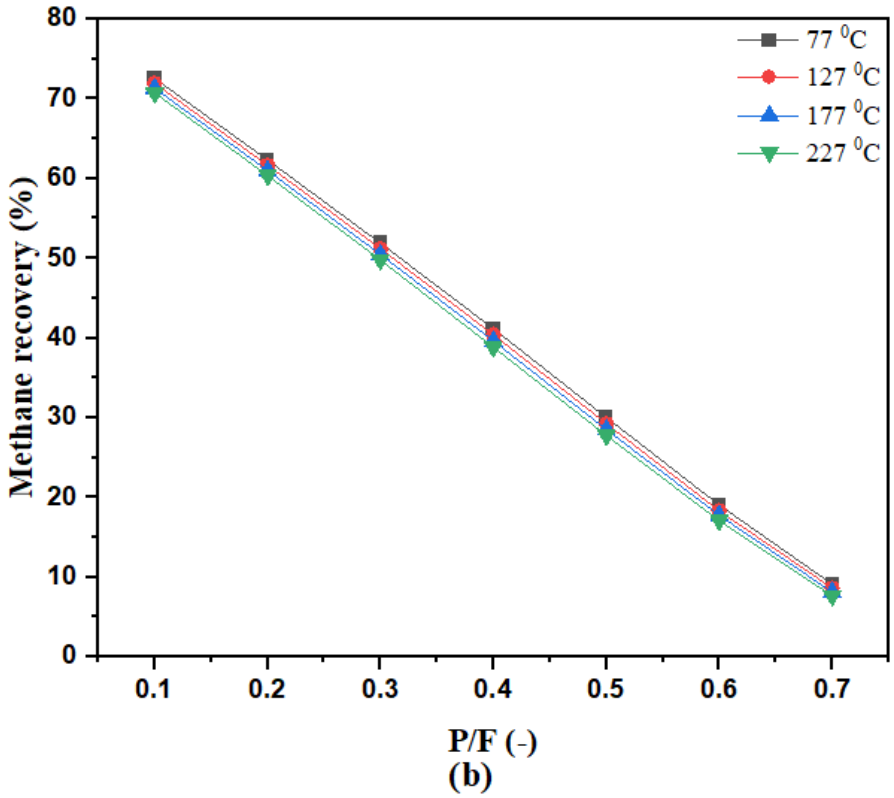

Figure 4.11: Effect of P/F on CH_4 a) Purity and b) Recovery

The combined analysis of Figures 4.11 (a) and (b) presented in Figure 4.12 highlights a clear trade-off between methane purity and recovery with increasing purge-to-feed flow rate ratio at varied regeneration temperatures. The intersection of methane purity and recovery occurred at a P/F range of 0.43 to 0.47, where both methane purity and recovery converged at about 82% - 83%. This intersection represents an optimal operating region in which neither the methane purity nor methane recovery was compromised. Although minor variations were observed for varied regeneration temperatures, the purge-to-feed flow rate ratio variable was more dominant to the methane purity and recovery balance in the thermal swing adsorption process.

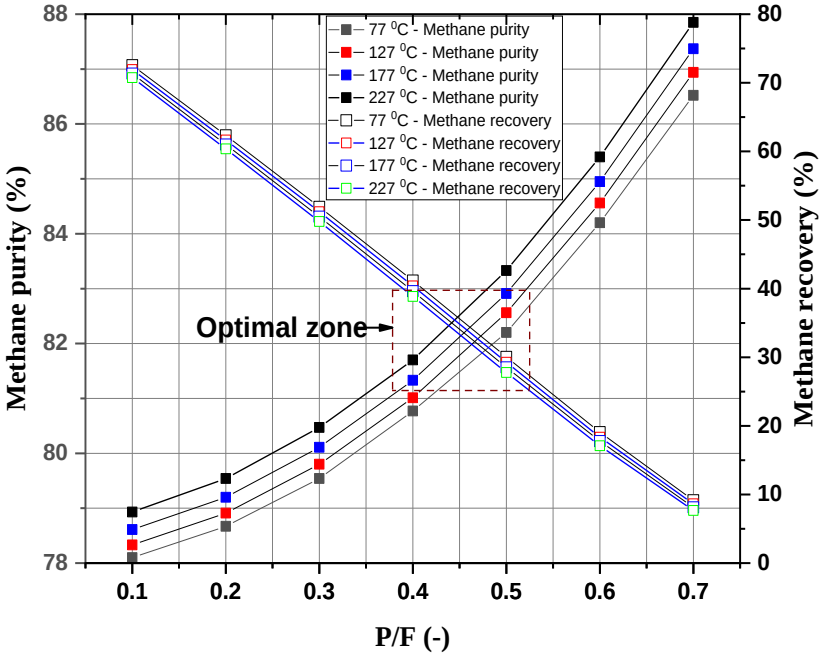

Figure 4.12: Combined Effect of P/F on Methane Purity and Recovery

4.7 Multi-Objective Optimization

To evaluate the sustainability of the biogas upgrading process, a multi-objective optimization approach was employed to maximize both methane purity and recovery. This aims to establish a good trade-off between methane purity and recovery. The Box-Behnken design response surface methodology was used to conduct the simulations. Particle radius, regenerating temperature, and purge-to-feed flow rate ratio were considered as decision variables, with methane purity and recovery as the output responses.

4.7.1 Regression Analysis

Table 4.6 presents the values of the selected independent decision variables used to generate a regression model. Particle radius, regenerating temperature, and purge-to-feed flow rate ratio —the independent decision variables — were considered to evaluate their influence on the methane purity and recovery response variables. The radius of the adsorbent particle used in the biogas upgrading process is crucial as it

influences the flow resistance across the column. It is also essential to optimize the purge-to-feed flow rate ratio, as it has an opposing effect on methane purity and recovery. Energy requirements linked to the regenerating temperature are crucial to ensure energy efficiency in upgrading biogas.

Multi-objective optimization is crucial due to the interaction between variables and the fact that one variable can have unintended consequences for other variables. The regression model equations used to predict the output responses for the various decision variables are presented in Equations (4.1) and (4.2). A comparison between the simulation results and the regression model, along with the residuals for each configuration, is also presented in Table 4.6. The regression models were considered satisfactory, with mean absolute percentage errors of 3.79% and 4.58% for methane purity and recovery, respectively.

$$BP = 77.994 - \ 0.0543A + \ 0.00267B - 1.877\ C + 0.00096A^2 + \ 0.000003B^2 \qquad 4.1$$

$$+ 18.56\ C^2 - 0.0001AB + 0.1354AC + 0.00733BC$$

$$BR = 84.159 + \ 0.0904A - \ 0.01693B - \ 105.35C - 0.00107A^2 + \ 0.000008B^2 \qquad 4.2$$

$$-0.218C^2 - 0.000067AB - 0.1208AC + 0.00389BC$$

Table 4.6: Independent and Response Variables for the Box-Behnken Design

Run	Decision variables			CH_4 purity (%)			CH_4 recovery (%)		
	Particle radius (mm)	Regenerating temperature (℃)	P/F (-)	Actual	Model	Residual	Actual	Model	Residual
1	5	152	0.4	81.24	81.2367	-0.0033	39.97	39.9667	-0.0033
2	5	227	0.7	88.08	88.0487	-0.0313	7.53	7.485	-0.045
3	5	152	0.4	81.23	81.2367	0.0067	39.97	39.9667	-0.0033
4	9	227	0.4	81.84	81.9287	0.0887	38.99	39.01	0.02
5	9	152	0.7	87.67	87.6125	-0.0575	8.18	8.2087	0.0287
6	5	152	0.4	81.24	81.2367	-0.0033	39.96	39.9667	0.0067
7	5	77	0.7	86.59	86.6587	0.0687	9.11	9.1375	0.0275
8	1	152	0.7	87.07	87.0900	0.02	8.38	8.3288	-0.0512
9	1	227	0.4	81.66	81.6713	0.0113	38.78	38.9363	0.1563
10	9	152	0.1	78.45	78.4300	-0.02	71.77	71.8213	0.0513
11	1	77	0.4	80.76	80.6713	-0.0887	40.96	40.8837	-0.0763
12	9	77	0.4	80.82	80.8087	-0.0113	41.25	41.0938	-0.1562
13	1	152	0.1	78.50	78.5575	0.0575	71.39	71.3612	-0.0288
14	5	227	0.1	78.93	78.8613	-0.0687	70.7	70.6725	-0.0275
15	5	77	0.1	78.10	78.1312	0.0312	72.63	72.635	0.005
Mean absolute percentage error (%)					**3.79**			**4.58**	

4.7.2 Analysis of Variance (ANOVA)

The statistical significance of the regression model was evaluated using analysis of variance (ANOVA) at a 95% confidence level. Table 4.7 presents the ANOVA results for both methane purity and recovery. The results show that both models were significant, having a p-value of less than 0.05. The purge-to-feed flow rate ratio variable had the most important contribution, accounting for over 90% of both methane purity and recovery, when compared to the particle radius and regeneration temperature variables. This is in agreement with the results presented in section 4.4.1 above. While the contribution percentages of the particle radius and regeneration temperature are less than 10%, they were considered significant to methane recovery, with a p-value of less than 0.05. The particle radius was, however, considered insignificant to the methane recovery model based on a p-value of 0.184, which is in agreement with the results presented in Figure 4.11. The $R^2_{adjusted}$ values for methane purity and recovery of 0.9994 and 1 respectively represents a high accuracy level for both models.

Table 4.7: Analysis of Variance Results

	CH_4 purity (%)					CH_4 recovery (%)				
Source	**dF**	**Adj SS**	**Contribution (%)**	**F-value**	**p-value**	**dF**	**Adj SS**	**Contribution (%)**	**F-value**	**p-value**
Model	9	169.843	99.98	2704.3	<0.0001	9	8027.56	100	36557.89	<0.0001
Particle radius (A)	1	0.078	0.05	11.18	0.02	1	0.06	0.00	2.37	0.184
Regenerating temperature (B)	1	2.247	1.32	322.03	<0.0001	1	7.90	0.10	323.81	<0.0001
P/F (C)	1	156.911	92.37	22485.4	<0.0001	1	8019.48	99.90	328689.58	<0.0001
A^2	1	0.001	0.02	0.13	0.737	1	0.00	0.00	0.04	0.842
B^2	1	0.001	0.03	0.17	0.697	1	0.01	0.00	0.31	0.600
C^2	1	10.303	6.06	1476.37	<0.0001	1	0.00	0.00	0.06	0.819
AB	1	0.004	0.00	0.52	0.505	1	0.00	0.00	0.07	0.808
AC	1	0.106	0.06	15.14	0.012	1	0.08	0.00	3.45	0.123
BC	1	0.109	0.06	15.61	0.011	1	0.03	0.00	1.26	0.313
Residuals	5	0.035	0.02	-	-	5	0.12	0.00	-	-
Total	14		100	-	-	14		100	-	-
	$R^2 = 0.9998;\ R^2_{adjusted} = 0.9994\ ;\ R^2_{predicted} = 0.9967$					$R^2 = 1;\ R^2_{adjusted} = 1\ ;\ R^2_{predicted} = 0.9998$				

4.7.3 Normal Probability and Residual Plots

The normality test was used to determine whether the residual variables in the regression model had a normal distribution. Figure 4.13 presents the normal probability and residual plots for the methane purity model. The data formed an approximately straight line, and the normal distribution appeared to be a good fit to the data, as presented in Figure 4.13(a). This represented normally distributed residuals. Random scattering of points on both sides of the zero-horizontal line was observed in the residual plots for Figure 4.13(b). The moderate scatter of the residuals indicated that no latent variables were likely to have affected the response during the modeling. Similar residual and normal probability plots for the methane recovery are presented in Figure 4.14.

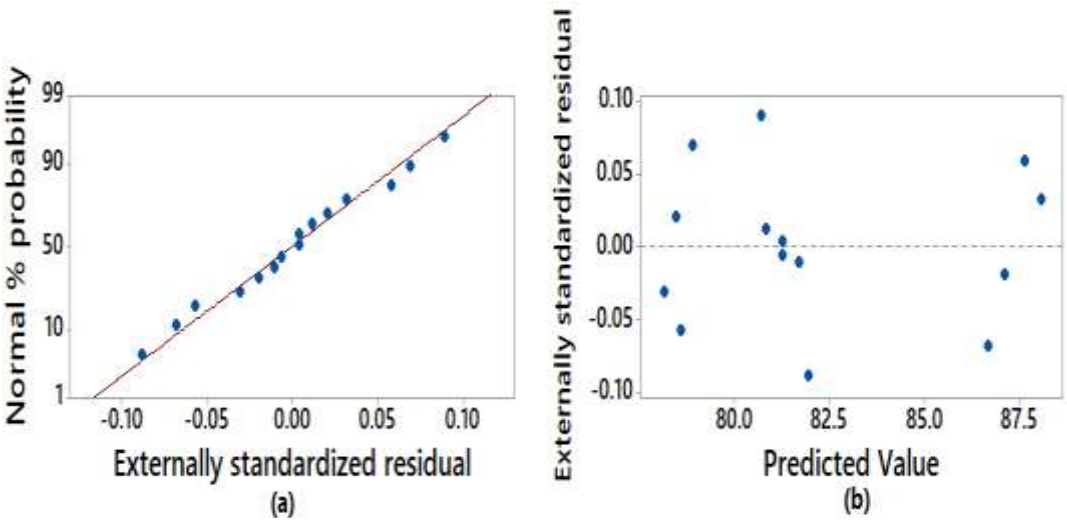

Figure 4.93: CH4 Purity (a) Normal Probability (b) Residuals

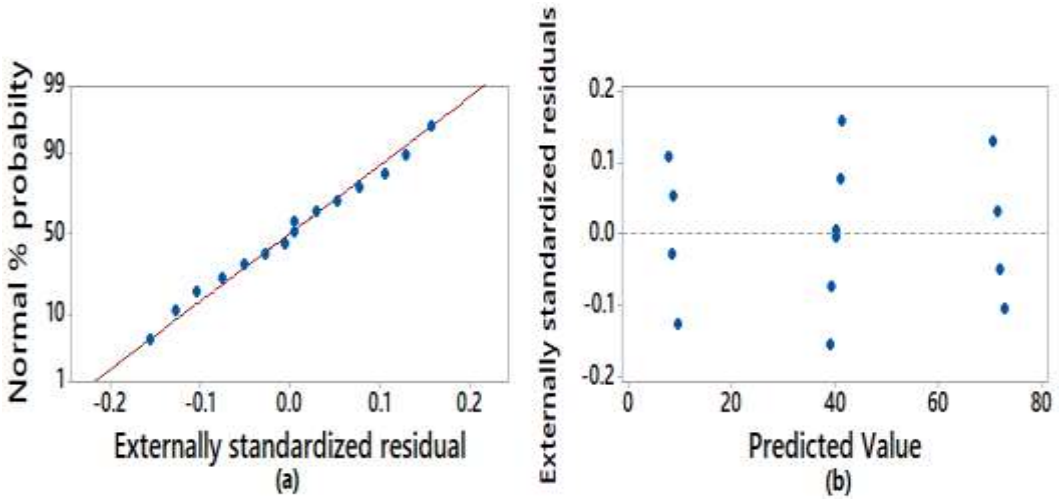

Figure 4.14: CH_4 Recovery (a) Normal Probability (b) Residuals

4.7.4 Multi-Objective Optimization Surface and Contour Plots

a) Methane Purity

Figures 4.15 to 4.17 present the 3D response surfaces and 2D contour plots of the decision variables about methane purity. It is evident from Figure 4.15(a) that the regenerating temperature had a higher influence on methane purity, resulting in a steeper gradient compared to the influence of the adsorbent particle radius. This is supported by the uniform colour-coded contours across the particle radius range presented in Figure 4.15 (b). The highest methane purity of above 81.8% was attained at the high regeneration temperature of 225°C and the largest particle radius of 9 mm. This was attributed to enhanced flow kinetics at elevated temperatures and adequate bed voidage that allowed for an improved bed desorption process.

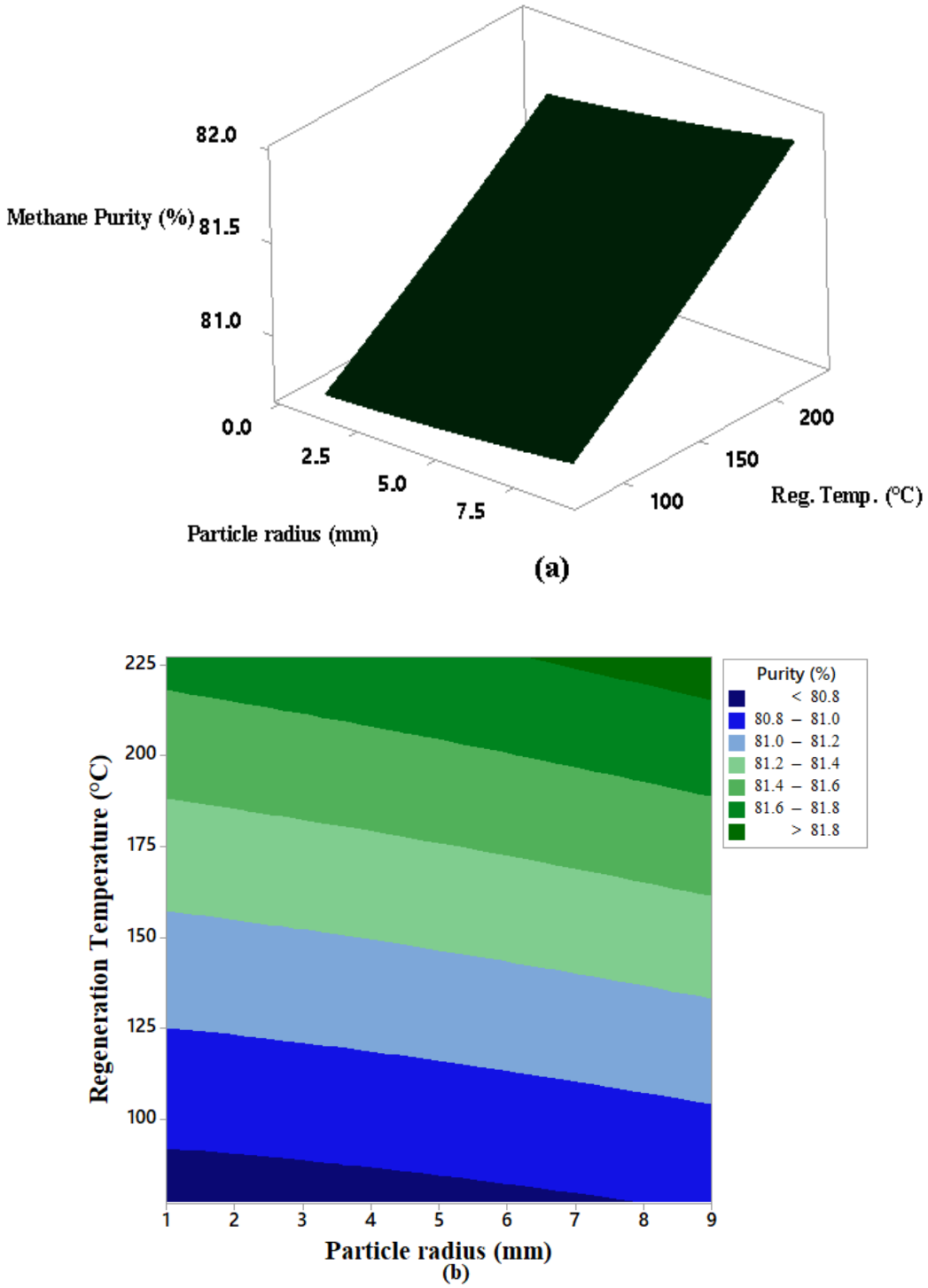

Figure 4.15: CH_4 Purity a) Surface Response and b) Contour Plots for Fixed P/F

From Figure 4.16, it was observed that the influence of purge-to-feed flow rate ratio on the methane purity was significantly greater when compared to that of the particle radius. Low purge-to-feed flow rate ratios, ranging from 0.1 to 0.3, resulted in the

lowest methane purity for all investigated adsorbent particle radii, as shown in Figure 4.16(b). This was attributed to slower intra-particle diffusion and incomplete desorption. Additionally, the possible agglomeration of tiny particles resulted in clogging of the bed, thereby decreasing the column's regeneration capacity. This slowed down the desorption process, negatively affecting the methane purity.

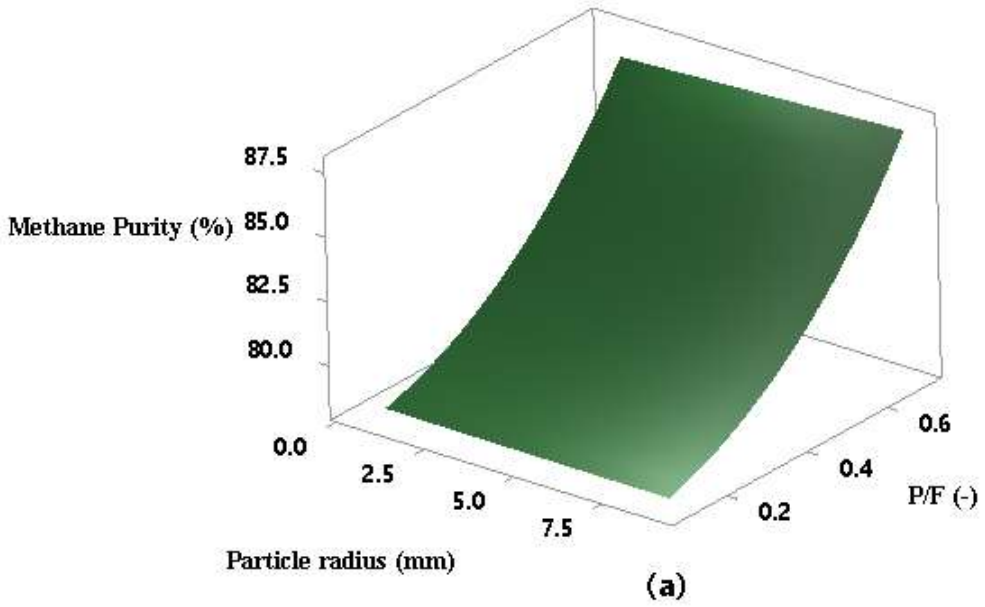

(a)

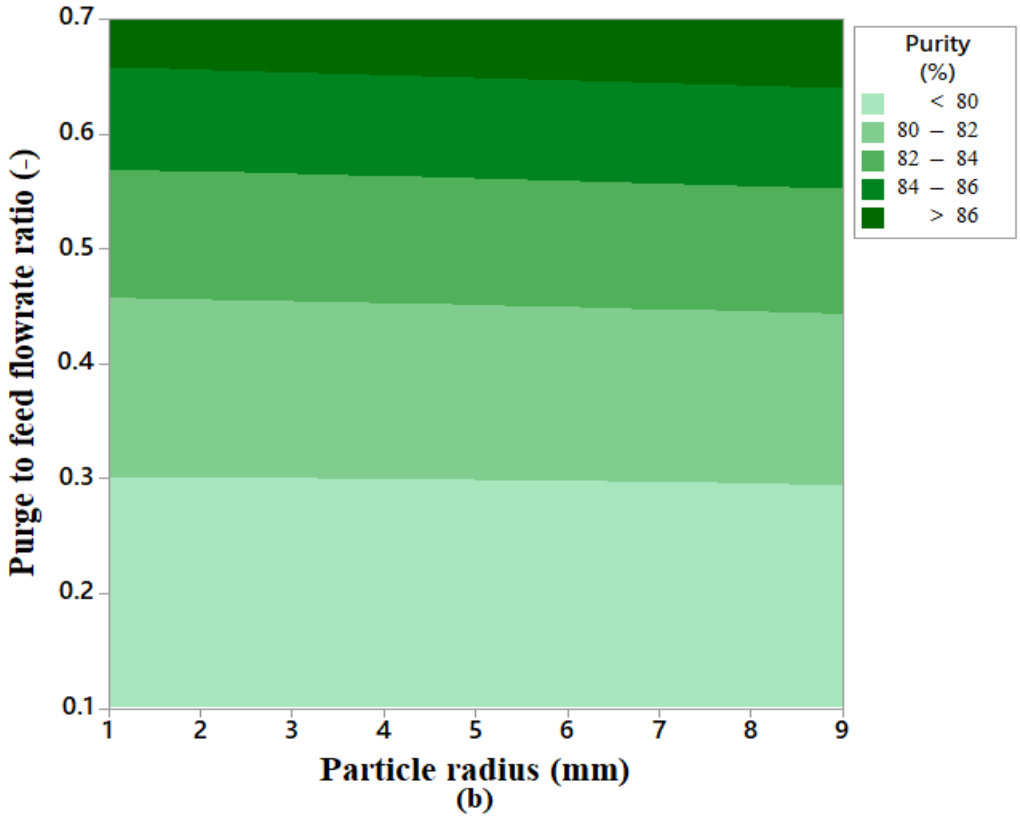

Figure 4.16: CH_4 Purity a) Surface Response and b) Contour Plots for Fixed Regenerating Temperature

A gradual increase in regenerating temperature and a corresponding increase in the purge-to-feed flow rate ratio resulted in a peak methane purity level, as shown in Figure 4.17(a). According to the contour grid direction, the maximum methane purity of over 88% was achieved at the highest regenerating temperature of 225°C and the highest purge-to-feed flow rate ratio of 0.7. This was attributed to the enhanced kinetic energy required for adsorbate molecules to overcome mass transfer resistance during the desorption process, resulting in complete bed regeneration for subsequent cycles. This highlights the crucial influence of gas flow properties on the biogas upgrading process compared to other variables, such as physicochemical properties.

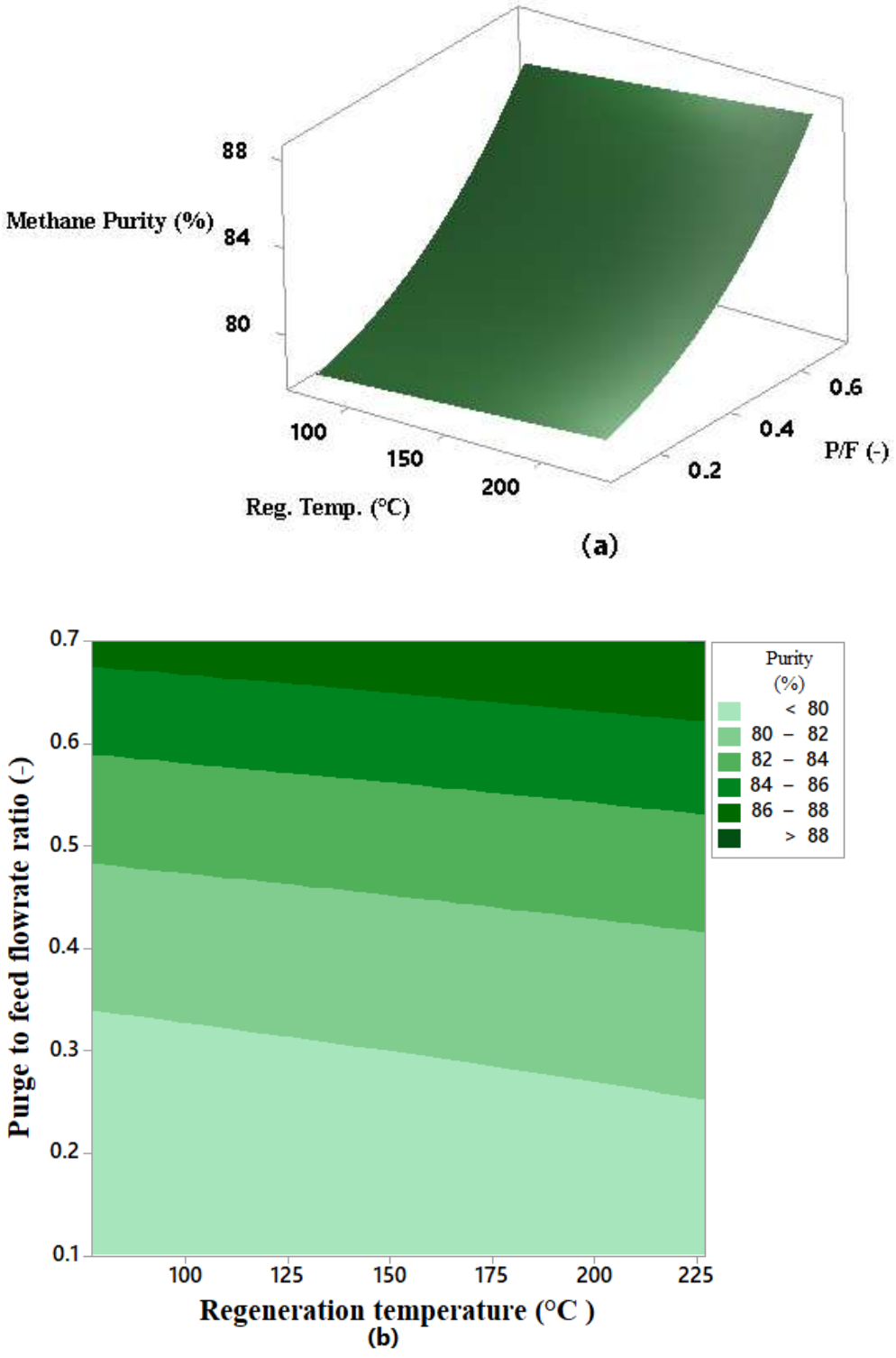

Figure 4.17: CH_4 Purity a) Surface Response and b) Contour Plots for Fixed Particle Radius

b) Methane Recovery

An increase in methane recovery was observed for increased particle radius between 1mm and 9mm, and decreased regeneration temperature between 77℃ and 227℃, as presented in Figure 4.18. The influence of the regeneration temperature is, however, more pronounced on the recovery process when compared to that of the particle radius, as shown in Figure 4.18 (b) contour plots. Increasing the particle radius reduced the pressure drop gradient across the adsorption column, resulting in a more uniform gas flow and, consequently, enhanced methane recovery. Regeneration temperatures above 150℃ resulted in a lower methane recovery of less than 40%. This can be attributed to thermal aging and degradation of the adsorbent at elevated temperatures, which negatively influenced its selectivity towards methane molecules.

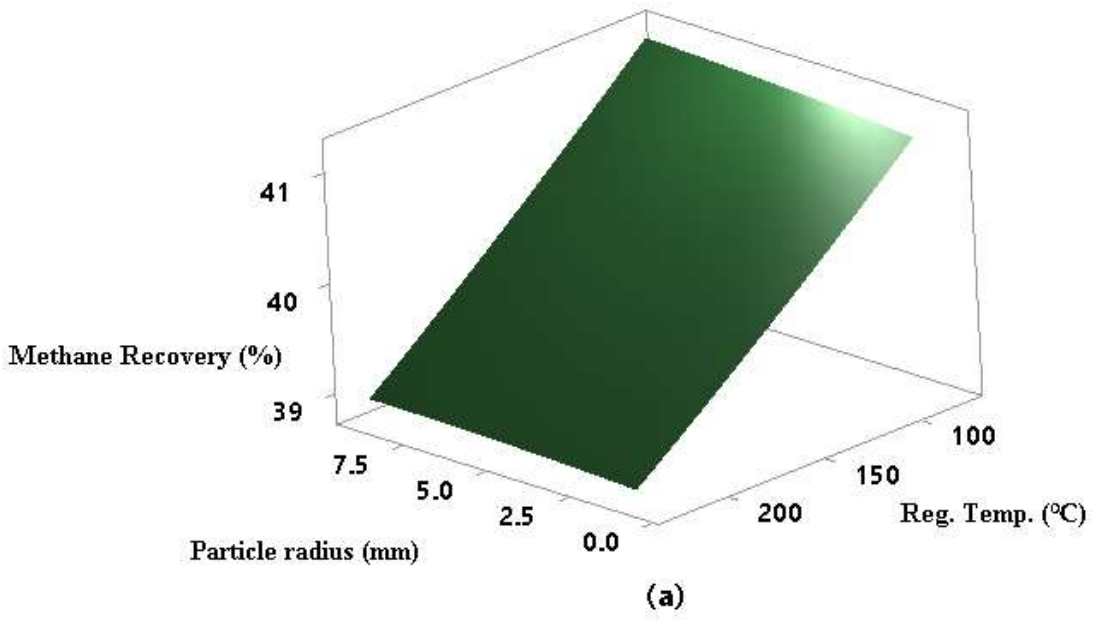

(a)

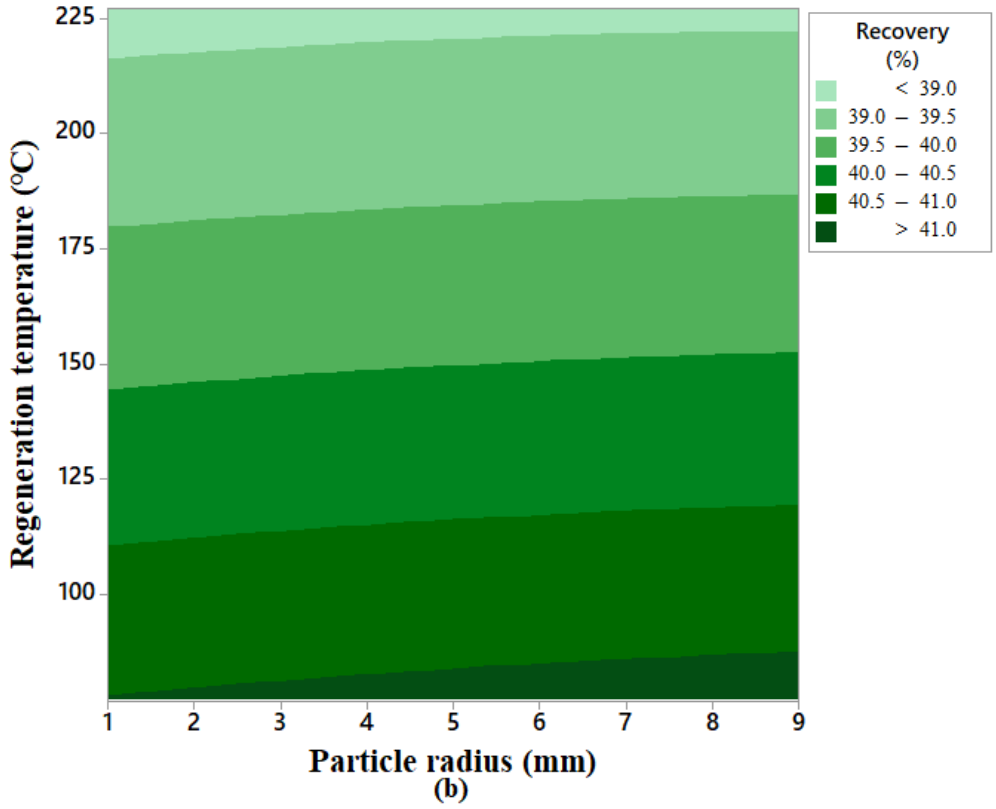

Figure 4.18: CH_4 Recovery a) Surface Response and b) Contour Plots for Fixed P/F

Variation in the particle radius had no significant influence on methane recovery when compared to the purge-to-feed flow rate ratio, as shown in Figures 4.19(a) and (b). A decrease in methane recovery was observed with an increase in the purge-to-feed flow rate ratio. At a purge-to-feed flow rate ratio of 0.7, methane recovery of less than 10% was achieved. This could be attributed to the increased volume of methane used during purging, resulting in its loss to the waste gas. While the high purge-to-feed flow rate ratio resulted in the highest methane purity, as shown in Figure 4.19(b), it generally decreases the methane recovery. A good trade-off between methane purity and recovery is required.

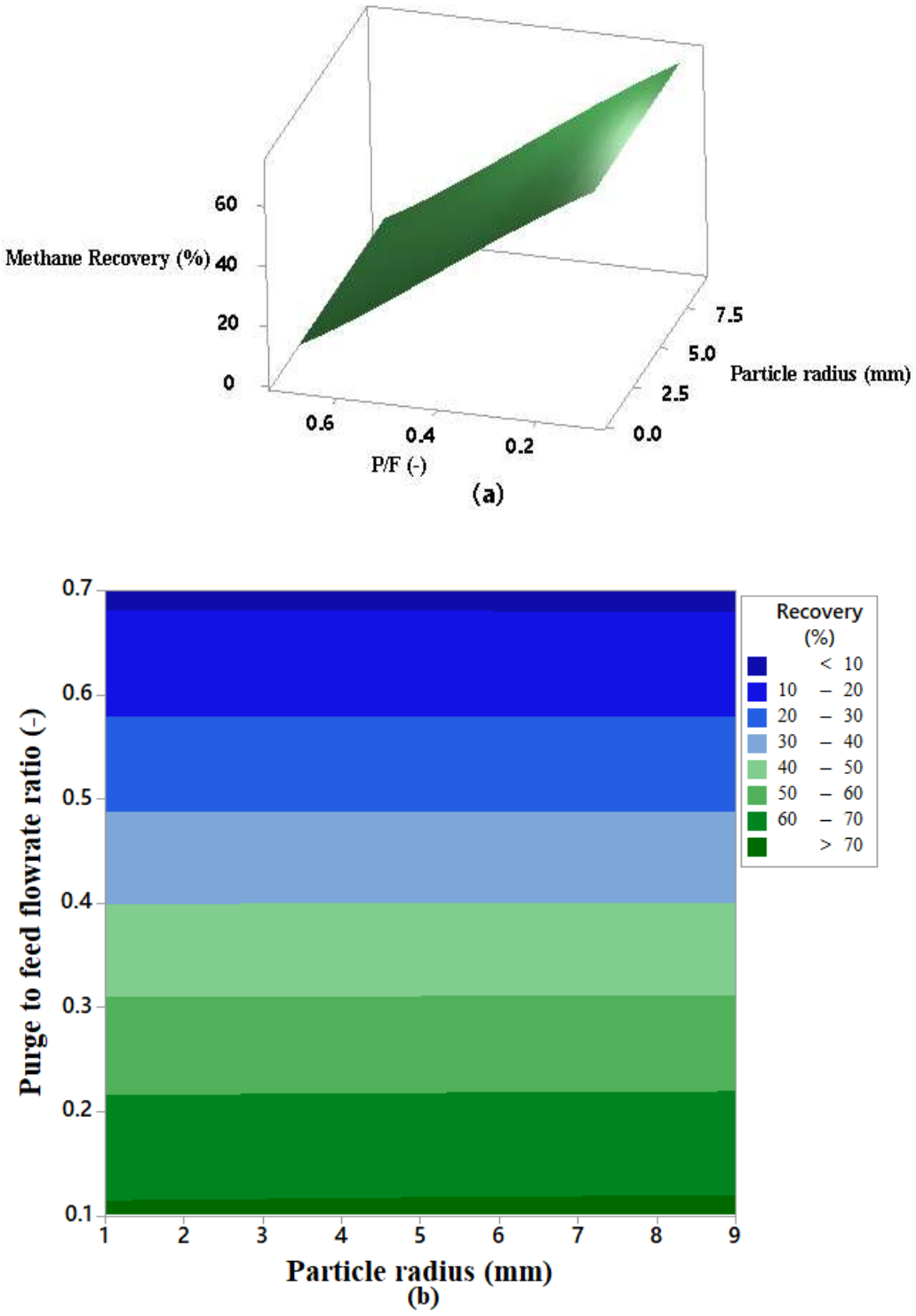

Figure 4.19: CH_4 Recovery a) Surface Response and b) Contour Plots for Fixed Regenerating Temperature

For a combined increase in the purge-to-feed flow rate ratio and regenerating temperature, there was a reduction in the methane recovery, as depicted in Figure 4.20. The highest methane recovery of above 70% was attained at a purge-to-feed flow rate ratio of 0.1 and regenerating temperatures below 100℃. Lower purge-to-feed flow rate ratios and regenerating temperatures result in targeted carbon dioxide desorption without disrupting the methane molecules retained in the adsorbent. This also ensured that the adsorbent's equilibrium was maintained, preventing the desorption of methane and ensuring its retention for separation. Furthermore, high purge flow rates and regeneration temperatures can lead to over-desorption, where methane is unnecessarily removed from the adsorbent, resulting in increased losses.

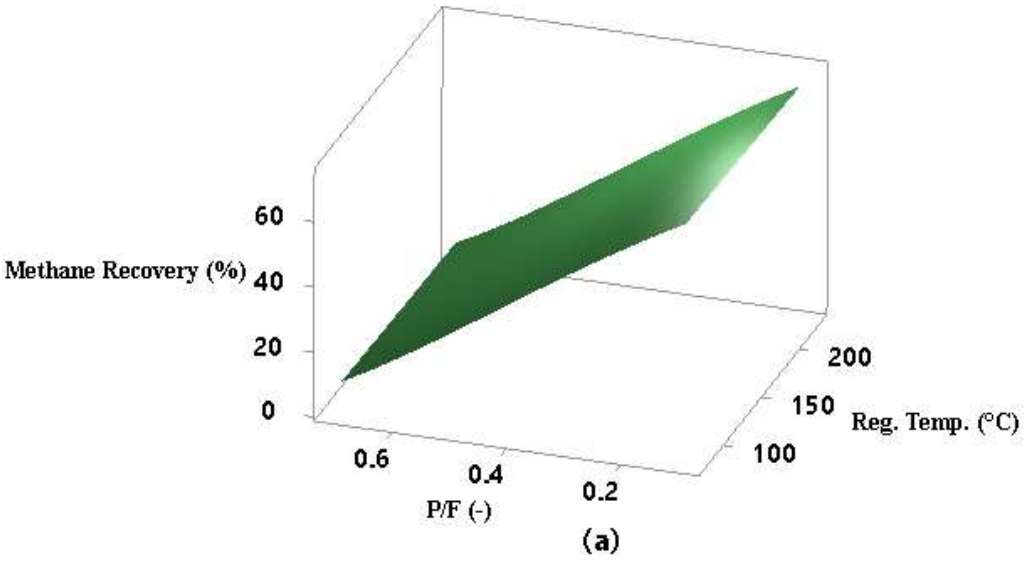

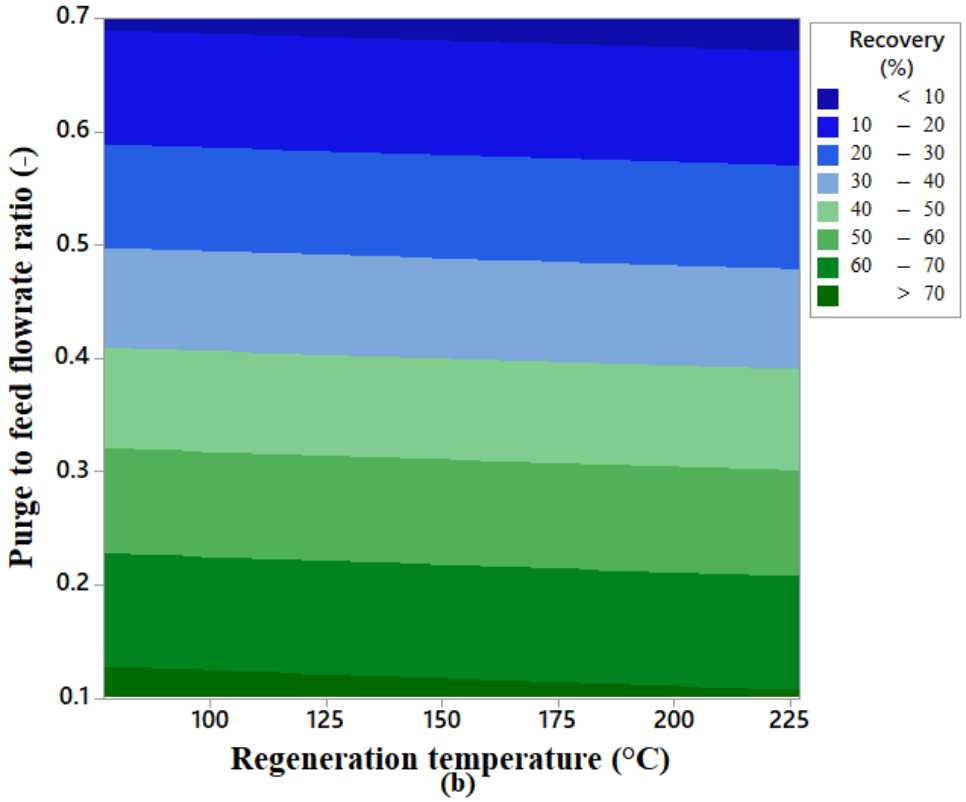

Figure 4.20: CH_4 Recovery a) Surface Response and b) Contour Plots for Fixed Particle Radius

4.7.5 Optimal Conditions

Multi-objective numerical optimization was used to maximize both methane purity and recovery for the thermal swing biogas upgrading process. This was achieved using the Box-Behnken design optimizer package in the Minitab software. Table 4.8 provides a summary of the optimization configuration considered. The objective function considered for the optimization is presented in Equation (4.3).

Table 4.8: Optimization Data

Response	Optimization goal	Range
Methane purity	Maximize	78.10 - 88.08
Methane recovery	Maximize	7.53 - 72.63

$$\text{Maximize}\{\text{Methane purity}\,(A, B, C),\ \text{Methane Recovery}\,(A, B, C)\} \qquad 4.3$$

Where $1 \leq A \leq 9\ mm,\ 77 \leq B \leq 227\ ℃,\ 0.1 \leq C \leq 0.7$

The optimal values for methane purity and methane recovery obtained were 82.12% and 37.21%, respectively, as shown in Figure 4.21. These optimal values were obtained for a particle radius of 9 mm, regenerating temperature of 227℃, and a purge-to-feed flow rate ratio of 0.4152. The validation test conducted in the Aspen Adsorption software under the optimal predicted conditions yielded a methane purity and recovery of 82.09% and 37.50%, respectively. This illustrates the high accuracy of the model to predict optimal configurations for the biogas upgrading process.

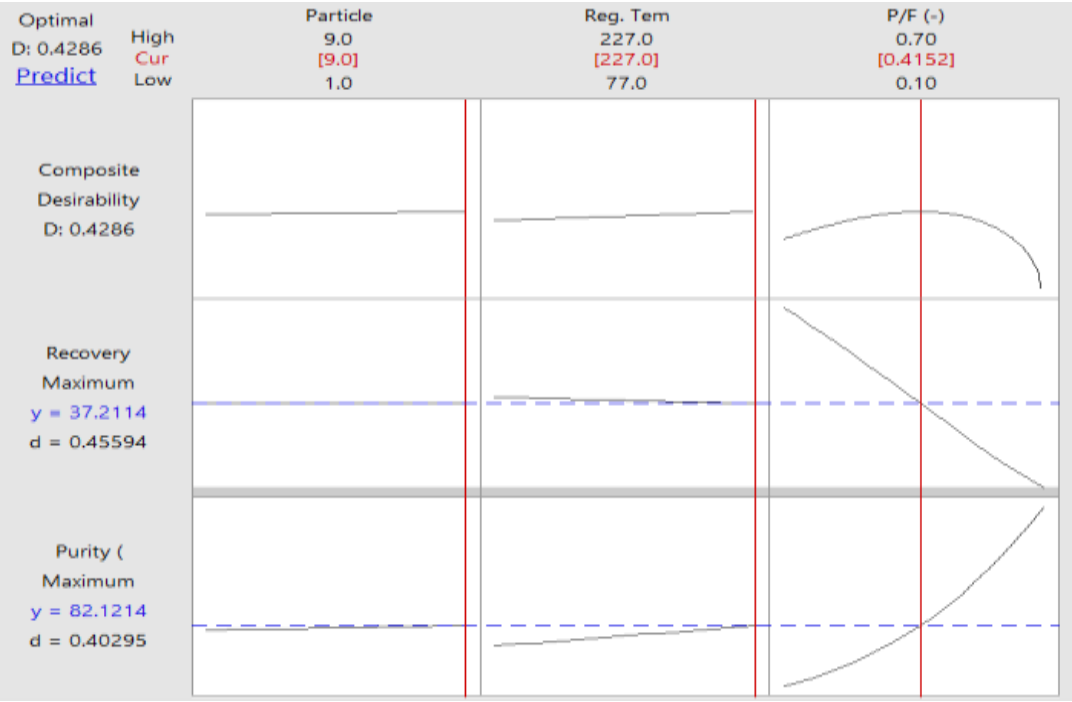

Figure 4.21: RSM Optimization Plot for Biomethane Purity and Recovery

CHAPTER FIVE

CONCLUSION AND RECOMMENDATIONS

5.1 Conclusion

This study investigated the influence of physicochemical properties and flow variables on the performance of a thermal swing adsorber for biogas upgrading. The developed model was optimized to maximize both methane purity and recovery. The following conclusions can be drawn from this study:

i. The energy efficiency of the developed laboratory-scale biogas upgrading system of 87% with a 2% mean absolute percentage error compared well with full-scale adsorption systems having an energy efficiency in the range of 87.3% to 89.8%. It can therefore be concluded that this technology is viable for adoption in water-deficient regions, suitable for both small-scale prototypes and large-scale systems.

ii. A particle radius increase from 1 mm to 9 mm decreased the methane purity by 1% and increased the methane recovery by 1%. It can hence be concluded that variation in adsorbent particle radius has a minimal influence on the biogas upgrading process.

iii. An increase in the purge-to-feed flow rate ratio from 0.1 to 0.7 enhanced the methane purity by 10% and decreased the methane recovery by 60%. It can therefore be concluded that flow variables are more crucial to the biogas upgrading process compared to the physicochemical properties of the adsorbent.

iv. The optimal values for methane purity and recovery of 82.12% and 37.21% respectively, were achieved at a particle radius of 9 mm, a steam regenerating temperature of 227°C, and a purge-to-feed flow rate ratio of 0.4152. These parameters favoured the column desorption process. It can hence be concluded that complete column regeneration is crucial in achieving maximum methane purity and recovery.

5.2 Recommendations

Based on the findings of this research, the following recommendations are proposed for consideration in the future. These recommended tasks were not carried out as they are considered beyond the scope of this research.

i. Performance of the developed dynamic adsorption model can be investigated for carbon dioxide capture from flue gases to assess its scalability.
ii. The feasibility of other biomass-based activated carbons as an adsorbent in the biogas upgrading process can be evaluated to allow for customization based on the available resources in various regions.
iii. Future work can evaluate the energy requirements of manufacturing activated carbon used in biogas upgrading and account for the exothermic nature of carbon dioxide adsorption in the energy analysis
iv. Future studies can investigate the impact of other physicochemical properties, such as particle shape, to enhance the accuracy of the developed biogas upgrading model.

REFERENCES

Abd, A. A., & Othman, M. R. (2022). Biogas upgrading to fuel grade methane using pressure swing adsorption: Parametric sensitivity analysis on an industrial scale. *Fuel*, *308*, 121986. https://doi.org/10.1016/j.fuel.2021.121986

Abd, A. A., Othman, M. R., & Helwani, Z. (2023). Unveiling the critical role of biogas compositions on carbon dioxide separation in biogas upgrading using pressure swing adsorption. *Biomass Conversion and Biorefinery*, *13*(15), 13827–13840. https://doi.org/10.1007/s13399-021-02106-4

Abdeljaoued, A., Querejeta, N., Durán, I., Álvarez-Gutiérrez, N., Pevida, C., & Chahbani, M. H. (2018). Preparation and evaluation of a coconut shell-based activated carbon for CO_2/CH_4 separation. *Energies*, *11*(7), 1–14. https://doi.org/10.3390/en11071748

Abdulsalam, J., Mulopo, J., Oboirien, B., Bada, S., & Falcon, R. (2019). Experimental evaluation of activated carbon derived from South Africa discard coal for natural gas storage. *International Journal of Coal Science and Technology*, *6(*3), 459–477. https://doi.org/10.1007/ s40789- 019-0262-5

Abuelnoor, N., AlHajaj, A., Khaleel, M., Vega, L. F., & Abu-Zahra, M. R. M. (2021). Activated carbons from biomass-based sources for CO2 capture applications. *Chemosphere*, *282*, 131111. https://doi.org/10.1016/j. chemosphere.2021.131111

Adnan, A., Ong, M., Nomanbhay, S., Chew, K. W., & Show, P. (2019). Technologies for biogas upgrading to biomethane: A review. *Bioengineering*, *6*(4), 1–23. https://doi.org/ 10.3390/bioengineering6040092

African Energy Commission. (2024). Key Africa Energy Statistics 2024. www.au-afrec.org

Ahmad, A., Yadav, A. K., Singh, A., & Singh, D. K. (2024). A comprehensive machine learning-coupled response surface methodology approach for

predictive modeling and optimization of biogas potential in anaerobic co-digestion of organic waste. *Biomass and Bioenergy, 180*. https://doi.org/10.1016/j.biombioe. 2023.106995

Akula, V. R. (2013). *Wetland biomass - suitable for biogas production?* Halmstan University.

Al-Ghouti, M. A., & Da'ana, D. A. (2020). Guidelines for the use and interpretation of adsorption isotherm models: A review. *Journal of Hazardous Materials, 393*. https://doi.org/10.1016/j.jhazmat.2020.122383

Aljeboree, A. M., Alshirifi, A. N., & Alkaim, A. F. (2017). Kinetics and equilibrium study for the adsorption of textile dyes on coconut shell activated carbon. *Arabian Journal of Chemistry, 10,* S3381–S3393. https://doi.org/10.1016/ j.arabjc.2014.01.020

Anand, A., Aier, I., Sakhiya, A. K., & Kaushal, P. (2021). Assessment of crop residues-based electricity generation potential for energy security in Bangladesh. *Bioresource Technology Reports, 15,* 100812. https://doi.org/10.1016/j. biteb.2021.100812

Anneli, P., & Arthur, W. (2009). Biogas upgrading technologies – developments and innovations. In IEA Bioenergy (Issue August).

Arifan, F., Abdullah, A., & Sumardiono, S. (2021). Effect of organic waste addition into animal manure on biogas production using anaerobic digestion method. *International Journal of Renewable Energy Development*, *10*(3), 623–633. https://doi.org/10.14710/ ijred.2021.36107

AspenTech. (2009). *Introduction to Aspen Adsorption AspenTech Customer Education Training Manual*. http://support.aspentech.com/contacts.

AspenTech. (2020). Aspen Adsim, Adsorption Reference Guide Description. http://www.adobe.com

Augelletti, R., Galli, S., Gislon, P., Granati, M., Monteleone, G., Murmura, M. A., & Annesini, M. C. (2020). Biogas upgrading through CO_2 removal by chemical absorption in an amine organic solution: Physical and technical assessment, simulation and experimental validation. *Biomass and Bioenergy*, *141*. https://doi.org/10.1016/j.biombioe.2020.105729

Aziz, I., Kurnianti, Y., Saridewi, N., Adhani, L., & Permata, W. (2020). Utilization of coconut shell as Cr2O3 catalyst support for catalytic cracking of jatropha oil into biofuel. *Journal of Scientific and Applied Chemistry*, *23*(2), 39–45. https://doi.org/10.14710/jksa.23.2.39-45

Azizian, S., Haerifar, M., & Basiri-Parsa, J. (2007). Extended geometric method: A simple approach to derive adsorption rate constants of Langmuir-Freundlich kinetics. *Chemosphere*, *68*(11), 2040–2046. https://doi.org/10.1016/j.chemosphere.2007.02.042

Baena-Moreno, F. M., le Saché, E., Pastor-Pérez, L., & Reina, T. R. (2020). Membrane-based technologies for biogas upgrading: A review. *Environmental Chemistry Letters*, *18*(5), 1649–1658. https://doi.org/10.1007/s10311-020-01036-3

Baena-Moreno, F. M., Mei, D., Leion, H., & Pallarès, D. (2023). Biogas upgrading through calcium looping: Experimental validation and study of CO2 capture. *Biomass and Bioenergy*, *176*. https://doi.org/10.1016/j.biombioe.2023.106918

Bahrun, M. H. V., Bono, A., Othman, N., & Zaini, M. A. A. (2025). Simultaneous production during biogas upgrading: Foundational insights from numerical simulation of dual-reflux pressure swing adsorption. *Next Energy*, 7. https://doi.org/10.1016/j.nxener.2025.100242

Ballesteros, Z. A., De Witte, N., Denayer, J. F. M., & Van Assche, T. R. C. (2022). Effect of pellet size on PSA performance: monolayer and multilayer bed

case study for biogas upgrading. *Adsorption*, *28*(5–6), 197–208. https://doi.org/10.1007/s10450-022-00365-9

Bardi, M. J., Mutunga, J. M., Ndiritu, H., & Koch, K. (2023). Effect of pyrolysis temperature on the physiochemical properties of biochar and its potential use in anaerobic digestion: A critical review. *Environmental Technology and Innovation*, *32*. https://doi.org/10.1016/j.eti.2023.103349

Bassey, J. B., Ekpo, D. D., & Gentle, V. U. (2024). Computational fluid dynamics analysis of flow characteristics in convergent and divergent section. *International Journal of Science, Engineering and Technology*, *2*. https://www.researchgate.net/publication/380760264

Bauer, F., Hulteberg, C., Persson, T., & Tamm, D. (2013). *Biogas upgrading – Review of commercial technologies*.

Bennett, D. A., Bradley, R., & Cross, M. (1986). A general ergun equation for a multilayered porous medium. *Numerical Mathematics and Applications* R. Vichnevetsky, J. Vignes, 85, 213–220.

Benyahia, F., & O'Neill, K. E. (2005). Enhanced voidage correlations for packed beds of various particle shapes and sizes. *Particulate Science and Technology*, *23*(2), 169–177. https://doi.org/10.1080/02726350590922242

Bioenergy strategy 2020-2027. (2020).

Boer, D. G., Langerak, J., Bakker, B., & Pescarmona, P. P. (2022). Binderless zeolite LTA beads with hierarchical porosity for selective CO_2 adsorption in biogas upgrading. *Microporous and Mesoporous Materials*, *344*. https://doi.org/10.1016/j.micromeso.2022.112208

Buivydas, E., Navickas, K., & Venslauskas, K. (2024). A life cycle assessment of methane slip in biogas upgrading based on permeable membrane technology with variable methane concentration in raw biogas. *Sustainability*, *16*(8). https://doi.org/10.3390/su16083323

Canevesi, R., & Grande, C. A. (2023). Biogas upgrading by pressure swing adsorption using zeolite 4A. Effect of purge on process performance. *Separation and Purification Technology*, *309*, 123015. https://doi.org/10.1016/j.seppur.2022.123015

Castley, J., Azimov, U., Combrinck, M., & Xing, L. (2022). Modeling and optimization of combined cooling, heating and power systems with integrated biogas upgrading. *Applied Thermal Engineering*, *210*. https://doi.org/10.1016/j.applthermaleng.2022.118329

Centi, G., & Perathoner, S. (2020). Chemistry and energy beyond fossil fuels. A perspective view on the role of syngas from waste sources. *Catalysis Today*, 342, 4–12. https://doi.org/10.1016/j.cattod.2019.04.003

Chen, D. L., Wang, N., Xu, C., Tu, G., Zhu, W., & Krishna, R. (2015). A combined theoretical and experimental analysis on transient breakthroughs of C2H6/C2H4 in fixed beds packed with ZIF-7. *Microporous and Mesoporous Materials*, *208*, 55–65. https://doi.org/10.1016/j.micromeso.2015.01.019

Chen, X. Y., Vinh-Thang, H., Ramirez, A. A., Rodrigue, D., & Kaliaguine, S. (2015). Membrane gas separation technologies for biogas upgrading. *RSC Advances*, *5*(31), 24399–24448. https://doi.org/10.1039/c5ra00666j

Chipo Mukonza. (2025). *Institutional Cooking with biogas in Kenya: Insights, innovations, and implementation challenges*.

Cutillo, E. A. (2024, May). Enhancing carbon dioxide adsorption in a hybrid fixed bed via structuring and thermal management: a numerical study. *Practical Aspects of Chemical Engineering PAIC.*

Czubaszek, R., Wysocka-Czubaszek, A., Banaszuk, P., Zając, G., & Wassen, M. J. (2023). Grass from road verges as a substrate for biogas production. *Energies*, *16*(11). https://doi.org/10.3390/en16114488

Djimtoingar, S. S., Derkyi, N. S. A., Kuranchie, F. A., & Yankyera, J. K. (2022). A review of response surface methodology for biogas process optimization. *Cogent Engineering*, *9*(1). https://doi.org/10.1080/23311916.2022.2115283

DOSH. (2016). *Guidelines on occupational safety and health in construction, operation and maintenance of biogas plant*.

Drosg, M. (2009). Dealing with uncertainties. In *Springer* (Issue 2). https://doi.org/10.1007/978-3-540-74757-4_7

Dubi, Y., & Ventra, D. M. (2009). Fourier's law: Insight from a simple derivation. *The American Physical Society*, *79*(4). https://doi.org/10.1103/PhysRevE.79.042101

Dungani, R., Munawar, S. S., Karliati, T., Malik, J., Aditiawati, P., & Sulistyono. (2022). Study of characterization of activated carbon from coconut shells on various particle scales as filler agent in composite materials. *Journal of the Korean Wood Science and Technology*, *50*(4), 256–271. https://doi.org/10.5658/WOOD.2022.50.4.256

Durán, I., Rubiera, F., & Pevida, C. (2022). Modeling a biogas upgrading PSA unit with a sustainable activated carbon derived from pine sawdust. Sensitivity analysis on the adsorption of CO2 and CH4 mixtures. *Chemical Engineering Journal*, *428*. https://doi.org/10.1016/j.cej.2021.132564

Energy Institute. (2024). Statistical Review of World Energy.

Energy Institute. (2025). *Statistical Review of World Energy 2025*. www.energyinst.org/statistical-review

Fatma A. Alfarjani. (2012). *Design and Optimization of Process Parameters in Bio-Gas Production Systems* (Issue January). Dublin City University.

Fenske, C. F., Kirzeder, F., Strübing, D., & Koch, K. (2023). Biogas upgrading in a pilot-scale trickle bed reactor – Long-term biological methanation under real application conditions. Bioresource Technology, 376.

Frankowski, J., & Czekała, W. (2023). Agricultural plant residues as potential co-substrates for biogas production. *Energies*, *16*(11). https://doi.org/10.3390/en16114396

Gan, J., Zhou, Z., & Yu, A. (2017). Effect of particle shape and size on effective thermal conductivity of packed beds. *Powder Technology, 311*, 157–166. https://doi.org/10.1016/j.powtec.2017.01.024

Gao, C., Long, J., Yue, Y., Li, B., Huang, Y., Wang, Y., Zhang, J., Zhang, L., & Qian, G. (2024). Degradation and regeneration inhibition of PCDD/Fs in incineration fly ash by low-temperature thermal technology. *Journal of Hazardous Materials, 477*. https://doi.org/10.1016/j.jhazmat.2024.135315

Gbangbo, K. R., Kouakou, A. R., Ehouman, A. D., Yao, B., Goli Lou, G. V. E., Gnaboa, Z., & Bailly, G. C. (2023). Influence of water content on hydrogen sulfide adsorption in biogas purification with musa paradisiaca biochar. *Chemistry Africa*. https://doi.org/10.1007/s42250-023-00610-w

Gholami, M., Verougstraete, B., Vanoudenhoven, R., Baron, G. V., Van Assche, T., & Denayer, J. F. M. (2022). Induction heating as an alternative electrified heating method for carbon capture process. *Chemical Engineering Journal, 431*(November 2021). https://doi.org/10.1016/j.cej.2021.133380

Gkotsis, P., Kougias, P., Mitrakas, M., & Zouboulis, A. (2023). Biogas upgrading technologies- Recent advances in membrane-based processes. *Hydrogen Energy, 48*, 3965–3993.

Golmakani, A., Ali Nabavi, S., Wadi, B., & Manovic, V. (2022). Advances, challenges, and perspectives of biogas cleaning, upgrading, and utilisation. *Fuel, 317*. https://doi.org/10.1016/j.fuel.2021.123085

Grande, C. A., Morence, D. G. B., Bouzga, A. M., & Andreassen, K. A. (2020). Silica gel as a selective adsorbent for biogas drying and upgrading. *Industrial and Engineering Chemistry Research*, *59*(21), 10142–10149. https://doi.org/10.1021/acs.iecr.0c00949

Grande, C. A., Ribeiro, R. P. P. L., & Rodrigues, A. E. (2009). CO_2 capture from NGCC power stations using electric swing adsorption. *Energy and Fuels*, *23*(5), 2797–2803. https://doi.org/10.1021/ef8010756

Guo, Z. Y., Liu, X. B., Tao, W. Q., & Shah, R. K. (2010). Effectiveness-thermal resistance method for heat exchanger design and analysis. *International Journal of Heat and Mass Transfer*, *53*(13–14), 2877–2884. https://doi.org/10.1016/j.ijheatmasstransfer.2010.02.008

Haddad, S., Rivera-Tinoco, R., & Bouallou, C. (2021). Cryogenic removal of CO_2 by frost formation from biogas. *Chemical Engineering Transactions*, *88*, 145–150.

Haider, S., Lindbrathen, A., & Hagg, M.-B. (2016). Techno-economical evaluation of membrane based biogas upgrading system: A comparison between polymeric membrane and carbon membrane technology. *Green Energy and Environment*, 222–234.

Hakawati, R., Smyth, B. M., McCullough, G., De Rosa, F., & Rooney, D. (2017). What is the most energy efficient route for biogas utilization: Heat, electricity or transport? *Applied Energy*, *206*, 1076–1087. https://doi.org/10.1016/j.apenergy.2017.08.068

Hasanpour Seyedlar, N., Zamir, S. M., Nosrati, M., & Rene, E. R. (2024). H2S mitigation for biogas upgrading in a full-scale anaerobic digestion process by using artificial neural network modeling. *Renewable Energy*, *232*. https://doi.org/10.1016/j.renene.2024.121016

He, S., Chen, G., Xiao, H., Shi, G., Ruan, C., Ma, Y., Dai, H., Yuan, B., Chen, X., & Yang, X. (2021). Facile preparation of N-doped activated carbon produced

from rice husk for CO2 capture. *Journal of Colloid and Interface Science, 582*, 90–101. https://doi.org/10.1016/j.jcis.2020.08.021

Herdem, H., Şahin, U., & Ülgen, A. (2024). An innovative approach to a pressurized water scrubbing system with several packing materials for upgrading biogas to biomethane. *Process Safety and Environmental Protection, 188*, 538–548. https://doi.org/10.1016/j.psep.2024.05.053

Higai, D., Huang, Z., & Qian, E. W. (2021). Preparation and surface characteristics of phosphoric acid-activated carbon from coconut shell in air. *Environmental Progress and Sustainable Energy*, *40*(2). https://doi.org/10.1002/ep.13509

Iovane, P., Nanna, F., Ding, Y., Bikson, B., & Molino, A. (2014). Experimental test with polymeric membrane for the biogas purification from CO2 and H2S. *Fuel, 135*, 352–358. https://doi.org/10.1016/j.fuel.2014.06.060

Jensen, M. B., Jensen, B., Ottosen, L. D. M., & Kofoed, M. V. W. (2021). Integrating H2 injection and reactor mixing for low-cost H2 gas-liquid mass transfer in full-scale in situ biomethanation. *Biochemical Engineering Journal, 166*. https://doi.org/10.1016/j.bej.2020.107869

Kalpana, R., V, S., Lokanadham, R., Amudha, K., Beena Bethel, G. N., Shukla, A. K., Kshirsagar, P. R., & Rajaram, A. (2023). Internet of things (IOT) based machine learning techniques for wind energy harvesting. *Electric Power Components and Systems*. https://doi.org/10.1080/15325008.2023.2293952

Kalsum, Z. P. (2025). Optimization of amine-based absorbent solutions for biogas purification from cow manure. *Jurnal Penelitian Pendidikan IPA*, *11*(11), 1044–1056. https://doi.org/10.29303/jppipa.v11i11.12070

Kamran, U., Choi, J. R., & Park, S. J. (2020). A role of activators for efficient CO2 affinity on polyacrylonitrile-based porous carbon materials. *Frontiers in Chemistry, 8*. https://doi.org/10.3389/fchem.2020.00710

Karimi, M., Siqueira, R. M., Shirzad, M., Ferreira, A. F. P., Rodrigues, A. E., & Silva, J. A. C. (2026). Integrated experimental, process simulation, and techno-economic assessment of biogas upgrading via pressure/vacuum swing adsorption. *Separation and Purification Technology*, *386*. https://doi.org/10.1016/j.seppur.2025.136571

Karuppiah, T., & Azariah, E. V. (2019). Biomass Pretreatment for Enhancement of Biogas Production. *Anaerobic Digestion*, 1–22. https://doi.org/10.5772/intechopen.82088

Keller, L., Lohaus, T., Abduly, L., Hadler, G., & Wessling, M. (2019). Electrical swing adsorption on functionalized hollow fibers. *Chemical Engineering Journal*, *371*(February), 107–117. https://doi.org/10.1016/j.cej.2019.04.029

Klinbun, W., Rattanadecho, P., & Pakdee, W. (2011). Microwave heating of saturated packed bed using a rectangular waveguide (TE10 mode): Influence of particle size, sample dimension, frequency, and placement inside the guide. *International Journal of Heat and Mass Transfer*, *54*(9–10), 1763–1774. https://doi.org/10.1016/j.ijheatmasstransfer.2011.01.015

Kong, J., Yue, Q., Huang, L., Gao, Y., Sun, Y., Gao, B., Li, Q., & Wang, Y. (2013). Preparation, characterization and evaluation of adsorptive properties of leather waste based activated carbon via physical and chemical activation. *Chemical Engineering Journal*, *221*, 62–71. https://doi.org/10.1016/j.cej.2013.02.021

Lee, W. H., Zhang, X., Banerjee, S., Jones, C. W., Realff, M. J., & Lively, R. P. (2023). Sorbent-coated carbon fibers for direct air capture using electrically driven temperature swing adsorption. *Joule*, 7(6), 1241–1259. https://doi.org/https://doi.org/10.1016/j.joule.2023.05.016

Li, G., Xiao, P., Xu, D., & Webley, P. A. (2011). Dual mode roll-up effect in multicomponent non-isothermal adsorption processes with multilayered bed

packing. *Chemical Engineering Science, 66*(9), 1825–1834. https://doi.org/10.1016/j.ces.2011.01.023

Lillia, S., Bonalumi, D., Grande, C., & Manzolini, G. (2018). A comprehensive modeling of the hybrid temperature electric swing adsorption process for CO2 capture. *International Journal of Greenhouse Gas Control, 74*(October 2017), 155–173. https://doi.org/10.1016/j.ijggc.2018.04.012

Malinowski, Z., Lenard, J. G., & Davies, M. E. (1994). A study of the heat-transfer coefficient as a function of temperature and pressure. In *Journal of Materials Processing Technology* (Vol. 41).

Masthan, S. K., Rao, K. S. R., Prasad, P. S. S., & Rao, P. K. (1992). Derivation of the expanded form of the BJH equation and its application to the pore structure analysis of mesoporous adsorbents. *Adsorption Science Technology*, *9*, 212–230. https://doi.org/10.1177/026361749200900401

Mbugua, J. K. (2021). *Fabrication and Optimization of an Effective Anaerobic Digester for Biogas Production Using Vegetable Waste From Wakulima and Kangemi Markets in Nairobi County, Kenya*. University of Nairobi.

McEwen, J., Hayman, J. D., & Ozgur Yazaydin, A. (2013). A comparative study of CO_2, CH_4 and N_2 adsorption in ZIF-8, Zeolite-13X and BPL activated carbon. *Chemical Physics*, *412*, 72–76. https://doi.org/10.1016/j.chemphys.2012.12.012

McLaren, R. L., Laycock, C. J., Brousseau, E., & Owen, G. R. (2021). Examining slit pore widths within plasma-exfoliated graphitic material utilising Barrett-Joyner-Halenda analysis. *New Journal of Chemistry, 45*(27), 12071–12080. https://doi.org/10.1039/d1nj01702k

Meloni, E., Martino, M., Pullumbi, P., Brandani, F., & Palma, V. (2021). Intensification of TSA processes using a microwave-assisted regeneration step. Chemical Engineering and Processing - *Process Intensification, 160*, 108291. https://doi.org/10.1016/j.cep.2020.108291

Mendel, N., Boon, J. J. P. J., Sîreţanu, I., Mugele, F., & Brilman, D. W. F. W. (2025). Cs-Bentonite clay for biogas upgrading: A numerical assessment. *Industrial and Engineering Chemistry Research, 64*(16), 8359–8374. https://doi.org/10.1021/acs.iecr.4c04491

Mertins, A., & Wawer, T. (2022). How to use biogas?: A systematic review of biogas utilization pathways and business models. *Bioresources and Bioprocessing, 9*(1). https://doi.org/10.1186/s40643-022-00545-z

Moinee, A. A., Rownaghi, A. A., & Rezaei, F. (2024). Challenges and opportunities in electrification of adsorptive separation processes. *ACS Energy Letters, 9*(3), 1228–1248. https://doi.org/10.1021/acsenergylett.3c02340

Moon, S. H., & Shim, J. W. (2006). A novel process for CO_2/CH_4 gas separation on activated carbon fibers-electric swing adsorption. *Journal of Colloid and Interface Science*, *298*(2), 523–528. https://doi.org/10.1016/j.jcis.2005.12.052

Mugagga, G. R., Omosa, I. B., & Thoruwa, T. (2023). Optimization and Analysis of a Low-Pressure Water Scrubbing Biogas Upgrading System via the Taguchi and Response Surface Methodology Approaches. *International Journal of Renewable Energy Development*, *12*(1), 99–110. https://doi.org/10.14710/ijred.2023.48269

Müller, R., Schuhmacher, D., & Mateu, J. (2022). *ANOVA for Data in Metric Spaces, with Applications to Spatial Point Patterns*. http://arxiv.org/abs/2201.08664

Mulu, E., M'Arimi, M., Ramkat, R. c., & Kiprop, A. (2021). Biogas upgrade using modified natural clay. *Energy Conversion and Management: X*, *12*. https://doi.org/10.1016/j.ecmx.2021.100134

Muriuki, T. E., Ayuya, O. I., & Oloo, B. O. (2024). Towards circular production system in the coconut value chain: actor, roles, linkage and constraints in Kilifi County, Kenya. *Cogent Social Sciences*, *10*(1). https://doi.org/10.1080/23311886.2024.2362903

Mutahi, P. M., Kimutai, S. K., & Adaramola, M. S. (2025). Barriers to the Growth and Implementation of Biogas Technology: The Kenyan Experience. *Energy Science and Engineering*, *13*(11), 5268–5283. https://doi.org/10.1002/ese3.70237

Mutunga, J. M., Ndiritu, H., Hawi, M., & Oketch, P. (2022, October). Technologies for Biogas Upgrading to Biomethane: A Review. *Sustainable Research and Innovation*.

Mutunga, J. M., Ndiritu, H., Hawi, M., & Oketch, P. (2024). Experimental study of four-step thermal swing adsorption cycle to upgrade biogas obtained from anaerobic digestion. *Energy Storage and Saving*, *3*(4), 278–287. https://doi.org/10.1016/j.enss.2024.10.001

Mutunga, J. M., Ndiritu, H., Hawi, M., & Oketch, P. (2025). Parametric study of biogas upgrading process using thermal swing adsorption techniques. *International Journal of Engineering Research in Africa*, *74*, 33–52. https://doi.org/10.4028/p-OZ6yag

Naeiji, E., Noorpoor, A., & Ghanavati, H. (2022). Energy, exergy, and economic analysis of cryogenic distillation and chemical scrubbing for biogas upgrading and hydrogen Production. *Sustainability (Switzerland)*, *14*(6). https://doi.org/10.3390/su14063686

Nam, G., Jeong, B., Kang, S., Lee, B., Choi, D., Environment, D., Technology, P., & Box, P. O. (2005). Equilibrium isotherms of CH_4, C_2H_6, CH_4, N_2, and H_2 on zeolite 5A using a static volumetric method. *Journal of Chemical Engineering Data*, *50*, 72–76.

Naquash, A., Qyyum, M. A., Haider, J., Bokhari, A., Lim, H., & Lee, M. (2022). State-of-the-art assessment of cryogenic technologies for biogas upgrading: Energy, economic, and environmental perspectives. *Renewable and Sustainable Energy Reviews*, *154*. https://doi.org/10.1016/j.rser.2021.111826

Nayeem, A., Shariffuddin, J. H., & Yousuf, A. (2023). Absorption technology for upgrading biogas to biomethane. In *Biogas to Biomethane: Engineering, Production, Sustainability* (pp. 69–84). Elsevier. https://doi.org/10.1016/B978-0-443-18479-6.00005-3

Njogu, P., Kinyua, R., Muthoni, P., & Nemoto, Y. (2015). Biogas Production Using Water Hyacinth (Eicchornia crassipes) for Electricity Generation in Kenya. *Energy and Power Engineering*, *07*(05), 209–216. https://doi.org/10.4236/epe.2015.75021

Njuguna, F. I. (2024). *Numerical Study for the Design of a Fluidized Bed Reactor for Biomass Gasification*. Jomo Kenyatta University of Agriculture and Technology.

Njuguna, F. I., Ndiritu, H. M., Gathitu, B. B., Hawi, M., & Munyalo, J. M. (2023). Experimental investigation and optimization of the gasification parameters of macadamia nutshells in a batch-fed bubbling fluidized bed gasifier with air preheating. *Energy Storage and Saving*, *2*(4), 559–570. https://doi.org/10.1016/j.enss.2023.07.001

Odero, V. O., Ochieng, F. X., & Njogu, P. M. (2025). Performance efficiency of locally available low-cost adsorbents in purification of biogas for high grade applications. *Journal of Agriculture, Science and Technology*, *23*(5), 128–144. https://doi.org/10.4314/jagst.v23i5.8

Ostrem, K. M., Millrath, K., & Themelis, N. J. (2004). Combining anaerobic digestion and waste-to-energy. *Proceedings of 12th Annual North American Waste to Energy Conference,NAWTEC12*, *6*, 265–271. https://doi.org/10.1115/nawtec12-2231

Owusu, P. A., & Asumadu-Sarkodie, S. (2016). A review of renewable energy sources, sustainability issues and climate change mitigation. *Cogent Engineering*, *3*(1), 1–14. https://doi.org/10.1080/23311916.2016.1167990

Papurello, D., Gandiglio, M., Kafashan, J., & Lanzini, A. (2019). Biogas purification : A comparison of adsorption wood-derived char using isotherm equations. *Processes*, *7*, 774.

Pérez-Huertas, S., Calero, M., Ligero, A., Pérez, A., Terpiłowski, K., & Martín-Lara, M. A. (2023). On the use of plastic precursors for preparation of activated carbons and their evaluation in CO_2 capture for biogas upgrading: A review. *Waste Management, 161*, 116–141. https://doi.org/10.1016/j.wasman. 2023.02.022

Piechota, G. (2021). Multi-step biogas quality improving by adsorptive packed column system as application to biomethane upgrading. *Journal of Environmental Chemical Engineering*, *9*(5). https://doi.org/10.1016/j. jece.2021.105944

Polat, S., & Sayan, P. (2019). Application of response surface methodology with a Box–Behnken design for struvite precipitation. *Advanced Powder Technology*, *30*(10), 2396–2407. https://doi.org/10.1016/j.apt.2019.07.022

Pöschl, M., Ward, S., & Owende, P. (2010). Evaluation of energy efficiency of various biogas production and utilization pathways. *Applied Energy*, *87*(11), 3305–3321. https://doi.org/10.1016/j.apenergy.2010.05.011

Punpee, S., Tongpadungrod, P., Suttikul, T., & Phalakornkule, C. (2023). Characteristics of CO_2 adsorption and desorption on activated carbon in comparison with zeolite 13X and carbon molecular sieve and applications in biogas upgrading using vacuum pressure swing adsorption. *Journal of Chemical Technology and Biotechnology*, *98*(11), 2677–2690. https://doi.org/10.1002/ jctb.7320

Raganati, F., Chirone, R., & Ammendola, P. (2020). CO_2 capture by temperature swing adsorption: Working capacity as affected by temperature and CO_2 partial pressure. *Industrial and Engineering Chemistry Research*, *59*(8), 3593–3605. https://doi.org/10.1021/acs.iecr.9b04901

Rainone, F., Balsamo, M., Lancia, A., & Erto, A. (2023). Adsorption technology for upgrading biogas to biomethane. In *Biogas to Biomethane: Engineering, Production, Sustainability* (pp. 85–115). Elsevier. https://doi.org/10.1016/B978-0-443-18479-6.00014-4

Rainone, F., D'Agostino, O., Erto, A., Balsamo, M., & Lancia, A. (2021). Biogas upgrading by adsorption onto activated carbon and carbon molecular sieves: Experimental and modelling study in binary CO_2/CH_4 mixture. *Journal of Environmental Chemical Engineering, 9*(5). https://doi.org/10.1016/j.jece. 2021.106256

Rajasekaran, N., Vinoba, M., Al-Sheeha, H., & Rana, M. S. (2021). The synergistic character of highly N-doped coconut–shell activated carbon for efficient CO_2 capture. *Chemistry Europe, 6*(34), 9149–9156. https://doi.org/10.1002/slct. 202102522

Rauch, J., & Haloua, F. (2018). Calorific value of biomethane: Comparative measurements using reference gas calorimeters. *Journal of Physics: Conference Series, 1065*(20). https://doi.org/10.1088/1742-6596/1065/ 20/202007

Ribeiro, R. P. P. L., Grande, C. A., & Rodrigues, A. E. (2014). Electric swing adsorption for gas separation and purification: A review. *Separation Science and Technology (Philadelphia), 49*(13), 1985–2002. https://doi.org/ 10.1080/0149639 5.2014.915854

Robinson, B. L., Clifford, M. J., & Selby, G. (2023). Towards fair, just and equitable energy ecosystems through smart monitoring of household-scale biogas plants in Kenya. *Energy Research and Social Science, 98*. https://doi.org/10. 1016/j.erss.2023.103007

Rohsenow, W. M. ., Hartnett, J. P. ., & Cho, Y. I. . (1998). *Handbook of heat transfer* . McGraw-Hill.

Rotunno, P., Lanzini, A., & Leone, P. (2017). Energy and economic analysis of a water scrubbing based biogas upgrading process for biomethane injection into the gas grid or use as transportation fuel. *Renewable Energy*, *102*, 417–432. https://doi.org/10.1016/j.renene.2016.10.062

Rouquerol, F., Rouquerol, J., Sing, K. S. W., Llewellyn, P., &, & Maurin, G. (2014). Adsorption by Powders and Porous Solids. In *Academic Press, Elsevier Ltd*.

Sakiewicz, P., Piotrowski, K., Ober, J., & Karwot, J. (2020). Innovative artificial neural network approach for integrated biogas – wastewater treatment system modelling: Effect of plant operating parameters on process intensification. *Renewable and Sustainable Energy Reviews*, *124*. https://doi.org/ 10.1016/j.rser.2020.109784

Saputra, N. A., Saputra, I. S., Yuniarti, K., & Andianto. (2020). Preparation and characterization of Gigantochloa robusta activated carbon to reduce COD levels of pharmaceutical waste. *IOP Conference Series: Materials Science and Engineering*, *935*(1). https://doi.org/10.1088/1757-899X/935/1/012045

Satayeva, A. R., Howell, C. A., Korobeinyk, A. V, Jandosov, J., Inglezakis, V. J., Mansurov, Z. A., & & Mikhalovsky, S. V. (2018). Investigation of rice husk derived activated carbon for removal of nitrate contamination from water. *Science of the Total Environment*, *630*, 1237–1245.

Schneider, T., Müller, D., & Karl, J. (2020). A review of thermochemical biomass conversion combined with Stirling engines for the small-scale cogeneration of heat and power. In *Renewable and Sustainable Energy Reviews* (Vol. 134). Elsevier Ltd. https://doi.org/10.1016/j.rser.2020.110288

Scholz, M. (2013). *Membrane Based Biogas Upgrading Processes*.

Selim, M. M., Tounsi, A., Gomaa, H., & Shenashen, M. (2024). Enhancing carbon capture efficiency in biogas upgrading: A comprehensive review on adsorbents and adsorption isotherms. *AIP Advances*, *14*(4). https://doi.org/10.1063/5.0208686

Seong, L. K., Abd, A. A., Al-Musawi, T. J., Kim, J., & Othman, M. R. (2024). Biogas upgrading to fuel quality by dynamic adsorption of activated charcoal under non-isothermal conditions. *Biomass Conversion and Biorefinery*. https://doi.org/10.1007/s13399-024-06222-9

Shah, G., Ahmad, E., Pant, K. K., & Vijay, V. K. (2021). Comprehending the contemporary state of art in biogas enrichment and CO_2 capture technologies via swing adsorption. *International Journal of Hydrogen Energy*, *46*(9), 6588–6612. https://doi.org/10.1016/j.ijhydene.2020.11.116

Shen, Y., Shi, W., Zhang, D., Na, P., & Fu, B. (2018). The removal and capture of CO_2 from biogas by vacuum pressure swing process using silica gel. *Journal of CO_2 Utilization*, *27*(May), 259–271. https://doi.org/10.1016/ j.jcou.2018.08.001

Shukla, S. K., Al Mushaiqri, N. R. S., Al Subhi, H. M., Yoo, K., & Al Sadeq, H. (2020). Low-cost activated carbon production from organic waste and its utilization for wastewater treatment. *Applied Water Science*, *10*(2), 1–9. https://doi.org/10.1007/s13201-020-1145-z

Siddiki, S. Y. A., Uddin, M. N., Mofijur, M., Fattah, I. M. R., Ong, H. C., Lam, S. S., Kumar, P. S., & Ahmed, S. F. (2021). Theoretical calculation of biogas production and greenhouse gas emission reduction potential of livestock, poultry and slaughterhouse waste in Bangladesh. *Journal of Environmental Chemical Engineering*, *9*(3). https://doi.org/10.1016/ j.jece.2021.105204

Solarte-Toro, J. C., Chacón-Pérez, Y., & Cardona-Alzate, C. A. (2018). Evaluation of biogas and syngas as energy vectors for heat and power generation using lignocellulosic biomass as raw material. *Electronic Journal of Biotechnology*, *33*, 52–62. https://doi.org/10.1016/ j.ejbt.2018.03.005

Solís, R. R., Calero, M., Pereira, L., Ramírez, S., Blázquez, G., & Martín-Lara, M. Á. (2024). Transforming a mixture of real post-consumer plastic waste into

activated carbon for biogas upgrading. *Process Safety and Environmental Protection*, *190*, 298–315. https://doi.org/10.1016/ j.psep.2024.07.022

Song, X., Gong, J., Zeng, Y., & Wang, L. (2022). Preparation and characterization of activated carbon modified by potassium for carbon dioxide/methane adsorption and separation. *Materialwissenschaft Und Werkstofftechnik*, *53*(12), 1592–1606. https://doi.org/10.1002 /mawe.202200022

Song, X., Gong, J., Zeng, Y., Zhan, X., & Wang, L. (2021). Adsorption and separation of carbon dioxide and methane on carbonaceous adsorbents. *Materialwissenschaft Und Werkstofftechnik*, *52*(11), 1267–1280. https://doi.org/ 10.1002/mawe.202100119

Sonnleitner, E., Schöny, G., & Hofbauer, H. (2018). Assessment of zeolite 13X and Lewatit® VP OC 1065 for application in a continuous temperature swing adsorption process for biogas upgrading. *Biomass Conversion and Biorefinery*, *8*(2), 379–395. https://doi.org/10.1007/s13399-017-0293-3

Sun, Q., Li, H., Yan, J., Liu, L., Yu, Z., & Yu, X. (2015). Selection of appropriate biogas upgrading technology-a review of biogas cleaning, upgrading and utilisation. *Renewable and Sustainable Energy Reviews*, *51*, 521–532. https://doi.org/10.1016/j.rser.2015.06.029

Surra, E., Ribeiro, R. P. P. L., Santos, T., Bernardo, M., Mota, J. P. B., Lapa, N., & Esteves, I. A. A. C. (2022). Evaluation of activated carbons produced from Maize Cob Waste for adsorption-based CO2 separation and biogas upgrading. *Journal of Environmental Chemical Engineering*, *10*(1). https://doi.org/10.1016/ j.jece.2021.107065

Swedish Gas Technology Centre Ltd (SGC). (2012). Basic Data on Biogas. In *Serviceförvaltningen i Lunds kommun, Lund* (Vol. 2). https://doi.org/10.1177/ 107755878003700411

Tabar, A. M., Hosseini, S. S., & Denayer, J. F. M. (2022). A multicolumn vacuum pressure swing adsorption biogas upgrading process for simultaneous CO_2

and N_2 separation from methane: Exergy and energy analysis. *Energy Conversion and Management*, *269*. https://doi.org/10.1016/j.enconman.2022.116060

Tan, V. W. G., Chan, Y. J., Arumugasamy, S. K., & Lim, J. W. (2023). Optimizing biogas production from palm oil mill effluent utilizing integrated machine learning and response surface methodology framework. *Journal of Cleaner Production*, *414*. https://doi.org/10.1016/j.jclepro. 2023.137575

Thommes, M., Kaneko, K., Neimark, A. V., Olivier, J. P., Rodriguez-Reinoso, F., Rouquerol, J., & Sing, K. S. W. (2015). Physisorption of gases, with special reference to the evaluation of surface area and pore size distribution (IUPAC Technical Report). In *Pure and Applied Chemistry* (Vol. 87, Issues 9–10). https://doi.org/10.1515/pac-2014-1117

Thrän, D., Billig, E., Persson, T., Svensson, M., Daniel-Gromke, J., Ponitka, J., & *et al*. (2014). *Biomethane Status and Factors Affecting Market Development and Trade. IEA Bioenergy Task 37* (Issue September).

Tsai, W. T., & Jiang, T. J. (2018). Mesoporous activated carbon produced from coconut shell using a single-step physical activation process. *Biomass Conversion and Biorefinery*, *8*(3), 711–718. https://doi.org/10.1007/s13399-018-0322-x

Valverde, A., Cabrera-Codony, A., Calvo-Schwarzwalder, M., & Myers, T. G. (2024). Investigating the impact of adsorbent particle size on column adsorption kinetics through a mathematical model. *International Journal of Heat and Mass Transfer*, *218*. https://doi.org/10.1016/j.ijheatmasstransfer.2023.124724

Verdade, A. G. A. (2020). *The potential of Aspen Adsorption software package to simulate pressure swing adsorption units*. University of Porto.

Verougstraete, B., Schoukens, M., Sutens, B., Vanden Haute, N., De Vos, Y., Rombouts, M., & Denayer, J. F. M. (2022). Electrical swing adsorption on

3D-printed activated carbon monoliths for CO_2 capture from biogas. *Separation and Purification Technology*, *299*(June), 121660. https://doi.org/10.1016/j. seppur.2022.121660

Vivo-Vilches, J. F., Pérez-Cadenas, A. F., Maldonado-Hódar, F. J., Carrasco-Marín, F., Faria, R. P. V., Ribeiro, A. M., Ferreira, A. F. P., & Rodrigues, A. E. (2017). Biogas upgrading by selective adsorption onto CO_2 activated carbon from wood pellets. *Journal of Environmental Chemical Engineering*, *5*(2), 1386–1393. https://doi.org/10.1016/j.jece.2017.02.015

Vogtenhuber, H., Hofmann, R., Helminger, F., & Schöny, G. (2018). Process simulation of an efficient temperature swing adsorption concept for biogas upgrading. *Energy*, *162*, 200–209. https://doi.org/10.1016/j.energy. 2018.07.193

Wang, J., & Guo, X. (2020). Adsorption kinetic models: Physical meanings, applications, and solving methods. In *Journal of Hazardous Materials* (Vol. 390). Elsevier B.V. https://doi.org/10.1016/j.jhazmat.2020.122156

Wantz, E., Benizri, D., Dietrich, N., & Hébrard, G. (2022). Rate-based modeling approach for High Pressure Water Scrubbing with unsteady gas flowrate and multicomponent absorption applied to biogas upgrading. *Applied Energy*, *312*. https://doi.org/10.1016/j.apenergy.2022.118754

Wasefi, S., Yapar, G., & Ramani, B. (2022). *CO2 Capture from Steel Gases - using Pressure Swing Adsorption model in Aspen Adsorption*. Univeresiteit Utrecht.

Werkneh, A. A. (2022). Biogas impurities: environmental and health implications, removal technologies and future perspectives. *Heliyon*, *8*(10). https://doi.org/10.1016/j.heliyon.2022.e10929

Wu, J. C., Jou, H. L., & Chang, C. H. (2023). Power conversion interface for a small-capacity photovoltaic power generation system. *Energies*, *16*(3). https://doi.org/10.3390/en16031097

Yin, C., Sun, W., Yang, H., & Zhang, D. (2015). Optimization of three-bed VPSA system for biogas upgrading. *Chemical Engineering Science*, *135*, 100–108. https://doi.org/10.1016/j.ces.2015.06.022

Yu, H., Seo, S. won, Mikšík, F., Thu, K., Miyazaki, T., & Ng, K. C. (2023). Effects of temperature and humidity ratio on the performance of desiccant dehumidification system under low-temperature regeneration. *Journal of Thermal Analysis and Calorimetry*, *148*(8), 3045–3058. https://doi.org/10.1007/s10973-022-11368-7

Zhai, J., Burke, I. T., & Stewart, D. I. (2021). Beneficial management of biomass combustion ashes. In *Renewable and Sustainable Energy Reviews* (Vol. 151). Elsevier Ltd. https://doi.org/10.1016/j.rser.2021.111555

Zhao, R., Liu, L., Zhao, L., Deng, S., & Li, H. (2018). Thermodynamic analysis on carbon dioxide capture by electric swing adsorption technology. *Journal of CO_2 Utilization*, *26*(March), 388–396. https://doi.org/10.1016/j.jcou.2018.05.026

Zheng, Y., Li, Q., Yuan, C., Tao, Q., Zhao, Y., Zhang, G., & Liu, J. (2019). Influence of temperature on adsorption selectivity: Coal-based activated carbon for CH_4 enrichment from coal mine methane. *Powder Technology*, *347*, 42–49.

Zhou, K., Chaemchuen, S., & Verpoort, F. (2017). Alternative materials in technologies for Biogas upgrading via CO_2 capture. *Renewable and Sustainable Energy Reviews*, *79*, 1414–1441. https://doi.org/10.1016/j.rser.2017.05.198

Zito, P. F., Brunetti, A., & Barbieri, G. (2022). Multi-step membrane process for biogas upgrading. *Membrane Science*, *652*.

APPENDICES

Appendix I: CO_2 Isotherm Fitting on (a) Langmuir, (b) Freundlich, and (c) Langmuir-Freundlich Models

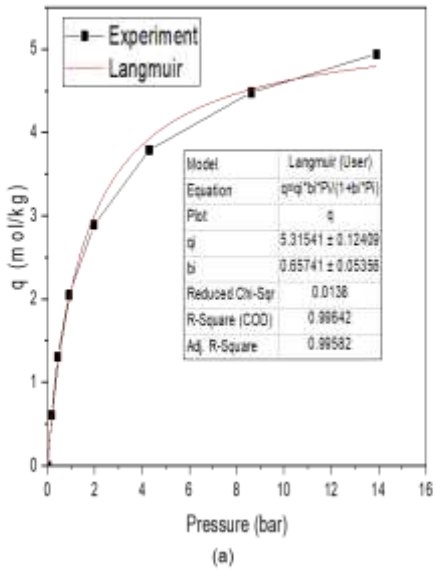

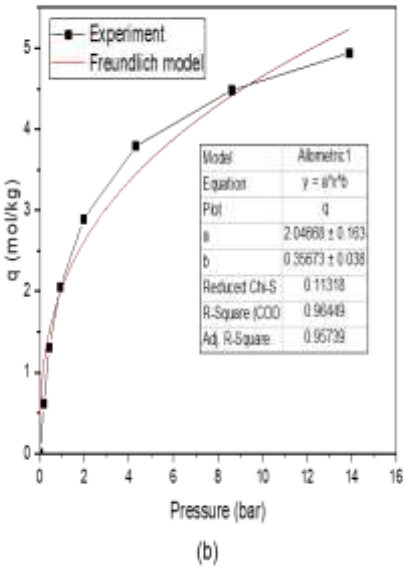

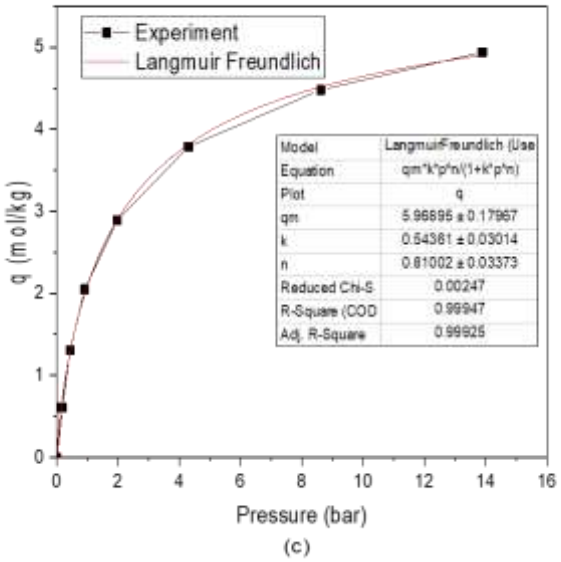

Appendix II: CH_4 Isotherm Fitting on (a) Langmuir, (b) Freundlich, and (c) Langmuir-Freundlich Models

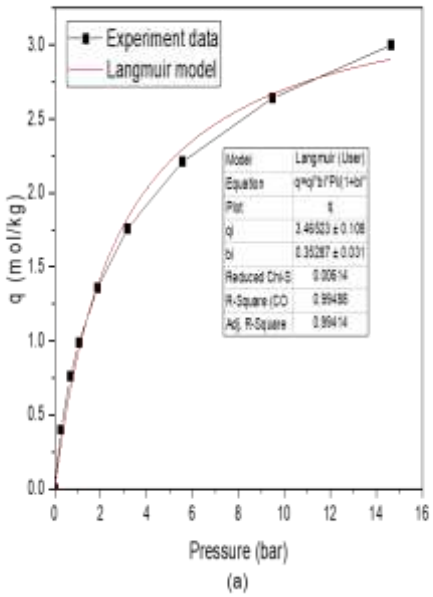

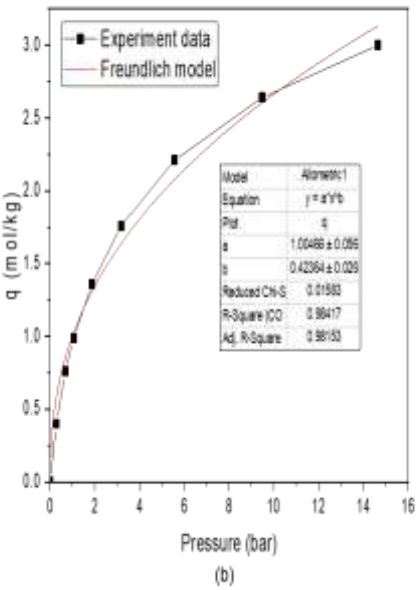

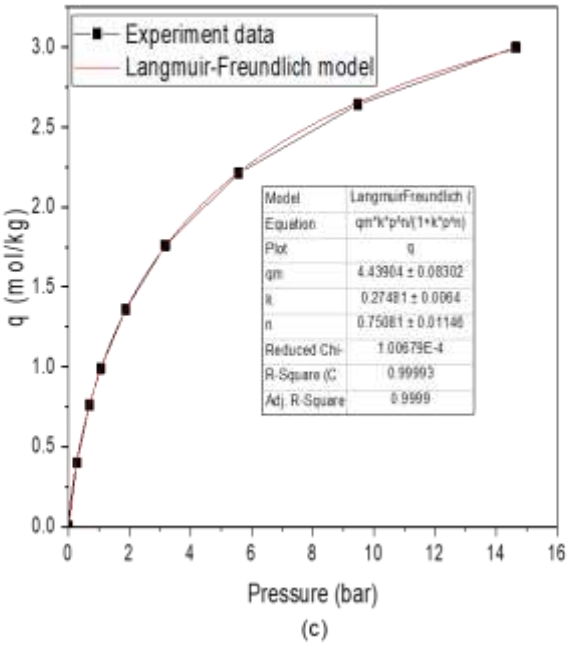

Appendix III: Experimental Measuring Equipment

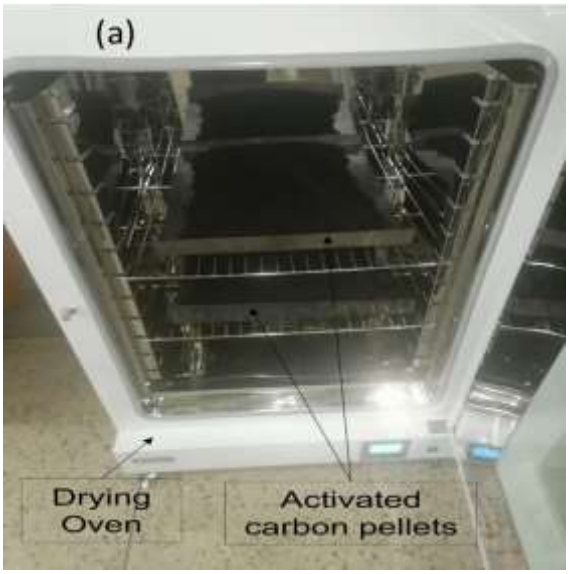

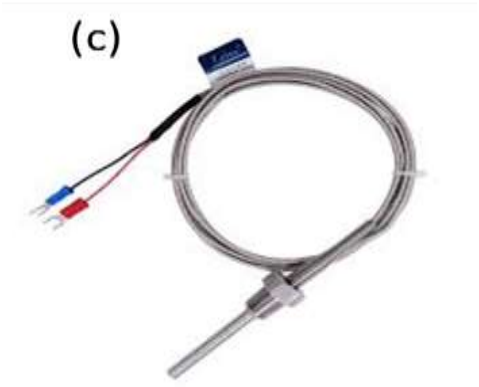

Equipment: (a) Commercial oven, (b) GASTiger, (c) K-type Thermocouples

Appendix IV: Classification of Adsorption Isotherms Combining Proposals from IUPAC

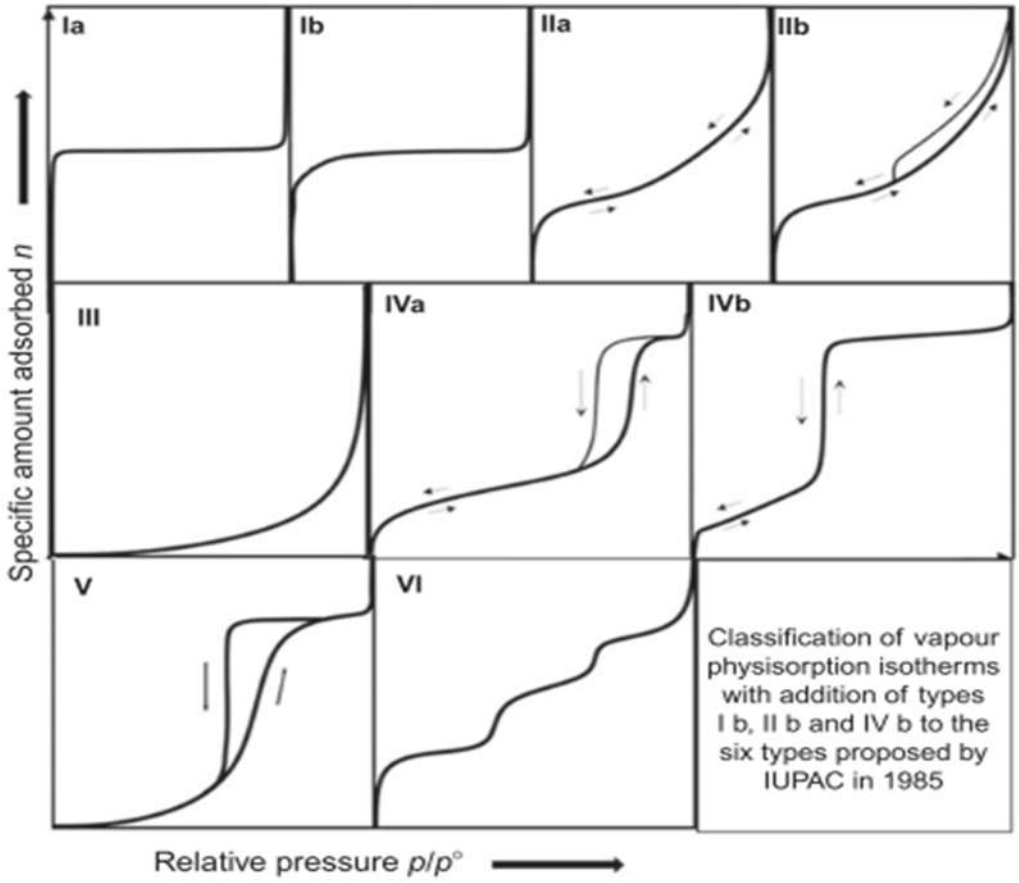

Appendix V: EDS Analysis Spectra of CSAC Samples